MODELING OF THE REBURN PROCESS WITH THE USE OF FEEDLOT BIOMASS AS A REBURN FUEL

A Thesis

by

GIACOMO COLMEGNA

Submitted to the Office of Graduate Studies of
Texas A&M University
in partial fulfillment of the requirements for the degree of

MASTER OF SCIENCE

May 2007

Major Subject: Mechanical Engineering

MODELING OF THE REBURN PROCESS WITH THE USE OF FEEDLOT BIOMASS AS A REBURN FUEL

A Thesis

by

GIACOMO COLMEGNA

Submitted to the Office of Graduate Studies of
Texas A&M University
in partial fulfillment of the requirements for the degree of

MASTER OF SCIENCE

Approved by:

Chair of Committee,	Kalyan Annamalai
Commettee Members,	Jerald Caton
	Adonios Karpetis
Head of Department,	Dennis O'Neal

May 2007

Major Subject: Mechanical Engineering

ABSTRACT

Modeling of the Reburn Process with the Use of Feedlot Biomass as a Reburn Fuel.

(May 2007)

Giacomo Colmegna, B.S., Politecnico di Milano

Chair of Advisory Committee: Dr. Kalyan Annamalai

Coal fired power plants will face many challenges in the near future as new regulations, such as the Clear Sky Act, are being implemented. These regulations impose much stricter limits on NO_x emissions and plan to impose limits on mercury emissions from coal fired boilers. At this time no technologies are currently being implemented for control of Hg and this explains the strong interest in this area by the Department of Energy (DOE).

Reburn technology is a very promising technology to reduce NO_x emissions. Previous experimental research at TAMU reported that Feedlot Biomass (FB) can be a very effective reburn fuel, for reduction of NO_x up to 90%-95%; however, little work has been done to model such a process with Feedlot Biomass as reburn fuel. The present work addresses the development of a reburn model to predict NO_x and Hg emissions.

The model accounts for finite rate of heating of solid fuel particles, mixing with NO_x laden hot gases, size distribution, finite gas phase and heterogeneous chemistry, and oxidation and reduction reactions for NO_x and Hg. To reduce the computational effort all the reactions, except those involved in mercury oxidation, are modeled using global reactions.

Once the model was validated by comparison with experimental findings, extensive parametric studies were performed to evaluate the parameters controlling NO_x reduction.

From DOE research programs some experimental data regarding the capture of mercury from power plant is available, but currently no experimental data are available for Hg emission with reburn process. This model has shown a very large mercury reduction using biomass as a reburn fuel.

The model recommends the following correlations for optimum reduction of NO_x: Equivalence Ratio should be above 1.05; mixing time should be below 100ms (especially for biomass); pure air can be used as the carrier gas; the thermal power fraction of the reburner should be between 15% and 25%; residence time should be at least 0.5s and the Surface Mean Diameter (SMD) of the size distribution should be as small as possible, at least below 100 μm.

ACKNOWLEDGMENTS

I would like to thank my committee chair, Dr. Annamalai, and my committee members, Dr. Caton, and Dr. Karpetis, for their guidance throughout the course of this research.

Thanks also to my friends in the Coal and Biomass Energy Laboratory who helped me with the development of my model. I wish to express my thanks to the Texas Commission for Environmental Quality, Austin, TX, and the Department of Energy, Golden, CO, for funding the project.

Finally, thanks to Dr. Boniardi for his guidance along my undergraduate and graduate studies.

NOMENCLATURE

CO	Carbon Monoxide
CO_2	Carbon Dioxide
CH_4	Methane
E	Activation Energy
ER	Equivalence Ratio
FB	Feedlot Biomass
FN	Fuel Bound Nitrogen
FC	Fixed Carbon
HAPC	High Ash Partially Composted Biomass
Hg	Elemental Mercury
HHV	Higher Heating Value
k	Pre Exponential Factor
LAPC	Low Ash Partially Composted Biomass
NO	Nitric Oxide
NO_x	Nitrogen Oxides
RTE	Reburner Thermal Fraction
SMD	Surface Mean Diameter
TCEQ	Texas Commission for Environmental Quality
TXL	Texas Lignite Coal
VM	Volatile Matter
WYO	Wyoming Subbituminous Coal

TABLE OF CONTENTS

Page

CHAPTER Page

LIST OF FIGURES

FIGURE Page

FIGURE Page

FIGURE Page

FIGURE Page

FIGURE Page

LIST OF TABLES

CHAPTER I

INTRODUCTION

In the United States, more than 50% of the electric power is generated from coal [1]. Year 2005 saw an increase in the coal consumption in the electric sector of 1.1% over the previous year [1].

Coal consumption in the power sector has been increasing in the recent years and there are no reasons to believe that this slow, but steady, growth will stop in the near future, as the electricity demand is growing and other fossil fuels such as natural gas have become increasingly expensive. Besides, the USA has huge reserves of coal, which represent a very stable source of energy as it does not rely on imports from foreign countries such as for oil or natural gas.

The combustion of coal, a solid fuel, poses many challenges as regulations about pollutant emissions become more stringent [2].

In fact exhaust from coal combustion normally contains many pollutants such as nitric oxides (NO_x), sulfur dioxide (SO_2), mercury, fly ash and particulate matter.

In addition, coal emits a larger amount of carbon dioxide than the other fossil fuels (see Table I.1), for the same amount of heat produced, and there is growing concern as CO_2 is believed to cause the phenomenon of global warming.

This thesis follows the style of *Combustion and Flame.*

Table I.1
CO_2 emission for different fuels

Fuel	Emission of CO_2 (kg/kWh)
Coal	0.34
Light Oil	0.28
Natural Gas	0.20
Methane (CH_4)	0.20
LPG - Liquid Petroleum Gas	0.20
Bioenergy	0

In particular much attention is focused on NO_x emission, as the United States Environmental Protection Agency reports that nitrogen oxides are one of the major air pollutants generated in the United States, and a large fraction comes from coal fired power plants [3].

Nitric oxides emissions cause concern, as they are one of the main ingredients involved in the formation of ground level ozone, which can trigger serious respiratory problems. Besides, they contribute to the formation of acid rain, to the deterioration of water quality and global warming [3].

Typical uncontrolled emissions from a 500MW coal plant can be as high as 0.75 – 1.2 lbm/MMBtu, depending on the furnace design and the kind of coal burnt [4].

Mercury is present in coal in tiny quantities (parts per billion). Approximately, around 40% of the mercury is released in oxidized form [5], which can be easily removed with the pollution control devices already installed in the power plants, and two thirds will be in elemental form. The main concern is with the elemental form, because only a small fraction of it is trapped by current clean up devices (such as wet scrubber), so the rest is emitted into the atmosphere.

Mercury emissions from human – related activities have steadily decreased in the United States since the 1960s as big sources such as Municipal Solid Waste Incinerators and mercury use in batteries and paints have been regulated [6].

Nowadays the mercury emission from human related activities in the USA can be estimated around 115 tons per year; coal power plants contribute for around 48 tons of mercury, representing the nation's largest source [6].

Emissions of elemental mercury represent a threat as this mercury will eventually settle in water or land and some microorganisms can change it into methylmercury, a highly toxic form that builds up in fish, shellfish and animals that eat fish.

Mercury exposure at high levels can harm the brain, heart, kidneys, lungs, and immune and nervous system of people of all ages and induce effects such as reduced reproduction and slower growth [6].

With coal likely to remain one of the nation's lowest cost source of electricity for the foreseeable future, and therefore to address the growing concerns about emission of pollutants, the Bush administration in 2002 passed the Clear Sky Initiative.

This initiative is very challenging and its targets, for coal power plants, are:

- Mercury emissions will be cut by 69%, from the present 48 tons per year to 26 tons per year in 2010 and 15 tons per year in 2018.
- Nitric oxide emissions will be cut by 67%, from the current 5 million tons per year to 2.1 million tons in 2008 and 1.7 million tons by 2018.

The Phase II of EPA's Acid Rain Program required NO_x level for coal fired boilers to be below 0.46 lbm/MMBtu by year 2000 [3]. After the implementation of the Clear Air Interstate Rule (that applies to 28 states in the East of the US), the region wide emission average for NO_x will be 0.14 lbm/MMBtu by 2010 and 0.11 lbm/MMBtu by 2015 [3].

NO_x control technologies (such as staged combustion, use of low nitrogen fuel, reburn process, etc.) are already available, but to achieve the new stringent levels they will need to be further developed, in order to get to these levels at competitive costs. The staged combustion consists in a gradual mixing of the air flow needed to burn the fuel: the main burner is operated slightly rich and then the remaining part of the air is provided gradually downstream, this way in the hottest part of the burner there is very little oxygen available and so the formation of NO_x is significantly reduced. The use of low nitrogen fuel (such a natural gas) reduces the emissions of NO_x because this way it is possible to avoid the formation of fuel NO_x, which is formed from the nitrogen contained in the fuel and in the case of coal it represents most of the NO_x formed in the burner. The reburn process will be better thoroughly exposed in the next chapter.

For mercury, the situation is even more challenging: the Clear Sky Initiative has set the very first caps on mercury emissions, as before, mercury emissions from coal

power plants has never been regulated. At the moment there are no commercially available, cost effective technologies capable of trapping mercury for all the power plant configurations or fuel types [5].

Brief description of a coal burner

In a conventional coal burner fuel is premixed with the so – called carrier air (almost 15 – 20 % of the total) and is injected in the combustion chamber. The rest of the air is preheated to around 500 K and is supplied with swirl injectors to better mix with the air and fuel in the chamber. In old burners all the fuel and all the air were injected together: this configuration led to very high emission of NO_x and has therefore been abandoned, at least in the large units. Modern burners use slightly rich combustion in the main burners (where air and fuel are premixed) to reduce NO_x and then secondary air (which is non premixed) to complete combustion as shown in Fig. I.1.

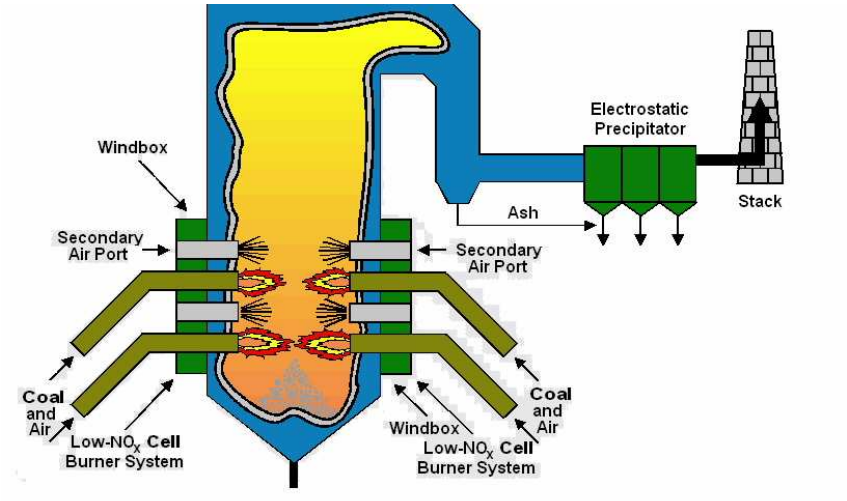

Fig. I.1. Schematics of a coal burner.

The advantage of keeping the main burner working in rich condition is that in this case there will be little oxygen available and so all the reactions trying to form NO_x will be slowed.

In some boilers downstream from the main burner there can be the reburn zone: here some extra fuel is injected and burned in a fuel rich zone whose primary purpose is to reduce NO_x. In this case further downstream there is the burn out zone in which some more air can be supplied to the exhaust to oxidize all the fuel left.

CHAPTER II

LITERATURE REVIEW

Chapter overview

This chapter provides a literature review on the main issues involved in this work. First a general review on the theories about NO_x formation is presented. Then, the various techniques to reduce NO_x are presented. Particular attention is paid on the reburn techniques to reduce NO_x and on the most important parameters in this process such as the reburn fuel. Finally, also a brief review on the mercury emission and control from coal fired power plants is presented.

NO_x formation

During the combustion process of hydrocarbons with air there is the possibility of forming, among many other pollutants, oxides of nitrogen in the exhaust. These oxides might be nitric oxide (NO), nitrous oxide (N_2O) or nitrogen dioxide (NO_2), and they are collectively called with the generic term of NO_x.

Theoretically, the formation of NO_x can take place in every part of the furnace, but often it is produced only in certain parts of the flame, and over 80% of the NO_x might be produced in only 10% of the flame volume.

N_2O is not significant in the case of coal combustion and also NO_2 only represents a small fraction of the oxides of nitrogen emitted at the stack. The largest fraction is by far composed by NO. Typically, in the atmosphere most of the NO is then converted into NO_2.

EPA regulations on reporting emissions of NO on mass basis require the use of molecular weight of NO_2. This means assuming that 1 NO leads to 1 NO_2, therefore this leads to more stringent limits than NO – based combustion.

The amount of NO_x formed depends on a variety of factors which include the fuel burned, the stoichiometry, the temperatures, the mixing and the residence time. The three main mechanisms of NO_x formation in the gas phase are: thermal NO_x, fuel NO_x and prompt NO_x [7].

Fuel NO is formed from the nitrogen contained in the fuel, and in the case of coal it can account for 60-80% of the total NO formed [7]. It is formed more readily than thermal NO as the bonds of nitrogen with coal or in the molecules emitted from coal (mainly HCN and ammonia) are much weaker than the triple bond of the molecular nitrogen present in the gas stream. Therefore the formation of fuel NO can be considered almost temperature independent.

Fuel bound nitrogen is normally emitted as molecular nitrogen, ammonia or HCN. Especially the last two species are the most significant, and their amount in the gas stream is a strong function of the kind of fuel [8]. In general high rank coals tend to emit most of their nitrogen as HCN, while low rank coals has also a significant fraction of ammonia [8]. It has been found that biomass emits a very large fraction of FBN as ammonia [9].

These species then react in the gas phase and they could either decay to NO or N_2, depending on the local stoichiometry, with more NO produced in the case of lean mixture [7].

Thermal NO_x originates from the reaction of oxygen in the gas stream with nitrogen at high temperatures [7]. This pathway has a very strong dependence on the temperature and on the oxygen concentration. This pathway can be described by the widely accepted two-step Zeldovich mechanism:

$$N_2 + O \Leftrightarrow NO + N \quad \text{(I.1)}$$

$$N + O_2 \Leftrightarrow NO + O \quad \text{(I.2)}$$

$$N + OH \Leftrightarrow NO + H \quad \text{(I.3)}$$

The third reaction is particularly important under rich flame conditions where the OH radicals are present in higher concentrations than atomic hydrogen or oxygen.

At mean temperatures below 1800 K, thermal NO formation is very slow [7]. Fig. II.1 presents the thermal NO_x equilibrium calculation for the combustion of methane according to the excess air provided [10]. It is noted that if the excess air is low, the NO_x formation becomes significant only for temperature roughly above 1800 K.

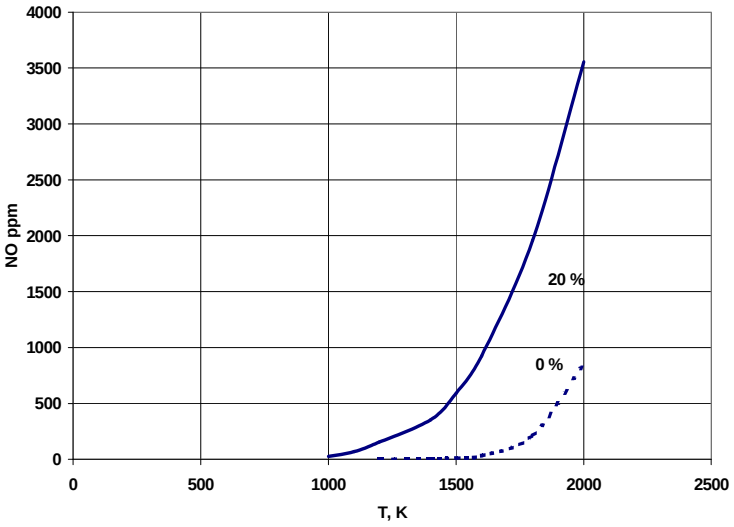

Fig. II.1. Thermal NO_x equilibrium calculation for methane for stoichiometric condition (0%) and lean mixture (20%).

In the case of coal flames, as flame temperature is normally below this threshold, the thermal NO_x formation is not very significant [7] unless you burn lean overall.

In the case of prompt NO_x, nitric oxide can be formed when hydrocarbons resulting from devolatilization process attack molecular nitrogen near the reaction zone of the flame [7].

The main reaction in this process is:

$$N_2 + CH \rightarrow HCN + N \qquad \text{(I.4)}$$

Then HCN reacts with oxygen to create NO. Prompt NO is more significant in fuel rich flames since it needs hydrocarbon to initiate the chain of NO formation [7]. Prompt NO_x is normally most significant in the case of clean fuels (that contain no nitrogen). In the case of coal combustion it is normally ignored [7].

Control of NO_x emission

The techniques to reduce NO_x emissions can be in general divided into two categories: combustion control and post combustion control. In the combustion control the parameters are optimized in order to avoid the formation of NO_x.

One such technique is to lower the flame temperature as in this way the thermal NO_x formation is directly affected. Another possible configuration is to create a fuel rich zone in the region with the maximum flame temperature: reducing the oxygen available the NO_x formation can be directly reduced. Alternatively, NO_x reduction can be achieved by lowering the residence time under oxidizing conditions. Combustion control systems such as fuel staging (rich followed by lean), reburning (lean followed by rich, followed by lean non premixed), flue gas recirculation, over-fire air and water / steam injection can provide substantial NO_x reduction. In the case of post combustion techniques, there is a dedicated clean up process that takes place after the combustion [4]. These techniques can be further divided into Selective Catalytic Reduction (SCR) and Selective Non-Catalytic Reduction (SNCR). Clearly the difference between the two is the presence or not of a catalyst. Using SCR it is possible to achieve NO_x reductions up to 90% [4]. The problem with SCR is the cost of catalysts, which have pushed the research to find new ways to gain high NO_x reduction at lower costs.

Reburning is a promising technique for NO_x reduction. In this case the furnace can be divided into three areas: main burner, reburner and burn out zone, (see Fig. II.2) [4].

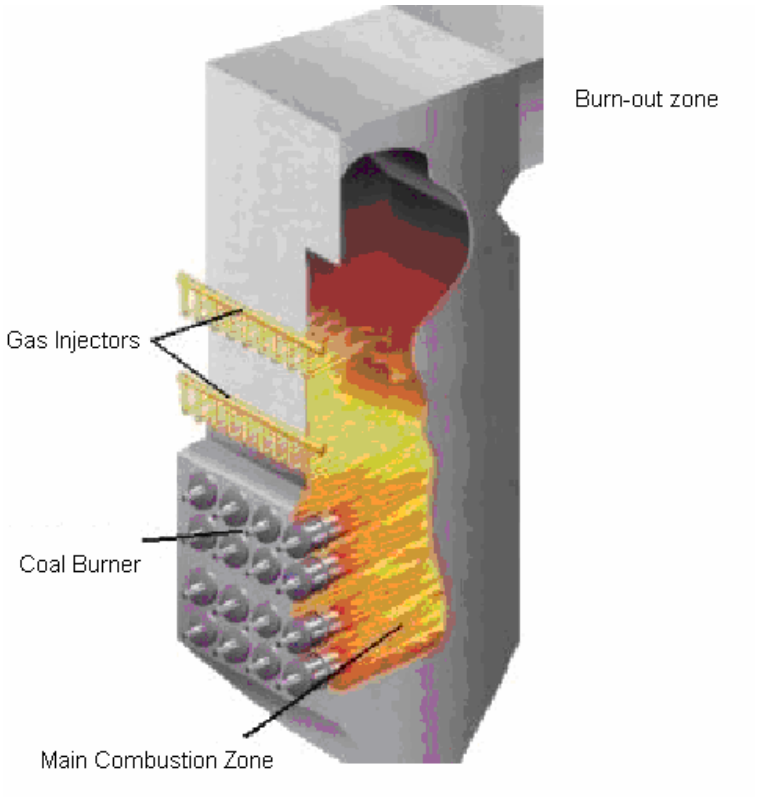

Fig. II.2. Reburner schematics.

In the main burner, the main fuel is injected along with a slight excess of air, providing most of the thermal power of the furnace. Downstream there is the reburn zone where the reburn fuel is injected in the gas stream and burned under fuel rich conditions. Here it is possible to convert a certain fraction of the NO_x generated in the primary zone into molecular nitrogen through the reverse prompt NO_x mechanism [11]. The extent of this conversion is strongly dependent on the reburn parameters such as type of reburn fuel, the stoichiometry and the mixing achieved [4, 11]. Further downstream, there is the burn out zone where more air is injected in the stream in order to oxidize the unburned hydrocarbons still present in the gas. The conditions in this zone must be optimized in order not to produce any more NO_x.

Under conventional operating conditions, and natural gas as a reburn fuel, it is reasonable to expect reductions in the order of 40 – 60% [4, 11]. This reduction is good but is still not enough to compete with SCR, therefore this kind of process needs to be optimized to gain a better NO_x reduction.

Table II.1 presents some example of the results obtained applying the reburn technology to pre existing coal fired furnace [4]. Some of these used natural gas as a reburn fuel, others coal.

Table II.1
Example of performances of reburn technology applications

Location (Retrofit Date) Boiler Type	Owner / Operator	MWe (net)	Reburn Heat %	NO_x emissions [lbm/MMBtu]		NO_x Reduction %
				Uncontrolled	Controlled	
Gas Reburning						
Hennepin (1991) Tangential	Illinois Power	71	18	0.75	0.25	67
Lakeside (1993) Cyclone	Springfield Water, Light & Power	33	23	0.97	0.39	60
Cherokee (1993) Wall	Pubblic Service of Colorado	158	18	0.73	0.27	63
Greenidge (1996) Tangential	(NY State Electric & Gas	100	10	0.5	0.25	50
Kodak Park (1995) Cyclone	Eastman Kodak	69	20	1.25	0.56	56
Kodak Park (1998) Cyclone	Eastman Kodak	50	14	1.2	0.51	58
Kodak Park (1999) Cyclone	Eastman Kodak	50	13	1.2	0.51	58
Coal Reburning						
Nelson Dewey (1991) Cyclone	Wisconsin Power & Light	100	25	0.82	0.39	52
Milliken (1997) Tangential Micronized Coal	NY State Electric & Gas	150	14	0.35	0.25	28
Kodak Park (1997) Cyclone Micronized Coal	Eastman Kodak	50	17	1.36	0.59	57

It is important to note that the reburn fuel does not have to be the same fuel used in the main burner, therefore this is one more parameter that can be studied to optimize the process.

Thermal de-NO_x is a process that relies on the injection of an N-agent (normally ammonia or urea) in the gas stream to destroy the NO_x content via a selective non catalytic reduction [12].

An evolution of the reburn process is the so called advance reburning (AR), in which besides the reburn fuel also an N-agent is injected in the furnace [11, 13-14]: this combines aspects of basic reburning with the thermal de-NO_x process which relies on the injection of an N-agent to reduce NO_x by a selective non – catalytic reduction. This process can achieve reductions up to 95% [13], therefore becoming competitive with the SCR as this reduction can be achieved at a cost which can be estimated as one third of SCR. Another advantage of the AR over the conventional reburning process is that it can work much closer to stoichiometric condition [11].

The NO reduction can be further improved adding promoter to the flue gases; the most effective promoters are normally alkalis, most notably sodium or potassium compounds. These compounds can be injected at the reburner or at the main burner of the furnace, but injection at the main burner has proved to be more effective [15].

Parameters that influence the NO_x reduction in reburner process

One of the most important parameters that influence the NO_x reduction in the reburn process is the equivalence ratio: as the mixture becomes rich there is a significant

decrease in the NO emission, as the lower concentration of oxygen does not favor its creation.

Another very important parameter is the residence time: it should not be too short (at least 0.5s typically required), in order to leave the time to the fuel to burn and to the reburn process to destroy the NO. The residence time required is a function of the fuel: natural gas requires a very short time as it can burn easily. Solid fuels require a longer time as they first have to devolatilize and to consume the char with the heterogeneous reactions. Kicherer [16] showed that as the residence time increases the results for solid fuels converge to the ones obtained with natural gas.

Also the mixing process is very important in the reburn technique, as it has relatively fast chemistry if compared to the mixing times of the reburn installations. The importance of the mixing process depends on the configuration of the burner and it is influenced by a variety of factors including the geometry of the injector and the swirl of the reburn jet. The mixing process and dispersion of the fuel is also determined by the velocity and momentum of the reburn jet [13].

The addition of alkalis to the gas flow has been reported to affect the NO reduction. This addition can be combined with the reburn process in order to maximize the reduction. Lissianski et al. [15] tested the injection of various alkalis compounds in a furnace fired with methane with a reburner fired with methane too. The reduction depended on the concentration of alkali injected; without reburner it was possible to achieve a NO reduction up to 30%, using also the reburner the reduction was up to 75%. The reduction obtained on the same facility using only the reburner, without the

injection of alkali was 65%. From this data it is clear that the effectiveness of the addition of alkali depends on the starting concentration of NO_x.

Reburning with different fuels

The most widely used fuel used in reburn process is methane [11], because it is a clean fuel as it contains no fuel bound nitrogen, sulfur or particulate matter and it reacts faster than liquid or solid fuels. Still, virtually every kind of fuel can be fired in a reburner and the strive to gain better performances and lower operating costs has pushed toward the study of different fuels. Also the increasing cost of natural gas has favored the research on different fuels. Detailed studies on the performance of NO_x reduction using different fuels has been conducted by Kicherer [16] and Maly [17] in which solid, liquid and gaseous fuels have been taken in consideration. It is important to note that the NO reduction mechanism in the case of solid fuels is different than in the case of gaseous fuels due to the presence of fuel nitrogen, the delay in the devolatilization and the presence of the heterogeneous reactions. In the case of solid fuels it has been found that also the size distribution has an effect on the NO reduction [16]: the smaller the particles, the better the NO reduction. This is not surprising as with small particles there is a more favorable area to volume ratio. Having a large area for the particles is particularly important as normally the reburn fuel is injected in a relatively cold area of the furnace; therefore the particle size is important in gaining an acceptable burn out. Hampartsoumian et al. [18] have studied the behavior of fifteen different coals as reburn fuels. These coals were very different and the proximate volatile content varied from 4% to 40%. They found a strong correlation between the effectiveness of the process and the

volatile content of the reburning fuel, with larger volatile content leading to better results. This result can be extended to all the solid fuels: the ones that perform better are the ones with a large content of volatiles (like biomass or low rank coals). High rank coal gains a NO_x reduction lower than natural gas, while low rank coal can achieve the same reduction as natural gas and Chen and Ma [19] even found a better NO reduction using lignite instead of natural gas. It is important to note that to get such good results with coal its parameters must be very well optimized, which include having a long residence time and small size particles. Wood has been tested successfully as reburn fuels gaining a reduction comparable with that of lignite.

Maly et al. [17] studied many different fuels including natural gas, coal, biomass and refused derived fuel. They found a NO reduction ranging between 44 and 50% for the various fuels using conventional reburning and a reduction ranging between 70 and 90% in the case of advanced reburning. In both cases the best performing fuel was biomass and the worst coal. The reduction could be further improved adding promoters (such as sodium compounds) to reductions ranging between 78 and 96%, also in this case the best performing fuel was biomass and the worst coal.

The use of biomass as a reburn fuel is very interesting as it has the potential to lead to results better than with other fuels. Maly [17] used refused wood as biomass. Goughnour [20] studied the potential of cattle biomass and in his experiments the NO reduction was up to 90%. Still the use of biomass can lead to problems especially regarding fouling and the handling of the fuel [20], but this depends strongly on the variety of biomass used. Also the reduction obtained depends strongly on the kind of

fuel used, as biomasses can be very different. For example Jensen et al. [21] used hog manure as reburn fuel with many technical difficulties, and hardly any effect on the NO reduction. It is important to note that such a poor result might have been influenced by the particular processing they used for the fuel.

Mercury emissions

Mercury emissions from coal power plant is a relatively new field of research, therefore there is not such an exhaustive literature, as it can be found on other forms of pollutants such as NO_x. Another problem that makes this kind of investigations more challenging than with the other types of pollutants is the fact that in this case the concentrations are in the order of parts per billion, therefore very accurate measurements are required [22].

Pavlish [5] reviewed the mercury control options for coal power plants, and he concluded that currently there is not a single best technology that can be applied broadly. It is reported that some techniques can be applied very successfully to some plants, but lead to very poor results in others.

With the technology currently installed in the power plants, on average, only around 40% of the mercury is trapped; the remaining 60% is emitted [5], but this result can vary widely according to the type of coal and the specific plant considered. Wet scrubbers can effectively trap most of the oxidized mercury but not the elemental form. Another promising technique to control the mercury emission is the use of activated carbon, which has proven to be able to trap a large fraction of mercury in high carbon fly ash [22].

Mercury is emitted in the elemental form and is partially oxidized in the gas phase (35 – 95%). Oxidation is promoted by the presence of chlorine, and it has been found that Appalachian Bituminous coals have a larger trapped fraction of mercury than Western Subbituminous coals even though they have about double the mercury than the second [23]. The reason is that Appalachian coals also have a larger content of chlorine that favors this oxidation.

It is seen from the literature review that there has not been significant effort on the modeling of the reburn process with FB as reburn fuel in order to have a deeper understanding of the NO_x and Hg reduction.

CHAPTER III

OBJECTIVE AND TASKS

The current research at the Coal and Biomass Energy Laboratory at Texas A&M University concentrates on the use of cattle biomass (CB), to be used as pure fuel or as cofired fuel with coal, and finally as a reburn fuel, as it has the potential to be a very cost effective method for reducing NO_x emissions from power plants near cattle feedlots. In previous experimental studies, it has already been shown that a much larger reduction is achieved when compared to coal as a reburn fuel. Besides, the use of biomass might lead to a larger amount of oxidized mercury, a development that would be very beneficial, as this form of mercury can be easily trapped with conventional technologies. The use of biomass, a renewable fuel, would be also beneficial as this is considered a CO_2 free fuel: the combustion of biomass does not add any CO_2 in the atmosphere as the CO_2 is used in the photosynthesis process.

The overall objective of this study is to develop a zero dimensional model that can predict the reburn performance of coal, feedlot biomass (FB) and their blends. In order to achieve the overall objective the following tasks are performed:

1. Development of a simplified model for mixing of reburn gas stream with main gas.
2. Inclusion of nitrogen and mercury release model.
3. Incorporation of the heterogeneous and homogeneous global reaction kinetics.
4. Accounting for the particle size distribution.
5. Prediction the NO_x and Hg emissions control performance.
6. Parametric studies on NO_x optimization and mercury capture.

CHAPTER IV

MODELING

Chapter introduction

This chapter presents the details of the model that has been developed in this work. The reference furnace that has been used is described. A general overview of the whole process is presented and all the assumptions made are stated. Then, all the parts of the model are individually presented, starting from the main burner model, to the reburn model, which includes the mixing model, the reactions modeling, the particle devolatilization modeling, the mass and energy conservation equations and finally the mercury modeling.

The experimental reburn facility is a laboratory-scale, down-fired furnace, providing a rated throughput of 100,000 Btu/hr (29.3 kW), based on the higher heating value (HHV) of the fuel. This facility is used for testing the potential for NO_x reduction of various solid fuels. Fig. IV.1 shows a schematics of the facility.

The main burner fires natural gas, with excess of air. Also a certain amount of ammonia is sprayed in the flame in order to generate a significant amount of NO_x in the exhaust leaving the main burner, as done in Zamansky [24] and Yang [25]. Downstream, the product gases, along with NO, enter the reburn zone (RZ). Here the reburn fuel is injected in the furnace along with carrier gas. The local stoichiometry in the RZ can be varied to study its effects on the performances. The facility is equipped with extensive diagnostics to keep track of the temperature along the furnace and to measure the gas composition at the exit of the furnace.

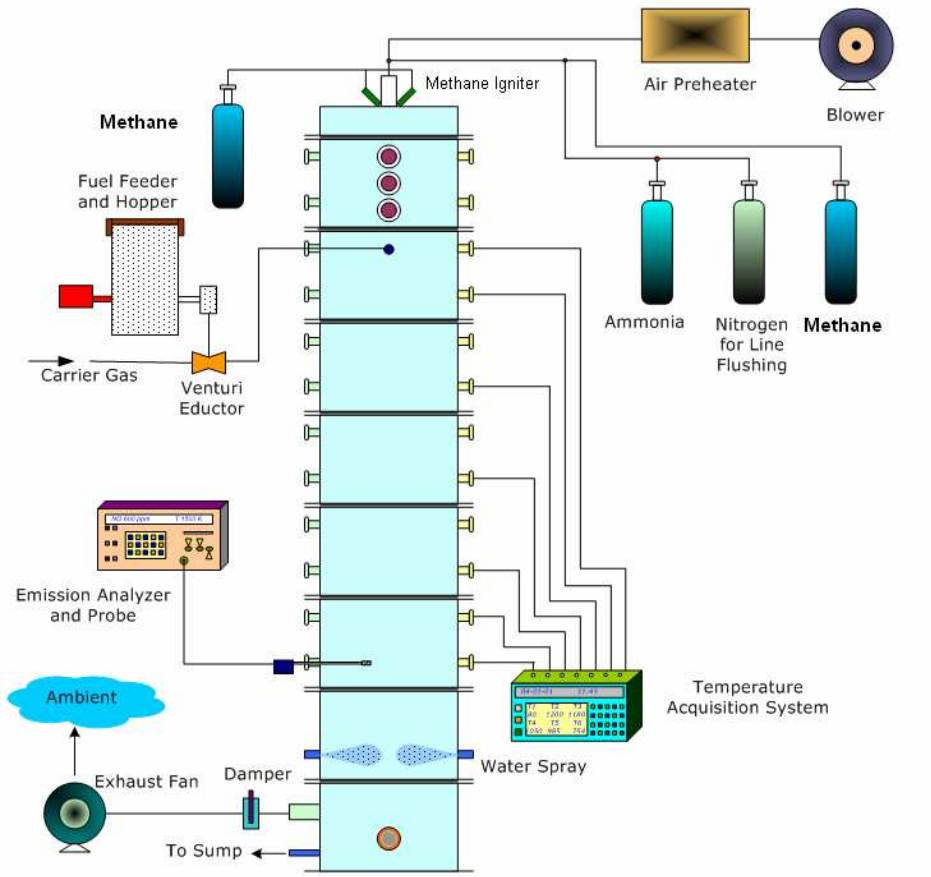

Fig. IV.1. Facility schematics.

A more detailed description of the facility can be found in Goughnour [20] and Arumugam [26].

General outline of the reburn model

Once the main burner and reburner thermal and heat input are fixed, it is possible to compute the mass flow of the main burner fuel as its heating value is known. The products of ammonia oxidation are assumed to be water and NO. Products from the main burner are computed assuming complete combustion. As shown in Fig. IV.2, the hot

gases, containing NO, then gradually mix with the reburn carrier gas (the gas injected along with the reburn fuel), which contains the reburn fuel.

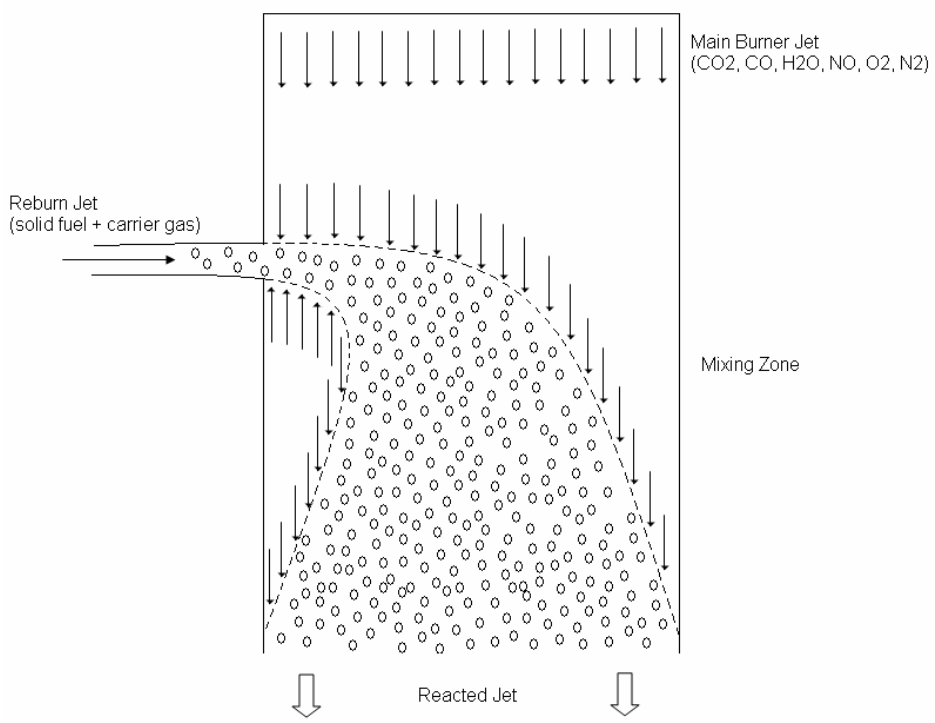

Fig. IV.2. Schematics of the reburner zone.

During the mixing with the hot gases, the reburn gases are heated up which in turn heat the solid particles. The particles release the volatiles and the fuel bound nitrogen, which undergoes homogeneous reactions. Simultaneously there is the combustion of the remaining fixed carbon and the heterogeneous reaction of nitrogen retained in the particles.

Fig. IV.3 depicts the heat and mass transfer process and reactions of a solid particle.

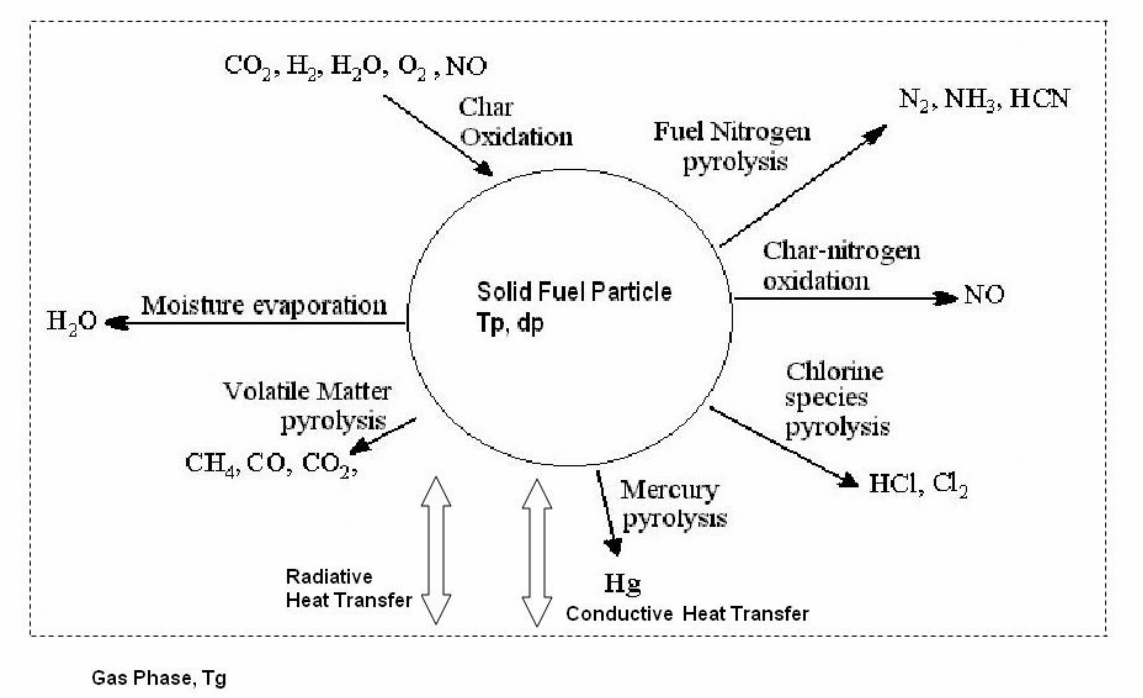

Fig. IV.3. Solid fuel particle: heat and mass transfer processes and chemical reactions.

Volatiles originating from the pyrolysis process are composed of many different species; normally the important species are CO, CO_2 and CH_4 [27, 28], especially under the very fast heating that takes place in the burners.

The species coming from the fuel bound nitrogen (FN) pyrolysis are normally HCN, N_2 and NH_3 [8, 9]. The pyrolysis of FN is a process that is still not completely understood yet. The models for evolution of N are as follows: i) finite kinetics [29] and ii) the emission of FN as proportional to the release of the volatiles [30]. Both these methods are discussed in the section on model description.

The reactions include four homogeneous reactions involving NO, three homogeneous reactions for the oxidation of CO, H_2 and CH_4, six heterogeneous

reactions involving solid carbon and one heterogeneous reaction involving solid nitrogen.

The gas phase mercury reactions are described by a two step reaction.

The code based on the model uses the following inputs:

Input to the code:

- Main burner heat input, fuel characteristics (including ultimate analysis, fuel N and chemical formula), excess air, inlet temperature of fuel and air and initial NO_x
- Reburner thermal heat input, proximate and ultimate analysis of the reburn fuels, size distribution, density, specific heat and heating value, inlet temperature and composition of the carrier gas, heterogeneous and homogeneous kinetics parameters, FN products composition and equivalence ratio in the reburn area
- Hg and Cl concentration in fuel

Output of the code:

- Temperature (T) versus time (t) for the reburn gas and for each particle diameter (d_p)
- Composition (Y_k) of the gas phase in the free stream and at the particle surface
- Mass (m_p), fixed carbon mass (FC), diameter (d_p) and density (ρ_p) of each class of particles
- Volatile matter (VM), rate of liberation of FN and elements left in the char
- The concentration of NO versus time
- Hg evolution and history of Hg oxidation

The gaseous species tracked are: CH_4, CO, CO_2, H_2, HCN, H_2O, N_2, NH_3, NO, and O_2. All the species are tracked on the total mass basis and at each temporal step, the molar and mass concentration of the gas are computed knowing the total mass of each species. Events are tracked using a Lagrangian frame of reference; this means that the observer travels with the gas from the reburner, and the mass tracked increases as the flow from the main burner mixes with the flow from the reburner, and the composition of the different species changes according to the various reactions taking place. For the mercury reactions, the extra species tracked are: Cl, Cl_2, HCl, Hg, HgCl, $HgCl_2$, OH.

At each temporal step the mass flow from the reburner is considered perfectly stirred, which means that the products coming from the main burner and from the particles are assumed to mix instantaneously with the main stream.

The choice of setting the observer as traveling with the reburn gases is called inverse mixing approach; alternatively it would have been possible to set the observer traveling with the main burner products: in this case it would have seen the flow increasing due to the mixing of the reburner gases. The choice of the inverse mixing approach depends on the fact that it was reported that this approach gives a more realistic description of the experimental data than the regular mixing [31, 32]. In the model, energy conservation is used to solve for local temperature of gas stream. Assuming all the different gases to be ideal, the enthalpy function is a non linear function of the temperature alone. Knowing the value of the enthalpy at some temperatures it is possible to set up enthalpy functions that interpolate the value of the

enthalpy between the successive intervals, once the temperature of the gas species is specified. The values used are from Annamalai et al. [10].

Assumptions

The assumptions are summarized as follows:

Main burner:

- Ammonia decomposes to water and NO
- NO in the main burner is generated only by the decomposition of ammonia. No thermal NO and fuel NO are considered
- Oxidation of Ammonia is complete
- The combustion at the main burner is complete and no dissociation is considered among its products

Reburner:

- The mixing between the reburner gases and the main burner gases is described by an exponential model

Gas phase:

- All the gases are treated as ideal gases
- The species are constantly perfectly mixed

Chemical reactions:

- All the reactions are described by simplified kinetics (except for mercury).

Solid fuels:

- Ash is evenly distributed in all particle sizes
- Ash is inert

- Moisture evaporates instantaneously as the fuel is injected in the furnace
- All oxygen or hydrogen atoms are released with volatiles
- Composition of volatiles and FN pyrolysis is constant throughout the process
- Chemical kinetics are independent of the particle size
- Particles are spheres
- In case detailed kinetics are not available for biomass, lignite kinetics are valid for biomass
- Temperature at the particle surface is the same as at the particle core
- Volatiles emission is described by a single reaction kinetics
- FN emission is either proportional to the volatiles emission or it can be described by a single reaction kinetics
- Gases coming from the particle mix instantaneously with the free stream of gas at each temporal step

Energy conservation:

- Energy transfer is at quasi steady state
- Gas mixing processes are isenthalpic
- Gases emitted from the particle surface are at the particle temperature
- Combustion of char occurs at constant density while pyrolysis occurs volumetrically (varying density) at constant diameter
- The boundary layer around the particle is at the particle temperature

Mercury:

- Mercury and chlorine are emitted along with pyrolysis gases

- Mercury is emitted in elemental form
- Mercury oxidation in the gas phase is described by a two step reaction
- All the Hg compounds are in trace amounts
- OH comes only from the dissociation of water and it is constantly at equilibrium concentration

General:

- The interior of the furnace is at atmospheric pressure

Main burner modeling

The main burner fuel is assumed to be represented by the formula $CH_xO_yN_z$ which is burned along with some NH_3 to simulate the desired amount of NO. The amount of ammonia to be fired with the fuel is adjusted in order to achieve the desired amount of NO.

The solution for complete combustion of a general fuel is:

$$CH_xO_yN_z + w\cdot NH_3 + \left(1+\frac{a}{100}\right)\cdot\left(1+\frac{x}{4}-\frac{y}{2}\right)\cdot\left(O_2+3.76\cdot N_2\right)\rightarrow CO_2+\left(\frac{x}{2}+\frac{3\cdot w}{2}\right)\cdot H_2O+ \\ +\left(\frac{a}{100}\cdot\left(1+\frac{x}{4}-\frac{y}{2}\right)-\frac{5\cdot w}{4}\right)\cdot O_2+w\cdot NO+\left[\frac{z}{2}+3.76\cdot\left(1+\frac{a}{100}\right)\cdot\left(1+\frac{x}{4}-\frac{y}{2}\right)\right]\cdot N_2 \quad \text{(IV.1)}$$

where *a* is the percentage excess of air based on the main burner fuel only.

This formula has been obtained with the atom balance of the species of the products and reactants. With this formula, it is possible to know the composition of the gas leaving the main burner zone. No dissociation has been taken in account. The excess air is fixed at 5%, therefore *a* is known.

In the experiments, the NO_x local concentration at the exit of the main burner has been fixed at 400 ppm dry basis, which is a typical value used in reburn experiments [24, 25, 33] in which the reburn fuel is injected in a gas stream that contains a significant amount of NO. In the configuration of Goughnour [20], the main burner fuel is burned with 5% excess air. So the initial NO_x can be also expressed as 391 ppm (at 3% excess oxygen), or 0.43 lbm/MMBtu. This will be the reference, the starting condition to evaluate the effectiveness of the reburn process with the various fuels and conditions.

Therefore, on dry basis:

$$X_{NOx} = 400 \cdot 10^{-6} = \frac{w}{1 + \left(\frac{a}{100} \cdot \left(1 + \frac{x}{4} - \frac{y}{2} \right) - \frac{5 \cdot w}{4} \right) + w + \left[\frac{z}{2} + 3.76 \cdot \left(1 + \frac{a}{100} \right) \cdot \left(1 + \frac{x}{4} - \frac{y}{2} \right) \right]} \quad \text{(IV.2)}$$

thus it is possible to compute *w* since *a* is known.

Now the amount of air and ammonia to be injected in the main burner fuel can be calculated and also the composition of the products coming from the main burner is known. In the experiments by Goughnour [20], the main burner fuel is natural gas which consists of over 95% of CH_4.

Table IV.1
Natural gas composition

Constituent	MOL %
Methane	95.32
Ethane	1.79
Carbon Dioxide	1.69
Nitrogen	0.41
Propane	0.4
Other	0.39

Therefore the main burner fuel can be approximated to be methane. In this case, there will be a complete combustion; besides the temperatures in the experiments are always below 1600K, therefore the NO at the exit of the main burner is generated mainly by ammonia. Even if there was some thermal NO_x, this would not have much effect on the overall model as simply less ammonia would be injected in the main burner; still the most important issue is simply to have a constant concentration of NO coming from the main burner.

As the thermal power coming from the main burner is fixed (70% of the total thermal power of the facility), it is possible to compute the mass flow of the main burner fuel:

$$\dot{m}_{fuel\,MB} = \frac{Thermal\ Rating_{MB}}{HHV_{fuel\,MB}} \quad \left[\frac{kg}{s}\right] \tag{IV.3}$$

Therefore the firing rate of ammonia is given by:

$$\dot{m}_{ammonia} = \frac{\dot{m}_{fuel\,MB} \cdot w \cdot M_{ammonia}}{M_{fuel}} \left[\frac{kg}{s}\right] \tag{IV.4}$$

The components of the various species from the main burner are represented in vector form as:

$$\dot{m}_{MB} = \frac{\dot{m}_{fuel,MB}}{M_{fuel,MB}} \cdot \begin{Bmatrix} 0 \\ 0 \\ 1 \cdot M_{CO_2} \\ 0 \\ 0 \\ \left(\frac{x}{2} + \frac{3 \cdot w}{2}\right) \cdot M_{H_2O} \\ \left[\frac{z}{2} + 3.76 \cdot \left(1 + \frac{a}{100}\right) \cdot \left(1 + \frac{x}{4} - \frac{y}{2}\right)\right] \cdot M_{N_2} \\ 0 \\ w \cdot M_{NO} \\ \left(\frac{a}{100} \cdot \left(1 + \frac{x}{4} - \frac{y}{2}\right) - \frac{5 \cdot w}{4}\right) \cdot M_{O_2} \end{Bmatrix} = \begin{Bmatrix} \dot{m}_{CH_4} \\ \dot{m}_{CO} \\ \dot{m}_{CO_2} \\ \dot{m}_{H_2} \\ \dot{m}_{HCN} \\ \dot{m}_{H_2O} \\ \dot{m}_{N_2} \\ \dot{m}_{NH_3} \\ \dot{m}_{NO} \\ \dot{m}_{O_2} \end{Bmatrix} \qquad \left[\frac{kg}{s}\right] \quad \text{(IV.5)}$$

The temperature of the gases leaving the main burner zone can be computed by applying the energy conservation equation between the products and the reactants and considering a fraction of heat to be lost, proportional to the heating value of the main burner fuel.

$$\dot{H}_{in,MB} = \dot{H}_{out,MB} + \dot{Q}_{lost} \quad \text{(IV.6)}$$

where the total enthalpy H is rate per unit time.

$$\frac{\dot{H}_{in,MB}}{\dot{m}_{fuel}} = h_{f,fuel} + h_{t,fuel} + \frac{\dot{m}_{NH3}}{\dot{m}_{fuel}} \cdot \left(h_{f,NH3} + h_{t,NH3}\right) + \frac{\dot{m}_{air,MB}}{\dot{m}_{fuel}} \cdot h_{t,air} \qquad \left[\frac{kJ}{kg_{MB,fuel}}\right] \quad \text{(IV.7)}$$

and

$$H_{out,MB} = \sum_{i=1}^{N\,species} \frac{\dot{m}_i}{\dot{m}_{fuel}} \cdot \left(h_{f,i} + h_{t,i}\right) \qquad \left[\frac{kJ}{kg_{MB,fuel}}\right] \quad \text{(IV.8)}$$

The enthalpies of formation are fixed while the thermal enthalpies are non-linear functions of the products' temperature; therefore this equation needs to be solved in implicit form. The enthalpy of formation of the fuel is computed from its heating value and considering its complete combustion with air:

$$h_{f,fuel} = \frac{\bar{h}_{f,CO2} + x/2 \cdot \bar{h}_{f,H2O}}{MW_{fuel}} + HV_{MB} \quad \left[\frac{kJ}{kg_{MB,fuel}}\right] \tag{IV.9}$$

The Heating Value of the fuel is directly measured on the various fuels used in this work.

It is difficult to quantify the heat loss in the main burner; if the temperature of the products of combustion of the main burner fuel is known, it is possible to specify it directly: this is the case used in this study, the previous case has been taken in consideration in order to make the model more general and usable also in case the temperature was not known.

The total mass leaving the main burner is the sum of the mass flow of ammonia, air and fuel supplied. The composition of the products is known, so also the mass flow rate of every species is known. The main burner is operated at the same conditions for all the different reburn conditions taken in consideration, so also the products flow from the main burner are the same for all the conditions.

Reburner modeling

Also the reburn fuel is known in the generic form of $CH_{x1}O_{y1}N_{z1}$. The reburn fuel is assumed to be a solid fuel, therefore it is necessary to model the release of

volatiles and FN and the heterogeneous reactions at the particle surface. In the case of blends there are two different solid fuels, each one with its formula and chemical composition. The chemical formula is obtained from the ultimate analysis (dry ash free), normalizing the carbon atom content to one; the ultimate analysis gives the mass based composition of the fuel; so using the molar weight of each element it is possible to get the empirical formula:

$$\begin{array}{lll} C: & c'_1 = \dfrac{C_{\%}}{M_C} & c_1 = \dfrac{c'_1}{c'_1} = 1 \\ H: & x'_1 = \dfrac{H_{\%}}{M_H} \quad \textit{normalizing} & x_1 = \dfrac{x'_1}{c'_1} \\ O: & y'_1 = \dfrac{O_{\%}}{M_O} & y_1 = \dfrac{y'_1}{c'_1} \\ N: & z'_1 = \dfrac{N_{\%}}{M_N} & z_1 = \dfrac{z'_1}{c'_1} \end{array} \qquad \text{(IV.10)}$$

Fuel pyrolysis is described by a finite kinetics [27, 34] and it depends on the type of fuel. The composition of the pyrolysis gas is considered to be constant throughout the pyrolysis process. The composition of the pyrolysis gas is determined using the atom conservation and the data from the proximate analysis which specifies the fraction of volatiles and fixed carbon in the fuel, and assuming that no oxygen or hydrogen is left in the particle after the pyrolysis [35] see equation IV.11. The composition of the FN gas stream is assumed from the literature [8, 33].

$$CH_{x1}O_{y1}N_{z1} \rightarrow a \cdot C(s) + b \cdot CO + c \cdot CO_2 + d \cdot CH_4 + e \cdot HCN + f \cdot NH_3 + g \cdot N_2$$

$$\begin{cases} C: & 1 = a + b + c + d + e \\ H: & x_1 = 4 \cdot d + e + 3 \cdot f \\ O: & y_1 = b + 2 \cdot c + 4 \cdot d + e + 3 \cdot f \\ N: & z_1 = e + f + 2 \cdot g \\ FC: & FC = \dfrac{a \cdot M_C}{M_{fuel\,RB}} \\ FN: & NH_{3\,frac} = \dfrac{f \cdot M_{NH3}}{e \cdot M_{HCN} + f \cdot M_{NH3} + g \cdot M_{N2}} \\ FN: & HCN_{frac} = \dfrac{e \cdot M_{HCN}}{e \cdot M_{HCN} + f \cdot M_{NH3} + g \cdot M_{N2}} \end{cases} \quad \text{(IV.11)}$$

In case of fuel blends this system has to be solved for the two fuels separately; from here it is possible to compute the compositions of the pyrolysis gases:

$$\dot{m}_{pyro\_vect} = \dot{m}_{pyro} \cdot \overline{Y} = \dot{m}_{pyro} \cdot \begin{Bmatrix} Y_{CH_4} \\ Y_{CO} \\ Y_{CO_2} \\ Y_{H_2} \\ Y_{HCN} \\ Y_{H_2O} \\ Y_{N_2} \\ Y_{NH_3} \\ Y_{NO} \\ Y_{O_2} \end{Bmatrix} = \dot{m}_{pyro} \cdot \begin{Bmatrix} \dfrac{d \cdot M_{CH_4}}{b \cdot M_{CO} + c \cdot M_{CO_2} + d \cdot M_{CH_4}} \\ \dfrac{b \cdot M_{CO}}{b \cdot M_{CO} + c \cdot M_{CO_2} + d \cdot M_{CH_4}} \\ \dfrac{c \cdot M_{CO_2}}{b \cdot M_{CO} + c \cdot M_{CO_2} + d \cdot M_{CH_4}} \\ 0 \\ 0 \\ 0 \\ 0 \\ 0 \\ 0 \end{Bmatrix} \left[\frac{kg}{s}\right] \quad \text{(IV.12)}$$

The mass flow rate of the reburn fuel is computed knowing the heat input of the reburner and the heating value of the fuel. For the general case of a blend, defining Y_{coal} and Y_{FB} as the mass fractions of the two fuels,

$$\dot{m}_{fuel\,RZ} = \frac{Thermal\ Power_{RZ}}{HV_{fuel\,FB} \cdot Y_{FB} + HV_{fuel\,coal} \cdot Y_{coal}} \qquad \left[\frac{kg_{fuel}}{s}\right] \qquad \text{(IV.13)}$$

$$\dot{m}_{FB} = \dot{m}_{fuel\,RZ} \cdot Y_{FB} \qquad \left[\frac{kg_{FB}}{s}\right] \qquad \text{(IV.14)}$$

$$\dot{m}_{coal} = \dot{m}_{fuel\,RZ} \cdot Y_{coal} \qquad \left[\frac{kg_{coal}}{s}\right] \qquad \text{(IV.15)}$$

Where $Y_{FB} = 1 - Y_{coal}$.

Note that in the experiments by Goughnour [20], it has been assumed that the fractions of fuel represent mass fractions. The mass flow rate of the air at the reburner is computed as the reburn zone (RZ) equivalence ratio (Φ_{RZ}) is specified.

Let ν_{O2} be the stoichiometric oxygen to fuel ratio (mass basis) for a generic fuel $CH_{x1}O_{y1}N_{z1}$:

$$\nu_{O2} = \left(1 + \frac{x_1}{4} - \frac{y_1}{2}\right) \cdot \frac{MW_{O2}}{MW_{fuel}} \qquad \text{(IV.16)}$$

The reburn zone equivalence ratio is defined as:

$$\Phi_{RZ} = \frac{\dot{m}_{O2,stoi}}{\dot{m}_{O2}} = \frac{\dot{m}_{coal,DAF} \cdot \nu_{O2,coal} + \dot{m}_{FB,DAF} \cdot \nu_{O2,FB}}{\dot{m}_{O2,MB} + \dot{m}_{O2,RB}} \qquad \text{(IV.17)}$$

$RB: reburner$

Where $\dot{m}_{O2,MB}$ is the flow of oxygen coming from the main burner: as the combustion in the main burner is with excess air, there is some oxygen left in its exhaust; solving for the required $\dot{m}_{O2,RB}$ supplied with the reburn fuel in order to achieve Φ_{RZ}, the oxygen flow rate results:

$$\dot{m}_{O2,RB} = \frac{\dot{m}_{coal,DAF} \cdot \nu_{O2,coal} + \dot{m}_{FB,DAF} \cdot \nu_{O2,FB}}{\Phi_{RZ}} - \dot{m}_{O2,MB} \qquad \left[\frac{kg_{O2}}{s}\right] \qquad \text{(IV.18)}$$

Knowing the mass percentage of oxygen in the carrier gas at the reburner (which may be different from the atmospheric), it is possible to compute the mass flow rate of carrier gas that needs to be injected with the reburn fuel:

$$\dot{m}_{carrier\ gas,RB} = \frac{\dot{m}_{O2,RZ}}{Y_{O2}} \qquad \left[\frac{kg_{RB,carrier\ gas}}{s}\right] \qquad \text{(IV.19)}$$

The composition of the carrier gas could be different from pure air as it may be diluted with nitrogen in order to simulate the use of recirculation gases to test its effects on the NO_x reduction. In the case of vitiated air the oxygen content of the air is 12.5% (volume basis) [20].

The solid fuels are characterized by a size distribution. The size distribution has been measured at the Coal and Biomass Energy Laboratory, Texas A&M University, for each fuel used by Goughnour [20]. See data in Chapter V. Each class is defined with its range of diameters. For the purpose of the modeling, each class is described with its mean diameter. For all the fuels there are 5 particle size groups. See Chapter V for details. All the properties (ultimate and proximate analysis) and kinetics of the solid fuels are assumed to be independent of the particle size.

The diameter of the various particles varies over time, because of the char consumption: as the fixed carbon is being oxidized the diameter of the particles shrinks; therefore the observer traveling with the particles sees the mean diameter of the class reducing over time.

Let the mass percentage for each class of the size distribution be Y_j. If five size classes are taken in consideration, then:

$$Total\ initial\ mass = \begin{Bmatrix} Y_1 \\ Y_2 \\ Y_3 \\ Y_4 \\ Y_5 \end{Bmatrix} \cdot \dot{m}_{fuelRZ} \qquad \left[\frac{kg}{s}\right] \tag{IV.20}$$

Similarly:

$$Initial VM = \begin{Bmatrix} Y_1 \\ Y_2 \\ Y_3 \\ Y_4 \\ Y_5 \end{Bmatrix} \cdot \dot{m}_{fuelRZ} \cdot VM \qquad \left[\frac{kg}{s}\right] \tag{IV.21}$$

$$Initial\ FC = \begin{Bmatrix} Y_1 \\ Y_2 \\ Y_3 \\ Y_4 \\ Y_5 \end{Bmatrix} \cdot \dot{m}_{fuelRZ} \cdot FC \qquad \left[\frac{kg}{s}\right] \tag{IV.22}$$

Where VM represents the volatile fraction of the fuel and FC represents the fixed carbon fraction. It is important to split all the components of the fuel in different classes according to the size distribution, as the behavior of the fuel during the combustion changes according to the size class taken under consideration, principally because the temperature profiles along the furnace are different for different particle sizes.

Assuming the particles to be spherical and calling d_j the mean diameter of class j, it is possible to compute the number of particles in each class:

$$n_{particles\ j} = \frac{Y_j \cdot \dot{m}_{fuelRZ}}{\frac{\pi}{6} \cdot d_j^3 \cdot \rho_{fuel}} \quad \text{(IV.23)}$$

Also this is computed for each size class of fuel injected in the reburner. At each temporal step, the total mass of each species in reburn gas mixture is known as:

$$Total\ mass\ originating\ \ from\ reburner = \begin{Bmatrix} m_{CH_4} \\ m_{CO} \\ m_{CO_2} \\ m_{H_2} \\ m_{HCN} \\ m_{H_2O} \\ m_{N_2} \\ m_{NH_3} \\ m_{NO} \\ m_{O_2} \end{Bmatrix} \quad \text{(IV.24)}$$

The mass and molar fractions and molar concentration at each temporal step are computed using:

$$Mass\ Fraction_i = Y_i = \frac{Mass\ of\ \ species_i}{\sum_{i=1}^{i=n\ species} Mass\ of\ \ species_i} \quad \text{(IV.25)}$$

$$Mole\ Fraction_i = X_i = \frac{\frac{Mass\ of\ \ species_i}{M_i}}{\sum_{i=1}^{i=n\ species} \frac{Mass\ of\ \ species_i}{M_i}} \quad \text{(IV.26)}$$

$$Molar\ Concentration_i = [\ \ ]_i = \frac{\frac{Mass\ of\ \ species_i}{M_i}}{\left(\sum_{i=1}^{i=n\ species} \frac{Mass\ of\ \ species_i}{M_i} \right) \cdot \frac{R \cdot T_g}{p}} \quad \left[\frac{kmol}{m^3} \right] \quad \text{(IV.27)}$$

$$Total\ Mass\ of\ Gas\ Phase = \sum_{i=1}^{i=n\,species} Mass\ of\ species_i \qquad [kg] \tag{IV.28}$$

$$Total\ Moles\ of\ Gas\ Phase = \sum_{i=1}^{i=n\,species} \frac{Mass\ of\ species_i}{M_i} \qquad [kmol] \tag{IV.29}$$

$$Molecular\ Weight\ of\ Mixture = \sum_{i=1}^{i=n\,species} X_i \cdot M_i \qquad \left[\frac{kg}{kmol}\right] \tag{IV.30}$$

The mass of each species varies over time as some species are produced and others are consumed; therefore the data of the masses of the gas phase is stored in a matrix, in which the rows correspond to the species *i* and the columns correspond to a certain temporal step *t*.

$$Time = \{\ 0 \ldots\ldots t \ldots\ldots t_{fin}\ \}$$

$$Total\ mass = \left\{ \begin{bmatrix} m_{CH_4} \\ m_{CO} \\ m_{CO_2} \\ m_{H_2} \\ m_{HCN} \\ m_{H_2O} \\ m_{N_2} \\ m_{NH_3} \\ m_{NO} \\ m_{O_2} \end{bmatrix} \ldots\ldots \begin{bmatrix} m_{CH_4} \\ m_{CO} \\ m_{CO_2} \\ m_{H_2} \\ m_{HCN} \\ m_{H_2O} \\ m_{N_2} \\ m_{NH_3} \\ m_{NO} \\ m_{O_2} \end{bmatrix} \ldots\ldots \begin{bmatrix} m_{CH_4} \\ m_{CO} \\ m_{CO_2} \\ m_{H_2} \\ m_{HCN} \\ m_{H_2O} \\ m_{N_2} \\ m_{NH_3} \\ m_{NO} \\ m_{O_2} \end{bmatrix} \right\} \tag{IV.31}$$

The same kind of matrix is built with the data regarding the fixed carbon and volatile matter over time. In this case there are two separate matrices for the two fuels (if using a blend) and the different rows indicate different particle sizes.

$$Time = \{\ 0 \ldots\ldots t \ldots\ldots t_{fin}\ \}$$

$$Volatiles\ fuel_1 = \left\{ \begin{Bmatrix} VM_1 \\ VM_2 \\ VM_3 \\ VM_4 \\ VM_5 \end{Bmatrix} \ldots\ldots \begin{Bmatrix} VM_1 \\ VM_2 \\ VM_3 \\ VM_4 \\ VM_5 \end{Bmatrix} \ldots\ldots \begin{Bmatrix} VM_1 \\ VM_2 \\ VM_3 \\ VM_4 \\ VM_5 \end{Bmatrix} \right\} \quad \text{(IV.32)}$$

And

$$Time = \{\ 0 \ldots\ldots t \ldots\ldots t_{fin}\ \}$$

$$Fixed\ Carbon_1 = \left\{ \begin{Bmatrix} FC_1 \\ FC_2 \\ FC_3 \\ FC_4 \\ FC_5 \end{Bmatrix} \ldots\ldots \begin{Bmatrix} FC_1 \\ FC_2 \\ FC_3 \\ FC_4 \\ FC_5 \end{Bmatrix} \ldots\ldots \begin{Bmatrix} FC_1 \\ FC_2 \\ FC_3 \\ FC_4 \\ FC_5 \end{Bmatrix} \right\} \quad \text{(IV.33)}$$

For Hg the mass vector which includes the elements is given as:

$$Total\ mass\ for\ Hg\ reaction = \begin{Bmatrix} m_{Cl} \\ m_{Cl_2} \\ m_{HCl} \\ m_{Hg} \\ m_{HgCl} \\ m_{HgCl_2} \\ m_{OH} \end{Bmatrix} \quad \text{(IV.34)}$$

Also for the mercury, there is a need to split the mercury and chlorine content between the different fuels and track the content of every fuel with time.

Mixing model

The mixing of the reburner gases with the main burner exhaust is a very important part of the reburn process; therefore it must be modeled carefully. Assuming

the mixing to be instantaneous is far from reality, as this process takes time to be completed; besides, previous work [32] has shown that the assumption of instantaneous mixing is a bad depiction of reality and leads to poor results. In this case the mixing of the reburner gases with the main burner gas is described using an exponential model [31, 36]; an alternative finite mixing model would be the linear mixing, as used [32]. More in details, an inverse mixing model (main burner gases into reburner gases: which means setting the observer traveling with the reburn gases) is used as it has been shown [32] that it leads to better results than direct mixing (reburner gases into main burner gases).

With respect to an observer traveling with the reburn mass, the total mass will be composed of the reburn mass and a fraction of the main burner mass that is added gradually over time, and will approach a total mass equal to the sum of reburn mass and main burner gases.

Considering exponential mixing model, the mass flow in the reburn zone due to mixing with main burner gases is:

$$\dot{m}_{RZ,t} = \dot{m}_{RZ,t=0} + \dot{m}_{prod,MB} \cdot \left(1 - \exp\left(-\frac{t}{\tau_{mix}}\right)\right) \qquad \left[\frac{kg}{s}\right] \qquad \text{(IV.35)}$$

Eq. IV.35 satisfies the initial ($t \to 0$) and final ($t \to \infty$) condition. The mixing time τ_{mix} depends on the geometry of the furnace and the reburn gases velocity. It is estimated from experimental data for the furnace and reburn injection configuration used for the experiment. τ_{mix} is estimated to be around 40ms, [20]. In the discussion of the results from the simulation, it is shown that reasonable variations of this constant will not affect

significantly the NO_x reduction, which is the most important parameter of this simulation and, most importantly, will hardly change the qualitative trend.

This is in agreement with what found by Lissianski [32]: the value of the mixing time is most critical at small values (close to the transition between instantaneous mixing and finite – rate addition of reagents); at higher values of τ_{mix}, its variations affect less the NO reduction. From equation IV.35, it is clear that as *t* increases the total mass seen by the observer increases.

The elemental amount of mass coming from the main burner that will be added over a period of time dt is given as:

$$dm_{MB} = \frac{\dot{m}_{prod,MB}}{\tau_{mix}} \cdot \exp\left(-\frac{t}{\tau_{mix}}\right) \cdot dt \qquad \text{(IV.36)}$$

The term dm_{MB} is a vector and contains the contribution of every gas species, and as well as contributes thermal energy to RB gases; the elemental mass dm decreases as time progresses as less and less mass is left to be mixed.

Since the composition of the gas coming from the main burner is known, it is possible to determine the quantity of each species at each temporal step of integration (considering only the contribution from the mixing process).

$$\dot{m}_{RZ,t+1} = \dot{m}_{RZ,t} + d\dot{m}_{MB,t} = \begin{Bmatrix} \dot{m}_{CH_4} \\ \dot{m}_{CO} \\ \dot{m}_{CO_2} \\ \dot{m}_{H_2} \\ \dot{m}_{HCN} \\ \dot{m}_{H_2O} \\ \dot{m}_{N_2} \\ \dot{m}_{NH_3} \\ \dot{m}_{NO} \\ \dot{m}_{O_2} \end{Bmatrix}_{RZ,t} + \frac{\exp\left(-\frac{t}{\tau_{mix}}\right)}{\tau_{mix}} \cdot \begin{Bmatrix} \dot{m}_{CH_4} \\ \dot{m}_{CO} \\ \dot{m}_{CO_2} \\ \dot{m}_{H_2} \\ \dot{m}_{HCN} \\ \dot{m}_{H_2O} \\ \dot{m}_{N_2} \\ \dot{m}_{NH_3} \\ \dot{m}_{NO} \\ \dot{m}_{O_2} \end{Bmatrix}_{MB} \cdot dt \quad \text{(IV.37)}$$

Chemical reactions

In order to reduce the computational effort, a simplified kinetics model has been adopted. The homogeneous reactions are the reactions that take place in the gas phase; for these reactions the species concentrations are directly computed knowing the composition of the gas phase stream.

NO reactions

A widely used model, for reduced NO reactions in the reburn process, is the one formulated by De Soete [37]. However, the simulations based on his kinetics have brought unsatisfactory results, especially with pure biomass or a blended fuel with a high content of biomass. It is speculated that the kinetics for ammonia reaction at low temperatures, plays a vital role in the case of reburn process with biomass. Further the De Soete's kinetics have been formulated based on data points at temperature mostly above 2000 K, while in this work, the temperatures are of the order of 1600 K. So the

two reaction rates from De Soete regarding ammonia will be substituted with the recent data by Brink et al. [38], which have been developed to describe the oxidation of volatile nitrogen in biomass combustion. The two reaction rates by De Soete regarding HCN will be substituted with the ones by He [39], that are a very slight modification on De Soete's ones. De Soete's kinetics parameters are reported in table 10.

I_N Ammonia oxidation [38].

$$NH_3 + O_2 \rightarrow NO + H_2O + 0.5 \cdot H_2$$

$$\dot{w}_{NH3,I_N} = -1.21 \cdot 10^{11} \cdot T_g^2 \cdot [NH_3] \cdot [O_2]^{0.5} \cdot [H_2]^{0.5} \cdot \exp\left(\frac{-8000}{T_g}\right) \left[\frac{kmol}{m^3 \cdot s}\right] \quad \text{(IV.38)}$$

II_N Ammonia reduction [38].

$$NH_3 + NO \rightarrow N_2 + H_2O + 0.5 \cdot H_2$$

$$\dot{w}_{NH3,II_N} = -\frac{8.73 \cdot 10^{20}}{T_g} \cdot [NH_3] \cdot [NO] \cdot \exp\left(\frac{-8000}{T_g}\right) \quad \left[\frac{kmol}{m^3 \cdot s}\right] \quad \text{(IV.39)}$$

III_N HCN oxidation [39].

$$HCN + O_2 \rightarrow NO + CO + 0.5 \cdot H_2$$

$$\dot{w}_{HCN,III_N} = -10^{11} \cdot X_{HCN} \cdot X_{O2}^{b} \cdot \frac{p}{R \cdot T_g} \cdot \exp\left(\frac{-280328}{R \cdot T_g}\right) \left[\frac{kmol}{m^3 \cdot s}\right] \quad \text{(IV.40)}$$

IV_N HCN reduction [39].

$$HCN + NO \rightarrow N_2 + CO + 0.5 \cdot H_2$$

$$\dot{w}_{HCN,IV_N} = -3 \cdot 10^{12} \cdot X_{HCN} \cdot X_{NO} \cdot \frac{p}{R \cdot T_g} \cdot \exp\left(\frac{-251000}{R \cdot T_g}\right) \left[\frac{kmol}{m^3 \cdot s}\right] \quad \text{(IV.41)}$$

The *b* exponent (used in reaction IV_N) is calculated by a curve fit from the experimental data from De Soete [37].

$$b = \begin{cases} 0 & if\ \ln X_{O2} \geq -3 \\ 233 \cdot \exp\left(\dfrac{28}{0.5 + \ln X_{O2}} \right) & if\ -5.67 < \ln X_{O2} < -3 \\ 1 & if\ \ln X_{O2} \leq -5.67 \end{cases} \qquad \text{(IV.42)}$$

Gas phase homogeneous oxidation reactions

These are other reactions, taking place in the gas phase, but in which NO is not involved.

I_G CO oxidation. Howard *et al*. [40].

$$CO + 0.5 \cdot O_2 \rightarrow CO_2$$

$$\dot{w}_{CO,I_G} = -1.3 \cdot 10^{17} \cdot [CO] \cdot [O_2]^{0.5} \cdot [H_2O]^{0.5} \cdot \exp\left(\frac{-125580}{R \cdot T_g} \right) \left[\frac{kmol}{m^3 s} \right] \qquad \text{(IV.43)}$$

II_G H_2 oxidation. Jones *et al*. [41].

$$H_2 + 0.5 \cdot O_2 \rightarrow H_2O$$

$$\dot{w}_{H2,II_G} = -0.68 \cdot 10^{19} \cdot \left(\frac{Y_{H2}}{2} \right)^{0.25} \cdot \left(\frac{Y_{O2}}{32} \right)^{1.5} \cdot \rho_g^{1.75} \cdot \exp\left(\frac{-20130}{R \cdot T_g} \right) \left[\frac{kmol}{m^3 s} \right] \qquad \text{(IV.44)}$$

III_G CH_4 oxidation. Van der Vaart [42].

$$CH_4 + 2 \cdot O_2 \rightarrow CO_2 + 2 \cdot H_2O$$

$$\dot{w}_{CH4,III_G} = -5.74 \cdot 10^{10} \cdot [CH_4]^{-0.5} \cdot [O_2]^{1.5} \cdot \exp\left(\frac{-60000}{R \cdot T_g} \right) \left[\frac{kmol}{m^3 s} \right] \qquad \text{(IV.45)}$$

From the stoichiometry of the reactions, it is possible to compute the reaction rates of each species k:

$$\dot{n}_{\mathrm{hom}\,o,i} = \sum_{k=1}^{\mathrm{hom}\,o\,react} \upsilon_{i,k} \cdot w_i \cdot \frac{R_{kg} \cdot m_{TOT,gas} \cdot T_g}{p} \qquad \left[\frac{kmol}{s} \right] \qquad \text{(IV.46)}$$

Where $\upsilon_{i,k}$ is the stoichiometric coefficient of species *i* in homogeneous reaction *k*, and it is positive if the species is being produced and negative if the species is being

consumed. It is zero if the species *i* does not appear in the reaction *k*. Knowing the molecular weight of each species, it is possible to compute the mass variation rate.

$$\dot{m}_{\mathrm{hom}o,i} = \dot{n}_{\mathrm{hom}o,i} \cdot M_i \qquad \left[\frac{kg}{s}\right] \qquad \text{(IV.47)}$$

Heterogeneous reactions

These reactions take place at the particle surface between the solid carbon and the solid nitrogen and the gas phase. The kinetics of these reactions depend strongly on the characteristics of the solid fuel (char porosity, dimension, condition of species diffusion etc). These kinetics have a way higher uncertainty than the reactions in the gas phase. When kinetics data are not available for specified biomass, they have been assumed to be the same as for lignite, as low rank coals are the closest to biomass in combustion characteristics.

I_{FC} Carbon complete oxidation. Annamalai et al. [43].

$$C + O_2 \rightarrow CO_2 \qquad \dot{w}_{C,I_{FC}} = 1.6 \cdot 10^5 \cdot \exp\left(\frac{-20000}{R \cdot T_p}\right) \qquad \left[\frac{m}{s}\right] \qquad \text{(IV.48)}$$

II_{FC} Carbon partial oxidation. Smoot, et al. [44] and Annamalai et al. [43].

$$C + 0.5 \cdot O_2 \rightarrow CO$$

$$\textit{for biomass}: \qquad \dot{w}_{C,II_{FC}} = 2.3 \cdot 10^7 \cdot \exp\left(\frac{-26000}{R \cdot T_p}\right)\left[\frac{m}{s}\right]$$

$$\textit{for lignite}: \qquad \dot{w}_{C,II_{FC}} = 1.22 \cdot T_p \cdot \exp\left(\frac{-10300}{R \cdot T_p}\right)\left[\frac{m}{s}\right] \qquad \text{(IV.49)}$$

$$\textit{for subbituminous} \qquad \dot{w}_{C,II_{FC}} = 10.4 \cdot T_p \cdot \exp\left(\frac{-11200}{R \cdot T_p}\right)\left[\frac{m}{s}\right]$$

III_{FC} Carbon partial oxidation with CO_2. Smoot, et al. [44].

$$C + CO_2 \rightarrow 2 \cdot CO \qquad \begin{array}{ll} \textit{for lignite} & \dot{w}_{C,III_{FC}} = 3.42 \cdot T_p \cdot \exp\left(\frac{-15600}{R \cdot T_p}\right)\left[\frac{m}{s}\right] \\ \textit{for subbituminous} & \dot{w}_{C,III_{FC}} = 6190 \cdot T_p \cdot \exp\left(\frac{-28900}{R \cdot T_p}\right)\left[\frac{m}{s}\right] \end{array} \quad \text{(IV.50)}$$

IV_{FC} Steam carbon reaction: this reaction rate can be defined as a function of the previous kinetics. Yoon, H., et al., [45].

$$C + H_2O \rightarrow H_2 + CO \qquad \dot{w}_{C,IV_{FC}} = 1.67 \cdot w_{C,III_{FC}} \left[\frac{m}{s}\right] \quad \text{(IV.51)}$$

V_{FC} Methane formation. Schoeters, [46].

$$C + 2 \cdot H_2 \rightarrow CH_4 \qquad \dot{w}_{C,V_{FC}} = 3 \cdot 10^{-3} \cdot w_{C,III_{FC}} \left[\frac{m}{s}\right] \quad \text{(IV.52)}$$

VI_{FC} Solid carbon and NO reaction. Mitchel et al., [47].

$$C + NO \rightarrow CO + 0.5 \cdot N_2 \qquad w_{C,VI_{FC}} = 1.57 \cdot 10^5 \cdot \exp\left(\frac{-34000}{R \cdot T_p}\right)\left[\frac{m}{s}\right] \quad \text{(IV.53)}$$

I_{FN} Solid nitrogen oxidation. Mitchel et al., [47].

$$N + 0.5 \cdot O_2 \rightarrow NO \qquad \dot{w}_{C,VII_{FC}} = \frac{m_N}{m_P} \cdot w_{C,II_{FC}} \qquad \left[\frac{m}{s}\right] \quad \text{(IV.54)}$$

The FC consumption rate for the k-th heterogeneous reaction, assuming non-interacting particle clouds, for one particle of size *j*, can be computed as:

$$\dot{m}_{C,SP,k,j} = \rho_{w,j} \cdot k_{C,k,j} \cdot Y_{i,jw} \cdot \pi \cdot d_{p,j}^2 \qquad \left[\frac{kg}{s}\right]_{for\ each\ particle} \quad \text{(IV.55)}$$

All the variables in the formula depend on the particle size, as the temperature of the particle and the composition of the boundary layer will be different according to the

size and this will affect the density, the mass fraction of the elements and the reaction rates as well.

Knowing the fixed carbon (FC) consumption rate and the stoichiometry of the heterogeneous reactions, it is possible to compute the amount of *i* species added to the gas phase:

$$\dot{m}_{i,hetero} = \sum_{j=1}^{J}\left[\sum_{k=1}^{hetero\,react}\left(\upsilon_{k,i}\cdot\dot{m}_{C,k,j}\right)\cdot N_{particles,j}\right]\cdot\frac{M_i}{M_C}\qquad\left[\frac{kg}{s}\right] \tag{IV.56}$$

where J is the number of size groups (five).

Note that to get the total variation of the gas phase component *i*, it is necessary to take in consideration all the heterogeneous reactions, paying attention that these reaction rates will be different according to the size of the particle; therefore there is the need for a double summation over all the reactions and over all the size groups. In the case of blends, this must be done for the two fuels separately. The density of the gas phase must be computed at the surface of the particle and also the mass concentration of the reactants must be computed in the boundary layer surrounding the particle.

The concentration of the i-th species of the gas phase at the particle surface, in the case of single particle combustion, can be computed as [48]:

$$Y_{i,w} = Y_i \cdot [\exp(X)] - \sum_{k=1}^{L} \frac{v_{i,k} \cdot \rho \cdot k_{C,k} \cdot Sn_l \cdot d_p \cdot (\exp(X) - 1)}{(X \cdot Sh \cdot \rho \cdot D)} \qquad \text{(IV.57)}$$

$$where \quad X = \frac{\dot{m}_p}{Sh \cdot \rho \cdot D \cdot \pi \cdot d_p}$$

$$Sh = 2 + 0.6 \cdot \mathrm{Re}^{1/2} \cdot Sc^{1/3}$$

$Sh = 2$ *for a quiescent atmosphere*

L *total number of heterogeneous reactions involving the species i*

$v_{i,k}$ *stoichiometric mass of species i in reaction k*

Sn_k $+1$ *if species i is produced by reaction k, otherwise* -1

$\dot{m}_p$ *total mass flow leaving the particle*

ρ *density of gas phase*

Sh stands for Sherwood number, a dimensionless number used in mass-transfer operations according to the conditions of flow. The surface reactions require concentration of reacting species; the gaseous mass liberated from the particle transport species i away from the surface by convection while the species gradient transport species i either towards the particle for positive gradient or away from the particle for negative gradient. This is familiarly known as blowing correlation. As $X \rightarrow 0$ $Y_{i,w} \rightarrow Y_i$.

Hence this equation takes in consideration the effects of the convection – diffusion of the various species in the boundary layer. From the previous equation it is possible to know the composition of the gas phase in the boundary layer, the mean molecular weight of the mixture in the boundary layer and the density can be computed using the ideal gas law. The temperature will be assumed to be the same as the particle.

Pyrolysis

For the release of volatiles it has been assumed a single reaction kinetics model, [33].

$$\left.\frac{dm_{pyro}}{dt}\right|_j = A_{pyro} \cdot VM_{remain,j} \cdot \exp\left(\frac{-E_{pyro}}{R \cdot T_{p,j}}\right), \qquad j = 1....5 \qquad \left[\frac{kg_{VM}}{s}\right] \qquad \text{(IV.58)}$$

For the five size groups (j=1…5):

$$\begin{Bmatrix} \dot{VM}_1 \\ \dot{VM}_2 \\ \dot{VM}_3 \\ \dot{VM}_{4,} \\ \dot{VM}_{5,} \end{Bmatrix} = A_{pyro} \cdot \begin{Bmatrix} VM_{remain,1} \cdot \exp\left(\frac{-E_{pyro}}{R \cdot T_{p,1}}\right) \\ VM_{remain,2} \cdot \exp\left(\frac{-E_{pyro}}{R \cdot T_{p,2}}\right) \\ VM_{remain,3} \cdot \exp\left(\frac{-E_{pyro}}{R \cdot T_{p,3}}\right) \\ VM_{remain,4} \cdot \exp\left(\frac{-E_{pyro}}{R \cdot T_{p,4}}\right) \\ VM_{remain,5} \cdot \exp\left(\frac{-E_{pyro}}{R \cdot T_{p,5}}\right) \end{Bmatrix} \qquad \left[\frac{kg_{VM}}{s}\right] \qquad \text{(IV.59)}$$

VM_{remain} represents the mass of volatiles left in a certain particle size group; its value needs to be updated at each integration step, as it drives the volatile emission kinetics. The activation energy E_{pyro} and the pre exponential factor A_{pyro} are different for coal and for biomass, but the same model is used. Note that T_p stands for particle temperature; as each size group has its own temperature, each group has a different rate of release of volatile matter. The VM content at the next temporal step can be computed as:

$$VM_{t+1} = \begin{Bmatrix} VM_{1,t+1} \\ VM_{2,t+1} \\ VM_{3,t+1} \\ VM_{4,t+1} \\ VM_{5,t+1} \end{Bmatrix} = \begin{Bmatrix} VM_{1,t} \\ VM_{2,t} \\ VM_{3,t} \\ VM_{4,t} \\ VM_{5,t} \end{Bmatrix} - \begin{Bmatrix} \dot{m}_{pyro1,t} \cdot dt \\ \dot{m}_{pyro2,t} \cdot dt \\ \dot{m}_{pyro3,t} \cdot dt \\ \dot{m}_{pyro4,t} \cdot dt \\ \dot{m}_{pyro5,t} \cdot dt \end{Bmatrix} \qquad \text{(IV.60)}$$

The total mass flow of gases from the particles to the gas phase can be computed summing the contribution of the different size classes:

$$\dot{m}_{pyro,TOT} = \sum_{j=1}^{J} \dot{VM}_j \qquad \text{(IV.61)}$$

The composition of volatile matter released is known (Eq. IV.11) and hence it is possible to compute species contribution to the gas stream. The pre exponential factors and activation energies have been selected from the literature paying attention to select data measured under very fast heating rate (1000 K/s – 10000 K/s) as this is close to the conditions the fuel encounters in the furnace.

Fuel nitrogen pyrolysis

The two most used ways to model the FN release rate are to assume either the FN release rate to be proportional to the pyrolysis rate[30] or to formulate a specific kinetics [29].

In the case of N release proportional to pyrolysis rate, the FN release rate is given as:

$$\left.\frac{dm_{FN,pyro}}{dt}\right|_j = \left.\frac{dm_{pyro}}{dt}\right|_j \cdot \frac{N_{initial}}{VM_{initial}} \qquad \left[\frac{kg_N}{s}\right] \qquad \text{(IV.62)}$$

Where $\left.\frac{dm_{pyro}}{dt}\right|_j$ is the pyrolysis rate. Note that also in this case the FN release rate will vary depending upon the size group.

In the second model, the FN emission is described with a single reaction model.

$$\left.\frac{dm_{N-pyro}}{dt}\right|_j = A_{FN} \cdot N_{remain,j} \cdot \exp\left(\frac{-E_{FN}}{R \cdot T_{p,j}}\right) \qquad \left[\frac{kg_N}{s}\right] \qquad \text{(IV.63)}$$

These parameters have been provided by Pohl, [29] and Peck [49]. Both these studies were based on coal, for Peck A = 8300 s^{-1} and E = 69840 kJ/kmol. The FN kinetics data is not available for FB.

There is one important difference between the pyrolysis rate formulation and the FN release rate formulation: the first rate is expressed in kg of volatiles released per second, therefore, knowing the mass composition of the volatiles it is possible to compute the flow rate of each component. On the other side the FN pyrolysis rate is expressed in terms of kg of solid nitrogen being released per second through the FN volatiles, and not directly as kg of FN products released per seconds. For this reason the N consumption rate must be multiplied by a constant in order to switch to the FN total mass flow rate. This constant k_{FN} depends on the FN composition and Appendix C explains a procedure to compute it.

So now:

$$\dot{m}_{FN,TOT} = \sum_{j=1}^{N\,class} \left. \frac{dm_{N-pyro}}{dt} \right|_j \cdot k_{FN} \qquad \left[\frac{kg_{FN}}{s} \right] \qquad \text{(IV.64)}$$

This is the total mass flow of gases released from the pyrolysis of the fuel bound nitrogen. For biomass, as a base case, it is assumed that the FN pyrolysis rate is proportional to the volatiles release rate, while for coal the base case will be FN pyrolysis with a specific kinetics.

There are studies available in the literature that have studied the emission rate of fuel nitrogen from coal, and in most of these cases the process has been modeled similarly to pyrolysis but with its own kinetics parameters. No studies of this kind have

been found in the literature for biomass. The nitrogen emission from biomass can be either modeled assuming the release to be proportional with the volatiles or to be modeled with its own kinetics. It is important to keep in mind that as no studies are available from the literature in the case of modeling using dedicated kinetics it would be necessary to use the same kinetics that have been developed for coal.

The choice on how to model the fuel nitrogen emission for biomass is important for the accuracy of the model, therefore results for the different assumptions have been compared in the parametric studies (see the figure on page 151). Still it is important to note that the N-bonds within a particle are very different for coal and biomass: in the case of animal waste biomass most of the nitrogen is in the form of urea and bond energy is low. Therefore in the case of biomass the base case will be assumed to be with the fuel nitrogen emitted along with the volatiles.

Gas stream mass conservation equations

The species concentrations in the free stream change with time due to various processes: they are produced / consumed by the homogeneous or heterogeneous reactions, mass is added from the main burner, the volatiles, the FN and species from the heterogeneous reactions.

In general it is possible to state:

$$\left.\frac{dm}{dt}\right|_{i,gas} = \dot{m}_{pyro,TOT} \cdot y_{pyro,i} + \dot{m}_{FN,TOT} \cdot y_{FN,i} + \dot{m}_{hetero,i} + \dot{m}_{\mathrm{hom}\,o.,i} + \dot{m}_{MB} \cdot y_{MB,i} \qquad \text{(IV.65)}$$

With the following formula it is possible to compute the variation of each species *i* at each temporal step of the integration:

$$m_{RZ,t+1} = m_{RZ,t} + \left.\frac{dm}{dt}\right|_{RZ} \cdot dt = \begin{Bmatrix} m_{CH_4} \\ m_{CO} \\ m_{CO_2} \\ m_{H_2} \\ m_{HCN} \\ m_{H_2O} \\ m_{N_2} \\ m_{NH_3} \\ m_{NO} \\ m_{O_2} \end{Bmatrix}_{RZ,t} + \dot{m}_{pyro,TOT} \cdot \begin{Bmatrix} y_{CH_4} \\ y_{CO} \\ y_{CO_2} \\ 0 \\ 0 \\ 0 \\ 0 \\ 0 \\ 0 \\ 0 \end{Bmatrix}_{pyro} \cdot dt + \dot{m}_{FN,TOT} \cdot \begin{Bmatrix} 0 \\ 0 \\ 0 \\ 0 \\ y_{HCN} \\ 0 \\ 0 \\ y_{NH_3} \\ y_{NO} \\ 0 \end{Bmatrix}_{FN} \cdot dt +$$

$$+ \begin{Bmatrix} \dot{m}_{CH_4} \\ \dot{m}_{CO} \\ \dot{m}_{CO_2} \\ \dot{m}_{H_2} \\ \dot{m}_{HCN} \\ \dot{m}_{H_2O} \\ \dot{m}_{N_2} \\ \dot{m}_{NH_3} \\ \dot{m}_{NO} \\ \dot{m}_{O_2} \end{Bmatrix}_{Hetero} \cdot dt + \begin{Bmatrix} \dot{m}_{CH_4} \\ \dot{m}_{CO} \\ \dot{m}_{CO_2} \\ \dot{m}_{H_2} \\ \dot{m}_{HCN} \\ \dot{m}_{H_2O} \\ \dot{m}_{N_2} \\ \dot{m}_{NH_3} \\ \dot{m}_{NO} \\ \dot{m}_{O_2} \end{Bmatrix}_{Homo} \cdot dt + \frac{\exp\left(-\frac{t}{\tau_{mix}}\right)}{\tau_{mix}} \cdot \begin{Bmatrix} 0 \\ 0 \\ y_{CO_2} \\ 0 \\ 0 \\ y_{H_2O} \\ y_{N_2} \\ 0 \\ y_{NO} \\ y_{O_2} \end{Bmatrix}_{MB} \cdot dt \qquad \text{(IV.66)}$$

Particle geometry

It is assumed that the volatile loss occurs volumetrically during the pyrolysis; a kind of spongy structure is left within the particle and without altering the external dimension. In coal it was observed that particle swells during the pyrolysis. The combustion of the fixed carbon will affect both the mass and the diameter, since the diameter of the particle shrinks as carbon burns. Therefore:

$$\left.\frac{d\left(d_p\right)}{dt}\right|_j = -\frac{2 \cdot \dot{m}_{C,j}}{\pi \cdot \rho_{p,j} \cdot d_{p,j}^2} \qquad \text{(IV.67)}$$

Mass loss from each particle of size class j:

$$\dot{m}_{p,j} = \dot{m}_{C,SP,j} + \frac{\dot{m}_{VM,j}}{N_{particles,j}} + \frac{\dot{m}_{FN,j}}{N_{particles,j}} \quad \text{(IV.68)}$$

where $\dot{m}_{C,SP,j}$ refers to the carbon consumption rate of a single particle.

So:

$$d_{p,t+1,j} = d_{p,t,j} + \left.\frac{d(d_p)}{dt}\right|_j \cdot dt \quad \text{(IV.69)}$$

The rate of change of diameter varies with the particle size class as $\dot{m}_C$ will be different depending upon the size. It is also possible to compute the mass of each particle at the next temporal step. For the size class *j* the formula is:

$$m_{particle,j,t+1} = m_{particle,j,t} - \left(\dot{m}_{C,j} + \frac{\dot{m}_{VM,j}}{N_{particles,j}} + \frac{\dot{m}_{FN,j}}{N_{particles,j}} \right) \cdot dt \quad \text{(IV.70)}$$

The new density will be computed at each temporal step as the new diameter is known and also the new mass is known. It has to be computed for each size class of the fuels:

$$\rho_{p,j,t+1} = \frac{m_{particle,j,t+1}}{\frac{\pi}{6} \cdot d^3_{p,j,t+1}} \quad \text{(IV.71)}$$

The formula for the diameter variation comes from geometric considerations assuming the particle to be a sphere.

Energy conservation for the solid phase

The particles exchange heat with the gas phase and the furnace walls through convection and radiation. A quasi-steady state behavior is assumed. The particles are assumed to have a uniform temperature from the surface to the core, since all the particles are very small. In fact the Biot number ranges between 0.00013 and 0.0005, so this justifies the assumption of uniform temperature in the particles. The oxidation reactions of the char are exothermic and tend to heat up the particle, while the gasification reactions require heat to proceed and tend to cool down the particle. Also the pyrolysis is typically endothermic and so tends to cool down the particle. Besides, the convective heat exchange with the gas phase and the radiation heat exchange with the walls of the furnace must be taken in consideration.

Chemical reactions:

$$\dot{q}_{ch,p,j} = \sum_{k=1}^{N_{hetero\,reaction}} \dot{m}_{C,k,j} \cdot HV_k + \dot{m}_{VM,j} \cdot HV_{pyro} \qquad \text{(IV.72)}$$

Convection term:

$$\dot{q}_{conv,j} = -h_j \cdot \left(T_P - T_g\right) \cdot \pi \cdot d_{p,j}^2 \cdot F_{B,j} \qquad \text{(IV.73)}$$

$$F_{B,j} = \frac{z_j}{e^{z_j} - 1}, \text{ [50]} \qquad \text{(IV.74)}$$

$$z_j = \frac{\dot{m}_{C,j} + \dot{m}_{VM,j} + \dot{m}_{FBN,j} + \dot{m}_{N-oxi,j}}{Sh \cdot \pi \cdot \rho_g \cdot d_{p,j}^2} \qquad \text{(IV.75)}$$

Radiation term:

$$\dot{q}_{rad} = -\sigma \cdot \varepsilon \cdot \left(T_p^4 - T_w^4\right) \cdot \pi \cdot d_{p,j}^2 \qquad \text{(IV.76)}$$

The radiation heat exchange takes place between the particles and the furnace wall. The wall is assumed to be at the same temperature of the gas. Considering that the particles are very small compared to the dimensions of the furnace, it is possible to assume the view factor from the particles to the wall to be one. The furnace has been in use for many years and so the walls are covered by a thick layer of ash. This is confirmed by inspecting the interior of the furnace. Therefore the walls can be assumed to have the same radiation property of silica which is the main component of ash. The radiation heat exchange is important only for the large particles as the small ones are constantly at a temperature very close to the gas one's.

For each particle size of diameter d_j it is necessary to set up the energy conservation:

$$\frac{d\left(c_{p,coal}\cdot m_{p,j}\cdot T_{p,j}\right)}{dt}=\dot{q}_{conv,j}+\dot{q}_{rad,j}+\dot{q}_{ch,p,j} \qquad \text{(IV.77)}$$

Therefore the new particle temperature is given as:

$$T_{p,j,t+1}=T_{p,j,t}+\frac{\left(\dot{q}_{conv,j}+\dot{q}_{rad,j}+\dot{q}_{ch,p,j}\right)}{c_{p,coal}\cdot m_{p,j,t}}\cdot dt \qquad \text{(IV.78)}$$

Energy conservation for gas phase

In the gas phase, it is necessary to take in consideration the mixing with the mass flow coming from the main burner as this flow is at a different temperature. First, it is necessary to compute the temperature of the gas stream after the mixing with the main burner gases; this process is assumed to be isenthalpic which assumes that heat loss is negligible.

$$H_{RB,t}(T_{RB,t}) + H_{MB}(T_{MB}) = H_{RB,t'}(T_{RB,t'}) \quad \text{(IV.79)}$$

$$H = \sum_{i=1}^{N\,species} m_i \cdot h_{T,i} \quad \text{(IV.80)}$$

Computing the total enthalpy of the gas flow as the sum of the enthalpies of the various species and summing the total enthalpy of the added mass, it is possible to compute the temperature at the next temporal step. This formulation is implicit as the enthalpy functions are non linear functions of the temperature, and is solved numerically.

Once this temperature has been computed it is possible to consider all the other energy balances. The gas flow receives the convective heat from the particle; also the gas stream originating from the particle is assumed to be at the particle temperature (which is different from the gas temperature). The oxidation reactions in the gas phase generate heat, which tends to heat up the gas phase.

As the gas phase is made out of different components, each one with different (and non linear) enthalpy functions the energy conservation is solved numerically at each step of integration:

$$H_{RB,t+1}(T_{RB,t+1}, m_{RB,t+1}) - H_{RB,t'}(T_{RB,t'}, m_{RB,t'}) = \dot{q}_{conv\,gas} + \dot{q}_{ch} + \dot{q}_m \quad \text{(IV.81)}$$

$$\dot{q}_m = \sum_{i=1}^{N\,sizes} \left(\dot{m}_{C,j} + \dot{m}_{pyro,j} + \dot{m}_{N-pyro,j} + \dot{m}_{N-oxi,j}\right) \cdot N_{particles,j} \cdot \left(h\left(T_{p,j}\right) - h\left(T_{RB,t+1}\right)\right) \quad \text{(IV.82)}$$

$$\dot{q}_{ch} = \sum_{i=5}^{7} w_i \cdot \frac{R_{kg} \cdot m_{TOT,gas} \cdot T_g}{p} \cdot HV_i \quad \text{(IV.83)}$$

The convection heat contribution can be computed from the relations presented previously for every size group, changing the sign and summing over the different particle sizes; the gas is assumed not to take part in the radiation heat exchange.

$$\dot{q}_{conv} = \sum_{j=1}^{J} - \dot{q}_{conv,j} \cdot N_{particles,j} \qquad \text{(IV.84)}$$

There is a need to account for the heat losses along the furnace to model the cooling of the gas flow. As in Han [13], this could be done by considering the heat transfer through the wall of the furnace to the ambient as proportional to the gas temperature. However this approach would not be very accurate, so it will not be used in this case.

In the experiments by Goughnour [20], the temperature of the gas flow is measured along the furnace so the gas temperature profile is known; therefore, in the simulation, the energy conservation equations for the gas phase (IV.79 to IV.84) are used only during the mixing where the temperature is not known, while downstream, the temperature at each point is set by the experimental data.

Thus the temperature description is closer to the one in the experimentally observed profile: in the first part, the heating up of the gas stream takes place in the middle of the reburn injection zone, which is not at direct contact with the walls, so ignoring the heat loss in this first part can be reasonable.

The spatial distance between two sampling points is known; to apply these measurements to this model it is necessary to know how much time it takes to the gas stream to flow from one sensor to the other (remember that the model is using

Lagrangian observer). This can be estimated knowing the volumetric flow rate in the reburner. See Appendix B for details.

This approach has been chosen because the temperature distribution is critical to the NO_x reactions, therefore it is important in the simulation to be as close as possible to the temperature profile in the furnace.

Mercury modeling

Mercury is released from the reburn fuel in the elemental form, while chlorine is released as Cl_2 and HCl. The partition of chlorine between Cl_2 and HCl is 0.1 and 0.9, mass fractions, assumed from literature [51].

The release of mercury from coal is a field still evolving and there is no kinetics data available to model this process, therefore it is assumed that the mercury and the chlorine are being emitted along with the volatiles.

Also in this case it is necessary to consider the mercury and chlorine content in different particle size groups, as they have different pyrolysis rates. Therefore the mercury release rate is:

$$\dot{H}g = \sum_{j=1}^{J} \dot{m}_{pyroj,t} \cdot \frac{Hg_{particle\ j,t=0}}{VM_{particle\ j,t=0}} \qquad \text{(IV.85)}$$

The evolution of chlorine is described in the same way. So the amount of mercury left in the particles at each temporal step is:

$$Hg_{t+1} = \begin{Bmatrix} Hg_{1,t+1} \\ Hg_{2,t+1} \\ Hg_{3,t+1} \\ Hg_{4,t+1} \\ Hg_{5,t+1} \end{Bmatrix} = \begin{Bmatrix} Hg_{1,t} \\ Hg_{2,t} \\ Hg_{3,t} \\ Hg_{4,t} \\ Hg_{5,t} \end{Bmatrix} - \begin{Bmatrix} \dot{m}_{pyro1,t} \cdot Hg_{particle1,t=0} / VM_{particle1,t=0} \cdot dt \\ \dot{m}_{pyro2,t} \cdot Hg_{particle2,t=0} / VM_{particle2,t=0} \cdot dt \\ \dot{m}_{pyro3,t} \cdot Hg_{particle3,t=0} / VM_{particle3,t=0} \cdot dt \\ \dot{m}_{pyro4,t} \cdot Hg_{particle4,t=0} / VM_{particle4,t=0} \cdot dt \\ \dot{m}_{pyro5,t} \cdot Hg_{particle5,t=0} / VM_{particle5,t=0} \cdot dt \end{Bmatrix} \quad \text{(IV.86)}$$

Similarly the variation of the mercury and chlorine species in the gas phase, due to the release from the particles is:

$$Hg_{t+1} = Hg_t + \dot{H}g_t \cdot dt \quad \text{(IV.87)}$$

$$Cl_{2t+1} = Cl_{2t} + Frac_{Cl_2} \cdot \dot{C}l_t \cdot dt \quad \text{(IV.88)}$$

$$HCl_{t+1} = HCl_t + Frac_{HCl} \cdot \dot{C}l_t \cdot dt \quad \text{(IV.89)}$$

The gas phase mercury reactions are described by a two step reaction, [52]:

$$I_{Hg}: \quad HCl + OH \rightarrow H_2O + Cl \qquad k = 2.71 \cdot 10^7 \cdot T^{1.65} \cdot \exp\left(\frac{937}{T}\right) \left[\frac{kmol}{m^3 \cdot s}\right] \quad \text{(IV.90)}$$

$$II_{Hg}: \quad Hg + Cl + M \rightarrow HgCl + M \qquad k = 2.4 \cdot 10^8 \cdot T^{1.4} \cdot \exp\left(\frac{7500}{T}\right) \left[\frac{kmol}{m^3 \cdot s}\right] \quad \text{(IV.91)}$$

$$III_{Hg}: \quad HgCl + Cl + M \rightarrow HgCl_2 + M \quad k = 2.19 \cdot 10^{18} \cdot \exp\left(\frac{-1614}{T}\right) \left[\frac{kmol}{m^3 \cdot s}\right] \quad \text{(IV.92)}$$

In his work Xu [52] provided many reactions regarding mercury, but only three have been selected. This is because the first two reactions have negative activation energy, therefore they are expected to be much faster than all the others that have positive activation energy, and the third is the one with the lowest activation energy. This reaction scheme is the same used also in [53].

OH is assumed to come from the dissociation of water according to the following equilibrium reaction:

$$H_2O \Leftrightarrow OH + \frac{1}{2} \cdot H_2 \qquad \text{(IV.93)}$$

The equilibrium constant is known, therefore it is possible to compute the amount of OH present in the gas phase at each temporal step. See Appendix C for details. The reaction is considered to be at equilibrium as there is plenty of water and the consumption of OH will be only in trace amounts. From these kinetics, at each step, it is possible to compute the variation of all the species involved in the mercury reactions.

As these species are in traces amounts they will not lead to any contribution to the overall energy conservation of the gas phase; additionally they do not affect the total number of moles in the gas phase.

The mercury oxidation strongly depends on the presence of elemental chlorine in the gas stream; for this reason three extra equilibrium reactions have been analyzed in order to consider if they affect the amount of elemental chlorine present in the gas stream.

These additional Cl equilibrium reactions are:

$$I_{Cl} \qquad Cl_2 \Leftrightarrow 2 \cdot Cl \qquad \text{(IV.94)}$$

$$II_{Cl} \qquad Cl + OH \Leftrightarrow OHCl \qquad \text{(IV.95)}$$

$$III_{Cl} \qquad HCl \Leftrightarrow H + Cl \qquad \text{(IV.96)}$$

For these equilibrium reactions the equilibrium strongly favors the presence of elemental chlorine at the temperatures of the furnace, therefore they have not been included in the model.

CHAPTER V

RESULTS AND DISCUSSION

Chapter introduction

This chapter presents all the results from the model. First all the input data for the code are presented. Then the results are reported and compared with the experimental data to evaluate the accuracy of the model. The results will be presented first for Texas lignite, which is the base case fuel taken in consideration, and then for LAPC biomass, Wyoming Coal and the blends. The results include the temperature profiles along the furnace, the evolution of volatile and the particles, and the mercury emissions. Results regarding mercury are exposed separately from the results for NO_x. Afterwards also the results from parametric studies are presented, in which the sensitivity of the process is studied varying many parameters.

Data input

Table V.1 and V.2 show data on main burner and reburner operating conditions.

Table V.1
Data for the main burner

Fuel	Methane (CH_4)
Total Power	29.3kW (100000 BTU/hr)
Main burner Rating	19.5kW (70000 BTU/hr)
LHV methane	50100 kJ/kg
HHV methane	57000 kJ/kg
% Excess air	5
NO simulated	400ppm (local concentration)
Inlet temperature of air and fuel	300K
Temperature gases from MB	1500K

Table V.2
General data for the reburner

Fuel	Coal, FB or Coal – FB blends
Reburner Rating	9.8 kW (30000 BTU/hr)
Equivalence ratio considered	1 to 1.15
Inlet temperature	300 K (80.33 F)
Mixing time	40 ms

Fuel properties are presented in Table V.3, the deduced empirical formula is presented in Table V.4 and the size distribution is presented in Table V.5.

Table V.3
Fuel data

Property		LAPC	HAPC	TXL	WYO
Proximate analysis [%]	Moisture	19.64	17	38.34	32.88
	Ash	16.5	53.85	11.46	5.64
	FC	11.54	3.36	25.41	32.99
	VM	52.33	25.79	24.79	28.49
Ultimate analysis (DAF) [%]	C	52.92	51.19	74.06	75.67
	H	5.72	4.782	4.22	4.44
	O	37.47	39.09	19.14	18.36
	N	3.087	3.863	1.35	1.074
Cl content (as received) [%]		0.831	--	0.004	0.007
Hg content [mg Hg / kg of fuel]		0.06	--	0.17	0.14
LHV as received [kJ/kg]		13283	5214	14306	18219
Density [kg/m3]		1100	1100	1300	1300
Pyrolysis kinetics	A [1/s] [27, 34]	6.7910^{9}	$6.79*10^{9}$	$1.67*10^{13}$	$1.67*10^{13}$
	B [kJ/kmol] [27, 34]	140000	140000	223000	223000
FN Pyrolysis kinetics	A [1/s] [30, 49]	Prop	--	8300	8300
	B [kJ/kmol] [30, 49]	Prop	--	69840	69840
Heat of Pyrolysis VM [kJ/kg] [54]		-400	-400	-400	-400
Specific heat reburn fuel [kJ/kg K]		1.1	1.1	1.1	1.1
FN distribution N_2:NH_3:HCN [8, 33]		1:6:3	1:6:3	0.1:1.2:8.7	0.01:1.61:8.28

Table V.4
Fuel empirical formula

Empirical formula	LAPC	HAPC	TXL	WYO
C	1	1	1	1
H	1.285	1.12	0.677	0.697
O	0.513	0.572	0.193	0.182
N	0.05	0.0645	0.015	0.012

Table V.5
Particle size distribution

Particle size distribution				
Mean Diameter [mm]	HAPC [%]	LAPC [%]	TXL [%]	WYO [%]
1596	0.01	0.05	0.01	0
1015	0.03	0.1	0.00	0
570	1.68	7.58	4.97	1.68
225	6.44	27.21	33.72	15.35
113	13.73	22.56	37.09	45.01
60	20.43	16.06	11.82	21.75
20	57.69	26.44	12.38	16.18
SMD [mm]	32.71	56.28	81.02	64.44

The fuel size distribution can also be described by the Rosin Rammler function:

$$R_p = 100 \cdot \exp\left(-b \cdot x^{n_p}\right) \quad \text{(V.1)}$$

Where R_p represents the mass percentage of fuel above the size x and b and n_p are parameters of the distribution. These two parameters can be easily computed as on a semi logarithm plot the cumulative fraction becomes a line (Table 9). Fig. V.1 shows how the experimental points align along the line from the Rosin Rammler distribution.

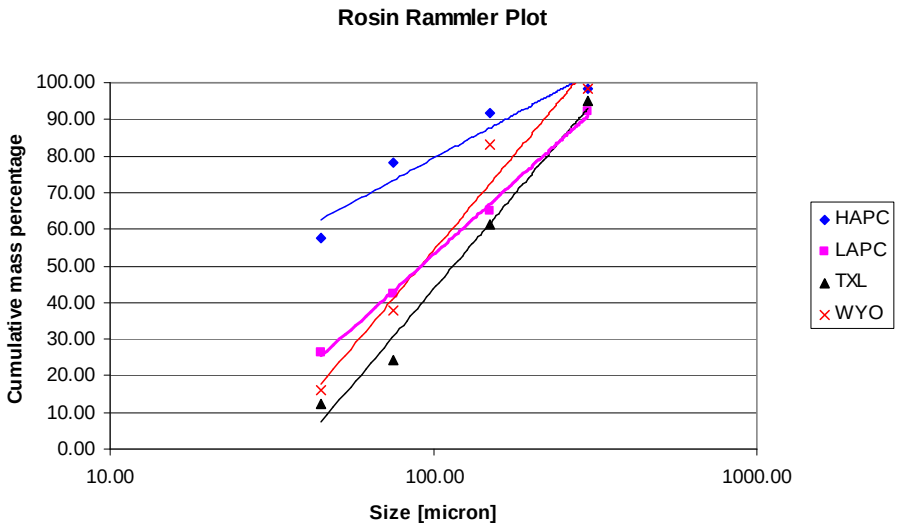

Fig. V.1. Rammler size distribution plot.

Table V.6
Rosin Rammler distribution factors

Values	HAPC	LAPC	TXL	WSB
n_p	2.33	2.01	3.00	3.13
b	9.35E-06	2.89E-05	3.12E-07	2.56E-07

The relevant kinetic data are presented in Table V.6 and V.7.

Table V.7
Kinetic data for homogeneous reactions

Reaction	A [m^3 – kmol - s]	E [kJ/kmol]	Reference
I_N	$1.21\ 10^{11}/T_g^2$	66500	[38]
II_N	$8.73\ 10^{20}\ T_g$	66500	[38]
III_N	10^{11}	280000	[39]
IV_N	$3\ 10^{12}$	251000	[39]
I_N (De Soete)	$4\ 10^{6}$	133900	[37]
II_N (De Soete)	$1.8\ 10^{8}$	113000	[37]
III_N (De Soete)	10^{10}	280000	[37]
IV_N (De Soete)	$3\ 10^{12}$	251000	[37]
I_G	$6.8\ 10^{18}$	20130	[40]
II_G	$5.74\ 10^{10}$	60000	[41]
III_G	$1.3\ 10^{17}$	125580	[42]

Table V.8
Kinetic data for heterogeneous reactions

Reaction		A [m/s]	E [kJ/kmol]	Reference
I_{FC}		$1.6\ 10^{5}$	20000	[43]
II_{FC}	Biomass	$2.3\ 10^{7}$	26000	[43]
	Lignite	$1.22\ T_p$	10300	[44]
	Subb	$10.4\ T_p$	11200	[44]
III_{FC}	Lignite	$3.42\ T_p$	15600	[44]
	Subb	$6190\ T_p$	28900	[44]
IV_{FC}		$1.67\ k_{IIIFC}$		[45]
V_{FC}		$3\ 10^{-3}\ k_{IIIFC}$		[46]
VI_{FC}		$1.57\ 10^{5}$	34000	[47]
$I_{N(s)}$		$m_N/m_p\ k_{VFC}$		[47]

Discussion of the numerical model

Following is a schematics of the model that summarize what has been presented before: after the data has been entered, and the condition of the main burner has been solved and the composition of the volatiles has been determined, the integration over time can start. First the contribution of the mixing process is considered at the particular temporal instant, afterwards it is possible to consider the effect of the mixing on the temperatures, then the devolatilization and the chemical reactions are taken in consideration, as well as the mercury evolution. Subsequently it is possible to compute the temperature of the gas and the particles at this temporal step. The temporal instant is then updated and it is checked whether the end of the integration has been reached or not. Fig. V.2 shows a schematics of the model.

In this model all the differential equations are integrated with an explicit scheme, in order to reduce the computational effort. A critical aspect in this kind of studies is the

choice of the temporal step for the integration. A large temporal step would lead to short computational time but would also bring to a bad solution or even to divergence as this is an explicit method and therefore is not always stable. On the other side, a very small temporal step would bring to a good solution but would require a massive computational effort. Therefore the temporal step must be carefully chosen to produce a good solution, but still not make the computational time excessively long.

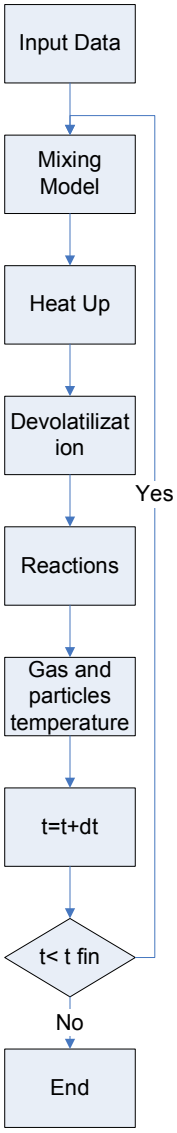

Fig. V.2. Model schematics.

In general the temporal step has to be smaller than the shortest characteristic time of the processes present in the model: it has to be small enough to guarantee a good accuracy even for the fastest events occurring in the simulation.

A standard way to check the sensibility to the temporal step is to consider the difference between its solution and the solution for a temporal step which is a half. If the variation between the two successive solutions is small then the temporal step chosen is fine, if it is not, it means that the solution has not converged yet, and it is necessary to use a smaller step.

This has been done for the present study, starting from the case of Texas lignite.

Fig. V.3 shows the NO_x profiles versus the equivalence ratio with different temporal steps as parameter.

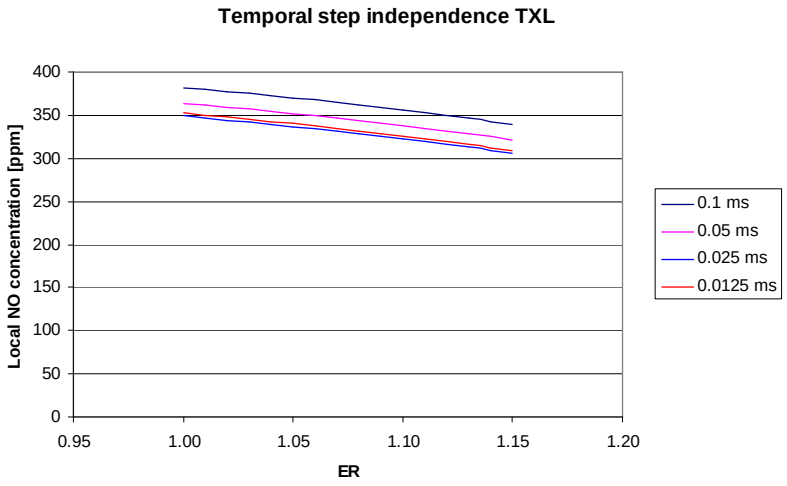

Fig. V.3. Choice of temporal ttep, Texas lignite.

As the temporal step is gradually reduced, the difference between two successive solutions becomes smaller and after the temporal step is 0.025ms the difference becomes negligible. So the 0.025ms is used as temporal step.

The same study has been repeated also for biomass and blends and in all the cases this temporal step has turned out to be similar.

NO_x results

The data from literature is directly used, without any changes to match with the experimental data. An alternative way is to adjust the kinetics to minimize the discrepancy between experiments and model, but this requires massive computational efforts, and besides, the experimental data available cannot be considered to be accurate enough to develop kinetics data based on them.

The residence time in the furnace is estimated to be of the order of 0.85s, and hence the numerical result for the NO emission is the value of the NO concentration considered at the residence time t = 0.85s. Appendix B presents the method used to compute the residence time. It is important to note that the only purpose of the residence time in the simulation is to know at what instant to select the results from the simulation and compare it with the experimental data. It might be argued that the method presented in Appendix B is too simplistic; to compute more accurately the residence time it would be necessary to go for complete fluid dynamic simulation. In fact the main result from this code is the NO concentration at the end of the furnace; since temperatures are already low all the NO reactions are already almost frozen well before the end of the furnace. Hence the NO concentration vs time flattens well before the end of the furnace

as the temperatures are decreasing. Under these circumstances it would make hardly any difference assuming a residence time of 0.7s or 1s.

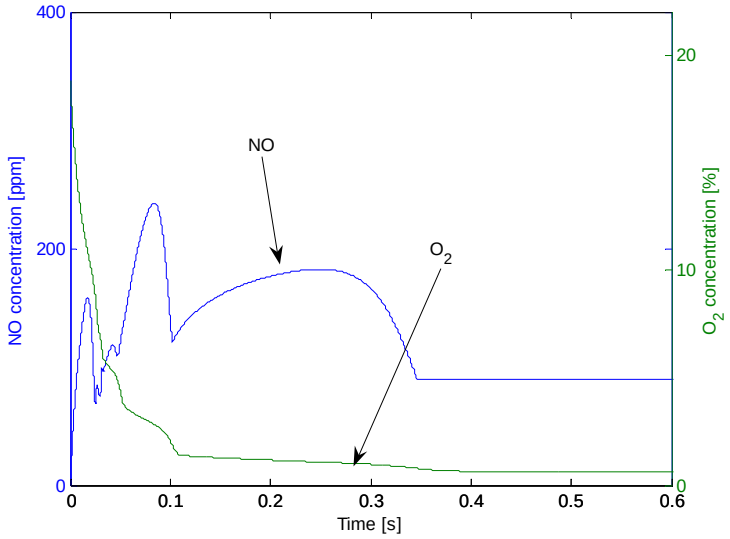

Fig. V.4. Example of NO concentration along the furnace.

Fig. V.4 shows the NO concentration along the furnace for the case of LAPC, ER = 1. It is clear that the NO concentration stabilizes well before the end of the furnace.

Sometimes the volatiles and FN release appear like spikes, see Fig. V.5.

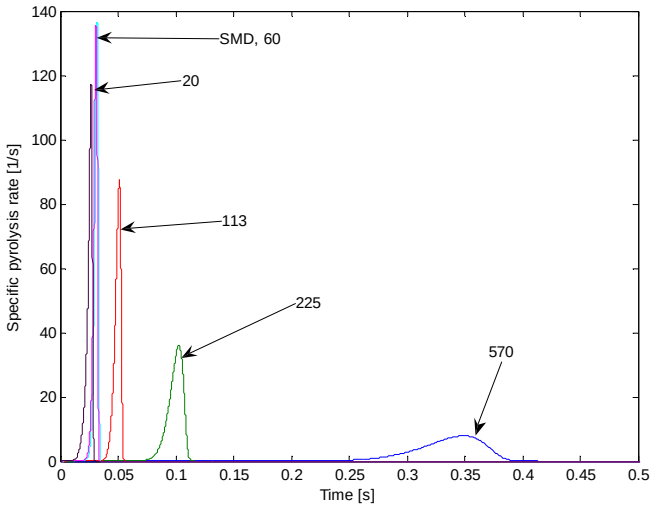

Fig. V.5. Effect of class size distribution on devolatilization rate.

Fig. V.5 presents the specific devolatilization rate for LAPC, ER = 1, and it is here presented to show the effect of a discrete number of size classes on this variable, the spikes are identified with the diameter of the corresponding class in micron.

This is due to the description of the particle size distribution with a finite number of size groups. The solid fuel size distribution is continuous, but in this model it is described by five size groups. This number has been chosen because this is the number of sieves used in the standard coal sieving machine in the laboratory; therefore a more detailed distribution was not available. Besides, more size groups would have resulted in more computationally intensive code.

With a finite size distribution, the process of release of the volatiles occurs when a certain size group reaches a certain temperature (e.g. pyrolysis temperature), its release rate becomes significant at that time. Correspondingly in the reactions that involve those

species, there is a spike as now there are more reactant species in the gas phase. With an infinite number of classes the release of volatiles would be a continuous function and hence the spikes can disappear. However using five size groups is a better description of reality than using just the SMD of the distribution and describing the reburn fuel with SMD: in that case there would be only one large spike and it is not possible to predict the effect of size distribution on the final NO concentration.

Many times small scale test data cannot be directly scaled to a large scale combustion system; however the ratios of reburn performance of fuel of interest to selected standard fuel which is coal, is typically scalable. Then Texas lignite is selected as standard fuel for the purpose of evaluating comparative reburn performance of LAPC biomass.

Texas lignite

Temperature effect

In all the graphs the different lines are identified by the mean diameter of that particle group, the unit being in micrometer (micron). The thick line represents the gas temperature profile. Besides the regular classes, also the line relative to the SMD is drawn. The fuel is still split in the five classes; the SMD line is drawn just to show what would have been the temperature profile for a particle of diameter equal to the SMD under these conditions.

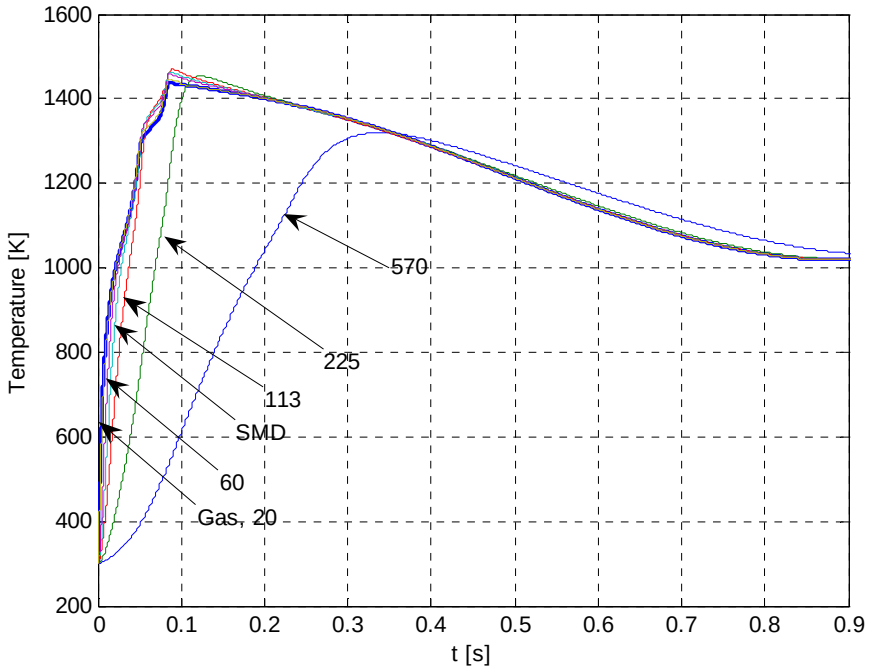

Fig. V.6. Temperature profiles for Texas lignite, pure air, ER = 1.

From Fig. V.6, it is possible to see the temperature profile for Texas lignite. The time required to reach the maximum temperature depends on the amount of volatiles present in the fuel. Specifically coal contains a smaller fraction of volatiles than biomass, so it takes it a longer time to reach the maximum temperature than for biomass (see the section with the results for biomass). A small content of volatiles implies that most of the energy is released from the char but char combustion takes a longer time to complete the combustion compared to the gaseous combustion of volatiles; this has a visible side effect on the temperature of the particles: comparing this graph with the one for biomass it is possible to see that in this case the particles are heated up faster than for biomass,

since more energy is released with FC and less energy within the particles is absorbed to emit the volatiles; this can be clearly seen for the large particles.

The temperatures of the particles become slightly higher than the temperature of the gas due to the large fraction of FC and hence significant heat is released inside the particles.

Fig. V.7 presents the temperature profile for the case of Texas lignite with vitiated air, ER = 1. It is seen that the heating rate is slower because in this case there is a significant amount of inert gas (nitrogen) which is heated up, and besides the lower concentration of oxygen slows down the oxidation reactions.

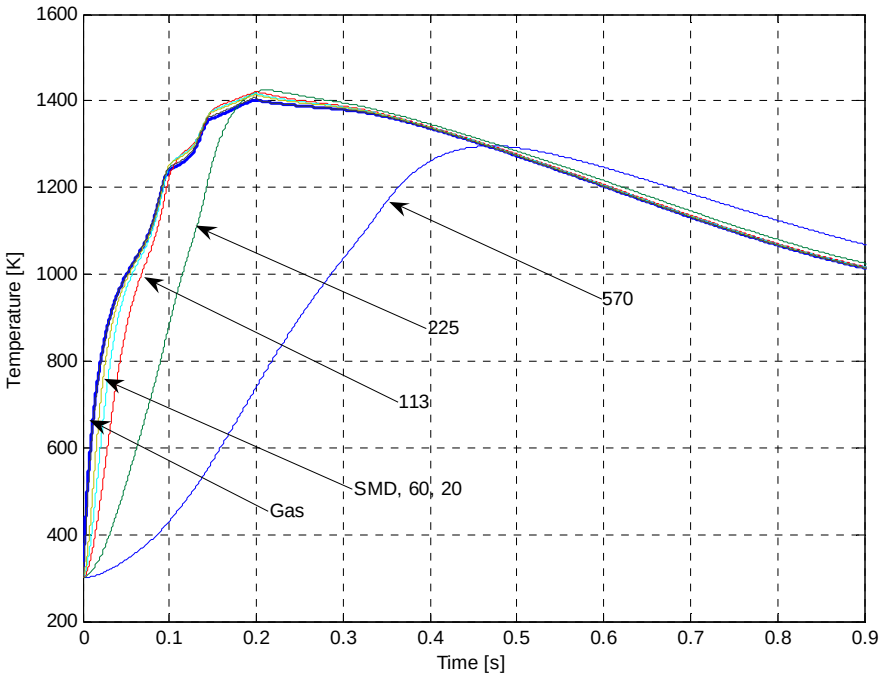

Fig. V.7. Temperature profile for Texas lignite, vitiated air, ER = 1.

Particle evolution

Fig. V.8 presents the volatiles emission rate of Texas lignite and it is seen that the spikes are much lower than those of LAPC (see the figure on page 97).

The rates are divided by the initial mass present in the size group it refers to:

$$Specific\ Pyrolysis\ Rate\ \ j = \frac{\frac{dm_{pyro,j}}{dt}}{m_{0,j}} \quad \left[\frac{1}{s}\right] \tag{V.2}$$

Such operation is necessary because the pyrolysis rate depends on the amount of volatiles present in a size group; if not divided, the pyrolysis rate of the groups with a small mass fraction would be hardly visible in the figure. It is also noted that the volatile emission in this case, for large particles, occurs at an earlier time than for biomass, see figure on page 97. It is important to note that this is not due to a faster kinetics (as it is not) but to the fact that the particles heat up faster and so the pyrolysis starts earlier.

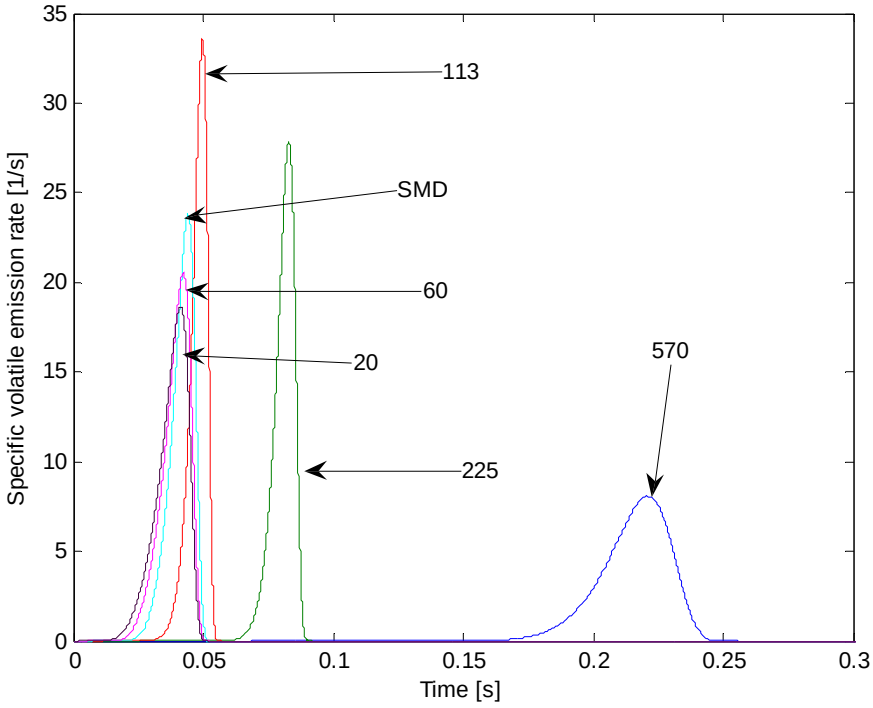

Fig. V.8. Volatiles emission rate, Texas lignite, pure air, ER = 1.

The larger the particle, the longer it takes to heat up and to release the volatiles. The difference between biomass and Texas lignite can also be seen drawing on the same figure the pyrolysis rate for the SMD of the two fuels (see Fig. V.9).

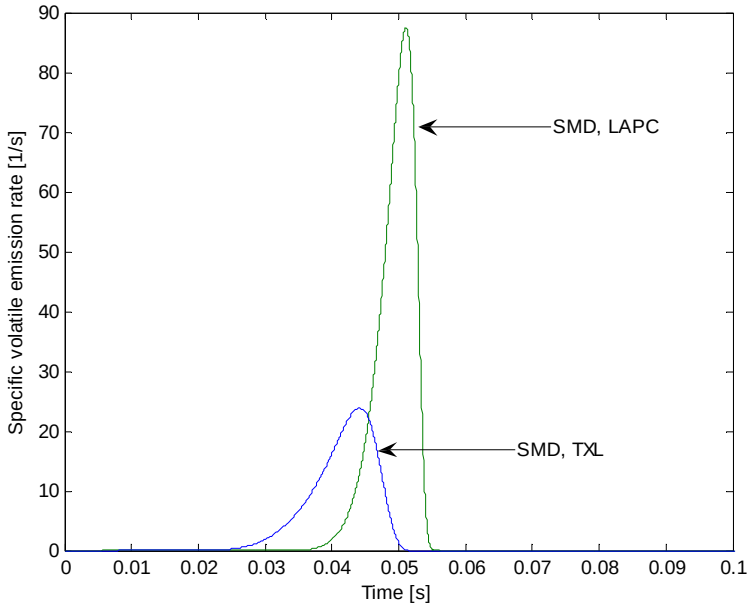

Fig. V.9. Comparison of volatile emission rate between LAPC and Texas lignite, pure air, ER = 1.

From Fig. V.9 the difference between the emission rates of the two fuels is evident. For the SMD, the temporal distance between the two fuels is almost negligible because such small particles are constantly at a temperature close to the gas temperature.

It was said that in the case of coal FN emission rate is modeled using specific kinetics parameters, different from the ones used for the volatiles emission. As the bonds of nitrogen with the char structure are typically strong, the FN emission rate will be slower than the emission of the volatiles. Fig. V.10 shows the normalized volatiles emission rate and the FN emission rate. It is important to pay attention on the different Y scale for the two curves. It is clear that the emission rate for FN is much slower and takes a much longer time than the emission of the volatiles. In fact the volatiles emission

looks more like a spike, while the FN emission is a much smoother curve. The curve presented is the one regarding particles with diameter equal to SMD. Also the fact that volatiles pyrolysis starts earlier is apparent from the graph.

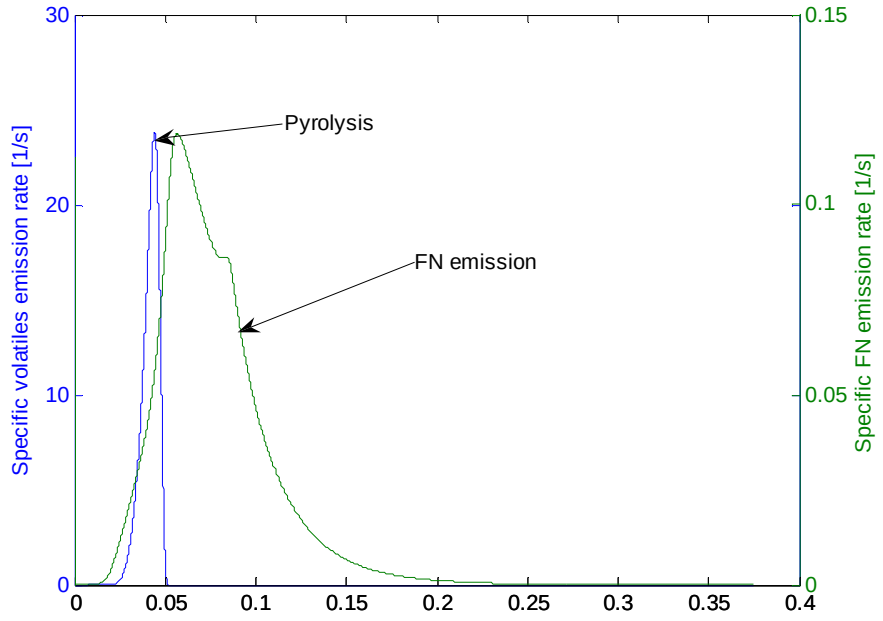

Fig. V.10. Comparison between specific volatile emission rate and FN emission rate, TXL, pure air, ER = 1.

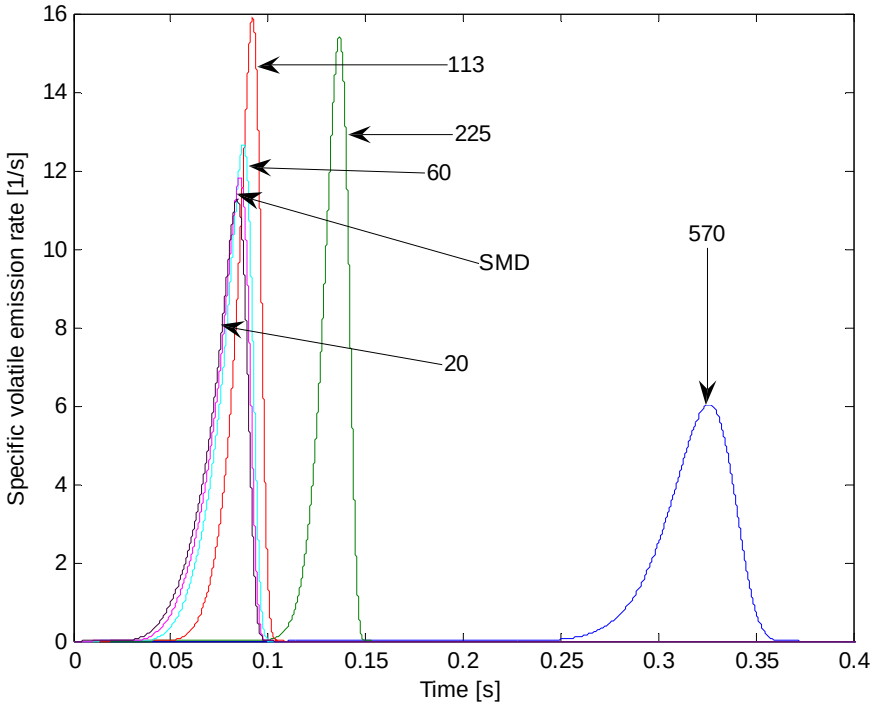

Fig. V.11. Comparison of volatiles emission rate, Texas lignite, vitiated air, ER = 1.

Fig. V.11 shows the effect of vitiated air on the pyrolysis rate for Texas lignite: the rates are lower and the volatile release is delayed, as the temperatures are lower. The rates of combustion of Texas lignite are illustrated in Figs. V.12 and V.13 for different size groups. Fig. V.12 plots the total specific mass while Fig. V.13 shows the fixed carbon fraction for each size group.

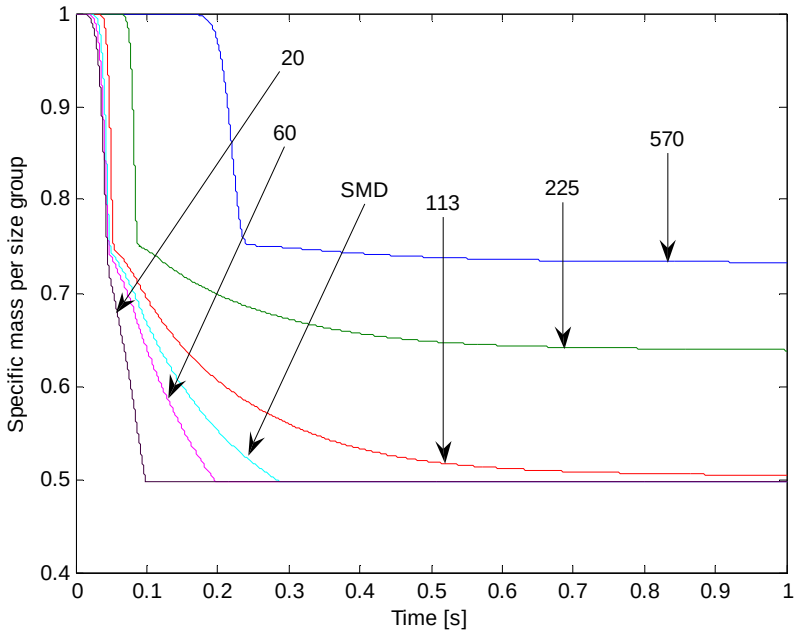

Fig. V.12. Specific mass content per size group, Texas lignite, pure air, ER = 1.

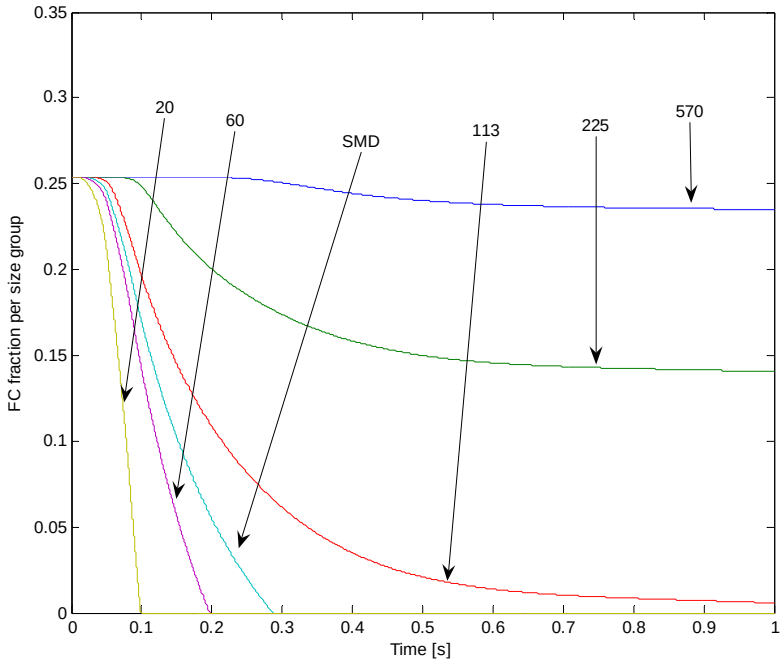

Fig. V.13. Fixed carbon fraction per size group, Texas lignite, pure air, ER = 1.

From Fig. V.12 it is seen that the first sharp drop of the mass content corresponds to the volatiles loss, while the second loss, which is less steep with time but still large, corresponds to the fixed carbon consumption; the FC loss is faster for the smaller size particles which are heated up faster, and also have a better surface to volume ratio to aid heterogeneous reactions to proceed. The largest particle size shows the volatile loss but it is not heated up enough to high temperature for the fixed carbon to react.

The same conclusions can be drawn from the plot of the fixed carbon. Only the two smallest particle size groups are able to consume all their fixed carbon. The size groups with diameter larger than 60 μm are able to consume only a part of their FC because it takes a longer time for them to be heated up and when they are ready to combust, the temperature of the gas phase starts decreasing, so their heterogeneous reactions proceed slowly; also their less favorable surface to volume ratio is important to explain their incomplete combustion. The largest particle size hardly consumes any fixed carbon.

Therefore, it is clear that the size of particles affects the degree of combustion; if the fuel is not burnt completely, there will be more oxygen available throughout the reburn process and therefore the reactions resulting in NO production are favored. On the other hand, a fuel that burns very fast (e.g. LAPC) consumes the oxygen in a short time, and so will simply block the reactions that tend to produce NO from the FN.

In Goughnour [20], it is reported that for TXL there is still a small amount of oxygen in the exhaust and this matches with what found in the simulation: the lignite is

not completely burned under these conditions and this, in part, explains the small NO reduction obtained.

Comparison with experimental data

Figs. V.14 and V.15 present a comparison of the experimental and the numerical results.

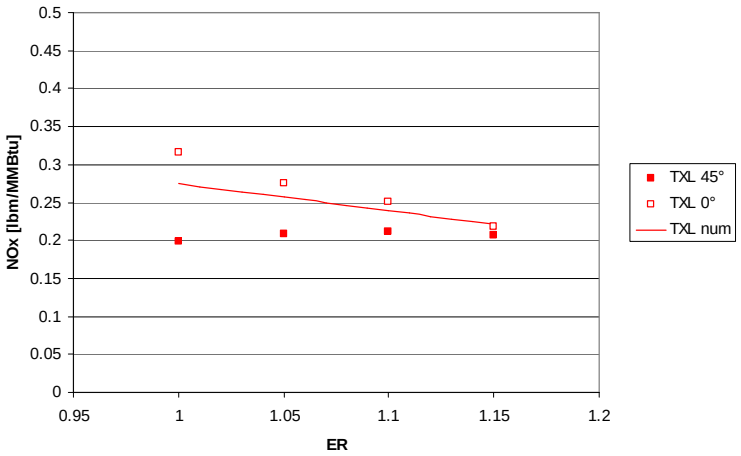

Fig. V.14. Comparison with experimental data, Texas lignite, pure air.

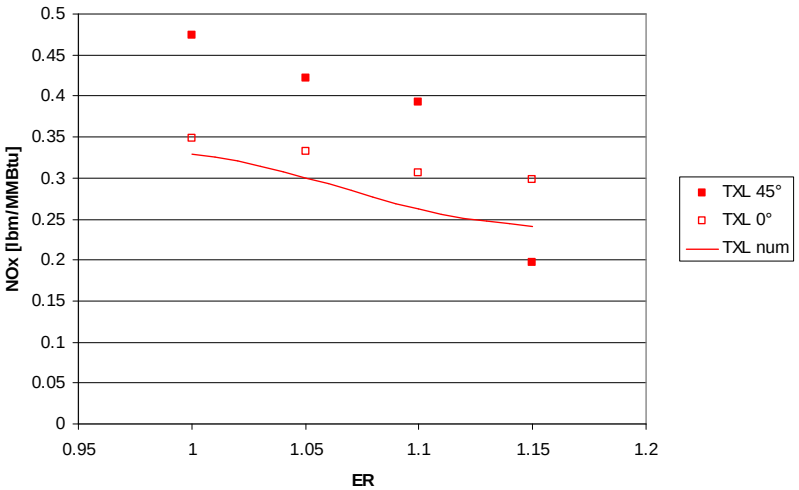

Fig. V.15. Comparison with experimental data, Texas lignite, vitiated air.

The agreement between the experimental and the numerical data results is satisfactory.

In the case of pure air, the prediction lies in between the experimental data (Fig. V.14). In the case of vitiated air there is under prediction, but still the discrepancy is reasonable and in the case of rich mixture the prediction is close to the experimental data (Fig. V.15).

It is important to note that the use of vitiated air for Texas lignite leads to poorer NO reduction than with regular air, and this result is confirmed both by the experiments and the simulation. The reason can be speculated to be in the fact that now the temperatures are lower and also the heating up is slower, therefore all the reactions become slower; also the fact that now the concentration of NO is lower is speculated to play a role in leading to this result.

NO data

Fig. V.16 shows the NO and O_2 concentration along the furnace. It is interesting to compare this plot with the one for biomass (see figure on page 104).

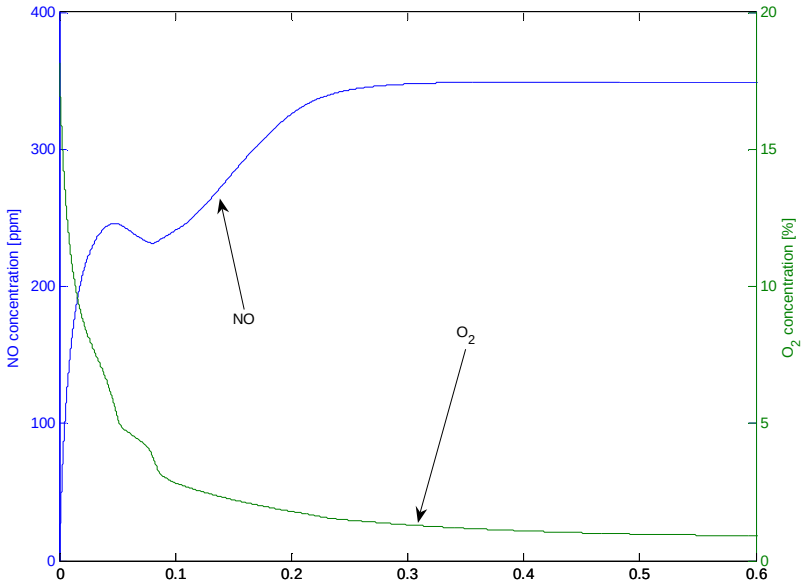

Fig. V.16. NO and oxygen concentration along the furnace, Texas lignite, pure air, ER = 1.

It is noted that there are not any large decreases in the NO concentration along the furnace which implies that the reactions that produce NO are always more significant than the ones that reduce NO.

A significant difference with LAPC biomass is represented by the oxygen concentration that is higher than for biomass (see Fig. V.31), especially in the very first part of the figure. This occurs due to less volatile matter which consumes less oxygen; the larger FC requires a longer time to be burned, and therefore to consume the oxygen. This is one of the reasons why the reburn process with Texas lignite is not as effective as with LAPC biomass.

Fig. V.17 shows the different NO concentration profiles along the furnace for different ERs and according to the use of pure air or vitiated air.

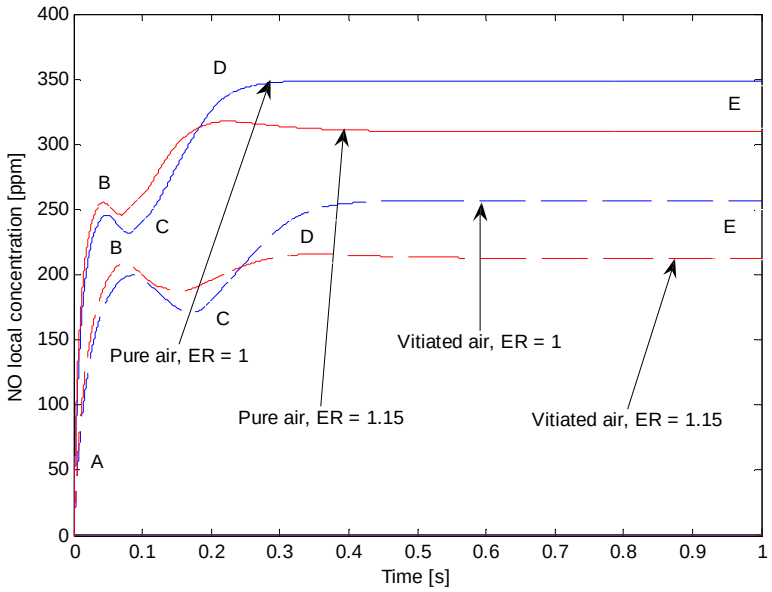

Fig. V.17. NO concentration along the furnace for Texas lignite.

It is seen from the diagram that the values for TXL are much higher than for LAPC biomass, and also the shape of the curves is vastly different, see Fig. V.32.

After the initial part in which the NO concentration rises due to the mixing with the flow from the main burner (AB), there is a small reduction (BC) and then the concentration rises steeply (CD) and only after 0.3 s it is possible to see a very small reduction (DE). It is important to note that still the NO_x concentration is slightly lower than the initial concentration, but the effectiveness of the reduction is much poorer than the one with LAPC biomass.

To compare the difference between the FN release for Texas lignite and Biomass the FN release rate (for a particle having diameter equal to the SMD fired along with the

regular fuel) for the two fuels is plotted on the same graph (see Fig. V.18). The specific rate is defined as ratio of release rate to initial mass of nitrogen contained in the fuel.

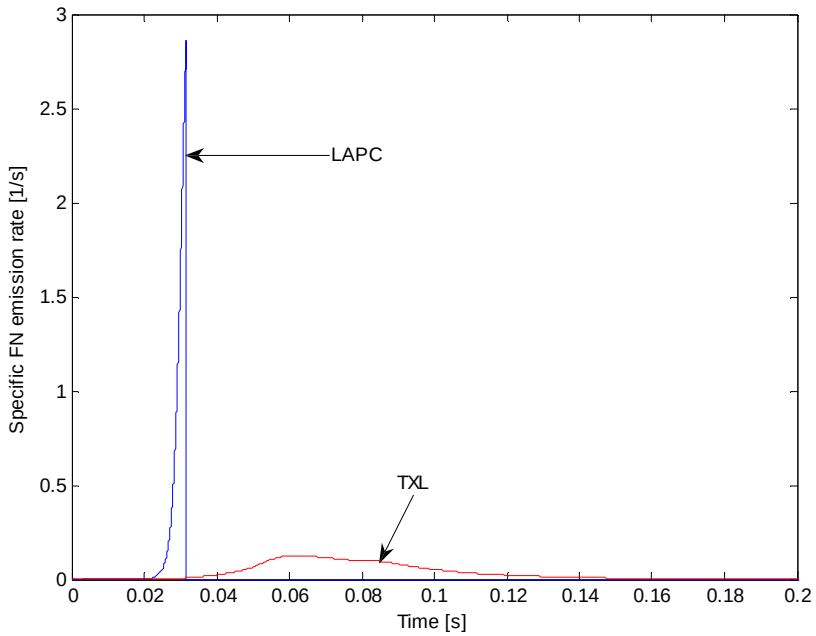

Fig. V.18. FN release rate comparison for Texas lignite and LAPC biomass, pure air, ER = 1.

The difference between the two fuels is evident: for biomass the release is very rapid and takes place over a very short time. For coal, the release is gradual and it takes much longer to complete the process. The absolute values depend on the kind of normalization chosen, but still the difference between the processes in the two cases is clear.

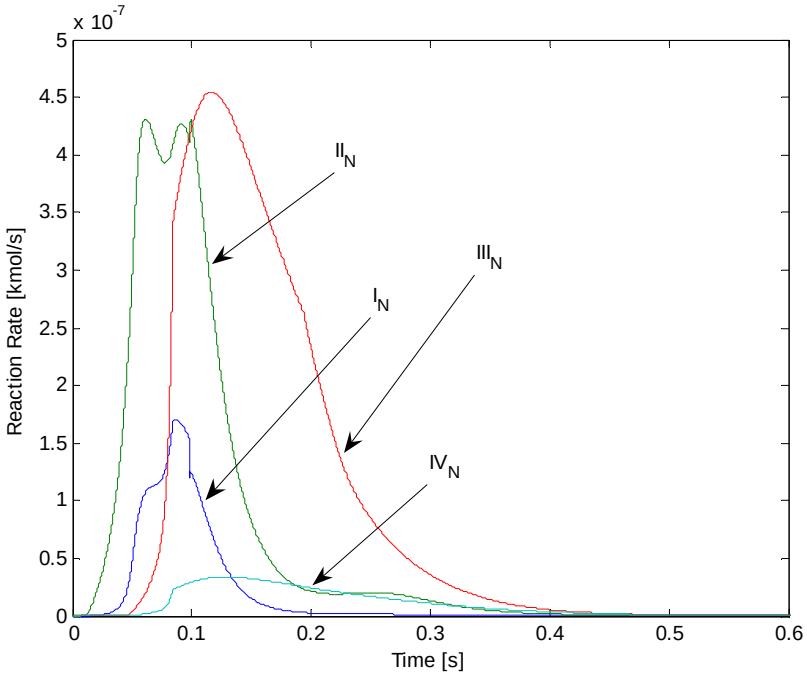

Fig. V.19. Reaction rates involving NO, Texas lignite, pure air, ER = 1.

From Fig. V.19 it is possible to see that the reaction rates are two orders of magnitude lower than those for LAPC (see figure on page 106). This happens because in the case of TXL most of the FN is released as HCN which is much less reactive than ammonia. The most important reactions are oxidation reaction to create NO (III_N) and the reduction reaction by ammonia with NO; however the others cannot be neglected.

It is interesting to note that under these conditions ammonia reacts more likely by (II_N), than by oxidation reaction to NO (I_N). The reason for this can be speculated from the reaction rate of reaction I_N, that depends also on hydrogen: in this case, as there is more oxygen left after the pyrolysis, and hence heterogeneous oxidation is favored instead of the gasification reactions that would produce hydrogen. The NO reduction with ammonia starts before the other reactions, but still it is not enough to provide any

significant NO reduction. There is a small temporal window (see Fig. V.16, around 0.1 s) in which NO is actually reduced, and this can be explained as at that moment reaction II_N is already fast while III_N has not become dominant yet.

The differences in the shape of the curves also depend upon the way FN is released. The figure for TXL does not show any spike when a size group becomes active.

Low Ash Partially Composted biomass (LAPC)

Temperature effect

Fig. V.20 shows the predicted temperature profiles of the gas and the various particle size groups for LAPC biomass.

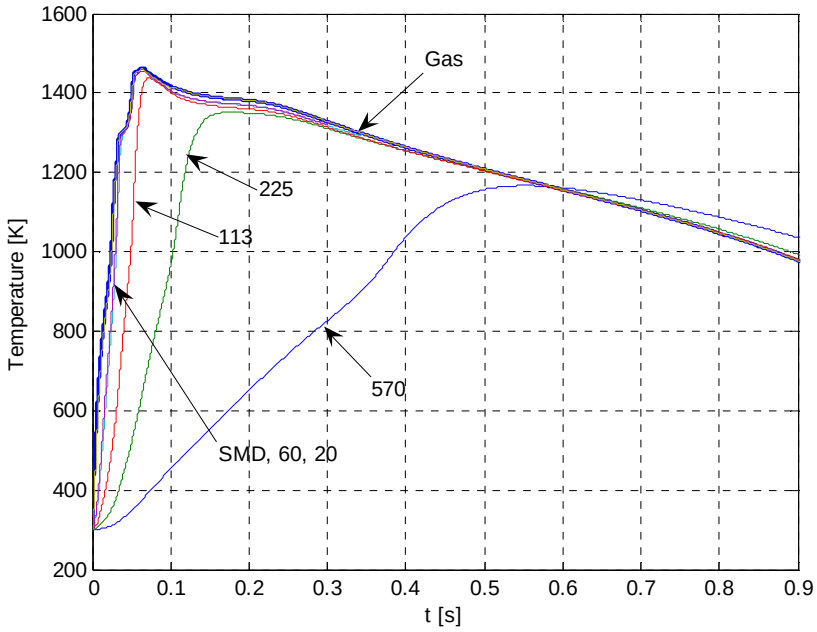

Fig. V.20. Temperature profile for LAPC, pure air, ER = 1.

It is seen that there is hardly any difference between the 20 micron, 60 micron and SMD classes, while the other larger classes have different temperature profiles.

As the main burner gases start mixing with reburn gases, the temperature of the reburn gas increases very rapidly; it reaches a peak and then it decreases as time passes and the gas moves down the furnace. As expected, the small particles heat up very rapidly, having curves that are hardly distinguishable from that of gas. On the other hand the large particles heat up slowly. It is possible to see that the temperatures of the particles always remain below the gas temperature since the fixed carbon content in biomass is very low and when particles reach a temperature where the heterogeneous reactions become fast, most of the oxygen has already been consumed by the combustion of the volatile gases; therefore the lack of oxygen at the particle surface tends to shift the reactions toward the endothermic gasification reactions which tend to cool the particles down.

The only exception is at the end of the furnace when the temperature of the gas is dropping: the temperature of the largest particles goes above the gas temperature, but this only happens due to the larger thermal inertia of these particles with respect to the small ones. The heat exchange coefficient h for large particles is smaller than for small particles (i.e. heat is transferred more rapidly out of particle with small d_p, than from the ones with large d_p).

Fig. V.21 shows the difference between the temperature profile of Texas lignite and LAPC.

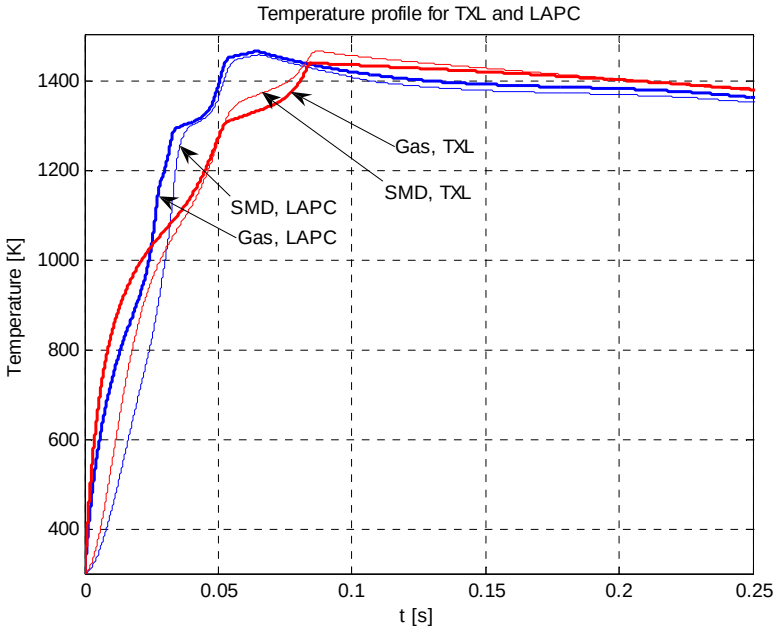

Fig. V.21. Comparison between temperature profile for Texas lignite and LAPC, pure air, ER = 1.

From this graph the delay between the combustion of LAPC and TXL is apparent.

Fig. V.22 shows the predicted temperature profile along the furnace for biomass with vitiated air.

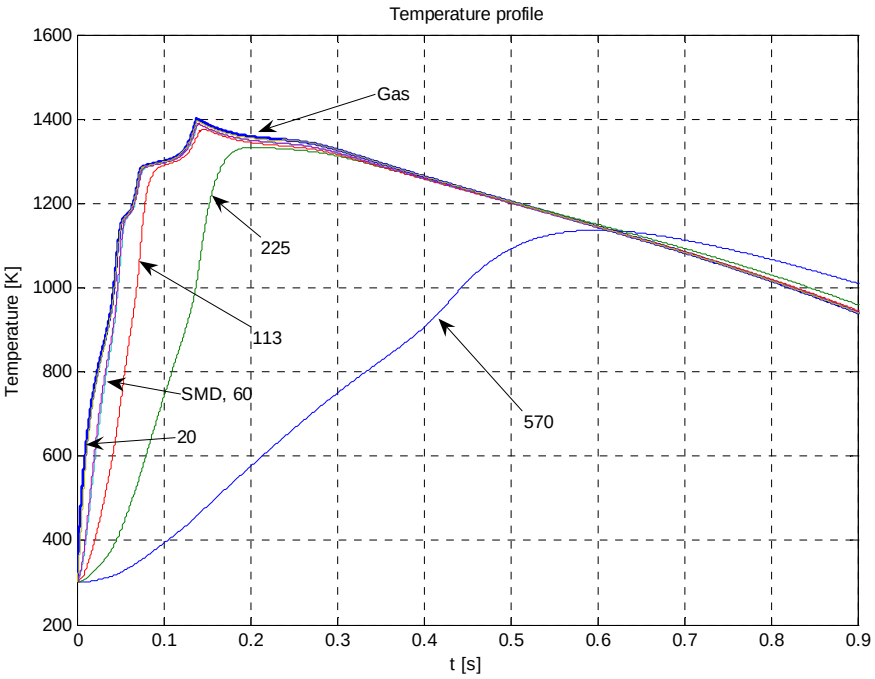

Fig. V.22. Temperature profile for LAPC, vitiated air, ER = 1.

The differences between the case of pure and vitiated air become apparent plotting the gas profile and the SMD profile for the two cases on the same figure, see Fig. V.23.

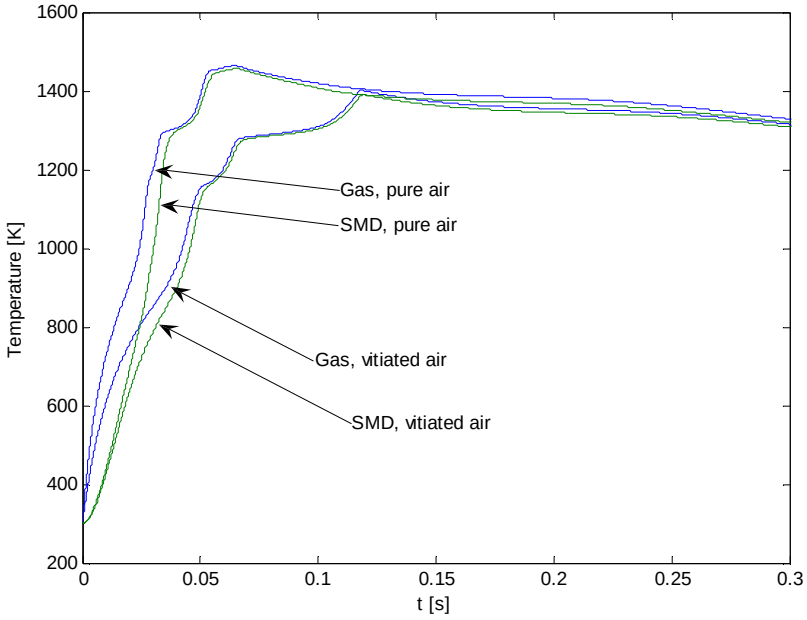

Fig. V.23. Comparison of temperature profiles for pure and vitiated air, LAPC, ER = 1.

The rate of heating up is slower and all the temperatures are lower than those with pure air. Note that the comparison is made at same Φ_{RZ}; since in the case of vitiated air the oxygen concentration is 12.5% more gas must be supplied to maintain the same Φ_{RZ}. Thus the mass of inert gas at the reburner is almost the double than before; so there is a large amount of inert gas to be heated up without giving any contribution to the combustion and this drives down the temperatures.

It is also interesting to study the effect of the size distribution on the temperature profile: Fig. V.24 shows this effect. In this figure the temperature profile for gas is plotted for the case of real distribution (five size groups) and in the case of monosized suspension with d_p = SMD. On the same plot T_p of the particle with d_p = SMD is plotted for both cases.

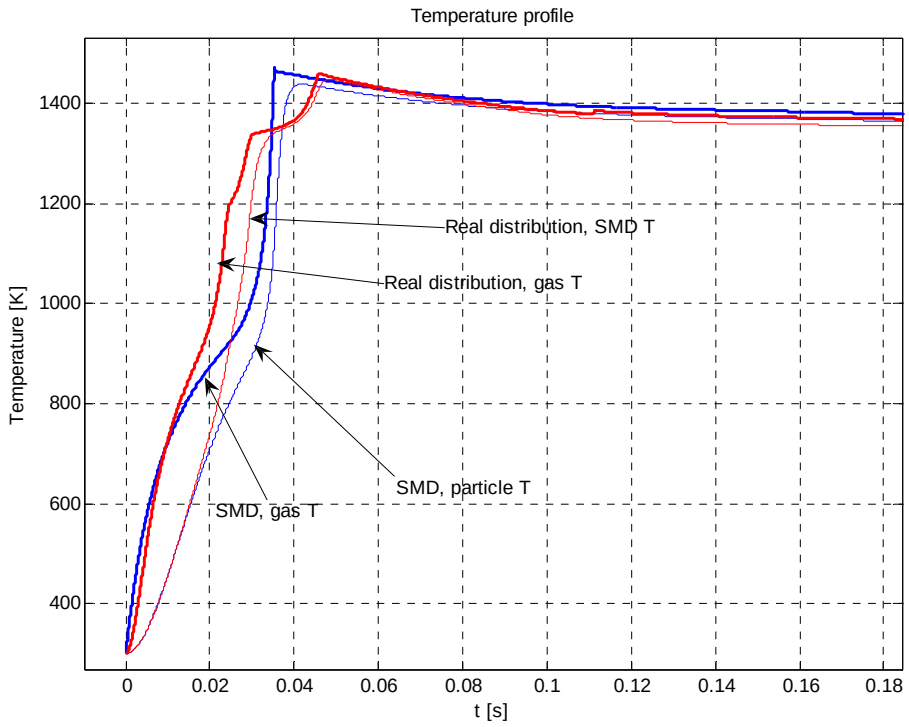

Fig. V.24. Comparison between temperature profile with real distribution and monosize, LAPC, pure air, ER = 1.

It is possible to see some differences in the temperature profiles: in the very first part the gas temperature in the case of real distribution increases faster than for the monosized distribution because in the case of real distribution there are particles smaller than the SMD that become combustible at earlier times. As these particles are burned out the rate of increase of T slows down, as now it is necessary to wait for the larger particles to burn. In the case of the monosized distribution, the particles are larger than the smallest particles of the real distribution, and hence it takes a longer time to heat up. Once they are combustible the temperature rise becomes much steeper than in the case of the real distribution, because the whole fuel becomes reactive at the same time. It is

apparent that it is possible to reach the maximum temperature faster for monosized distribution than with the real distribution, because in the case of real distribution the small particles do not provide enough energy to reach the highest temperature.

Particle evolution

Let now consider the volatile release rate for the LAPC biomass, see Fig. V.25;

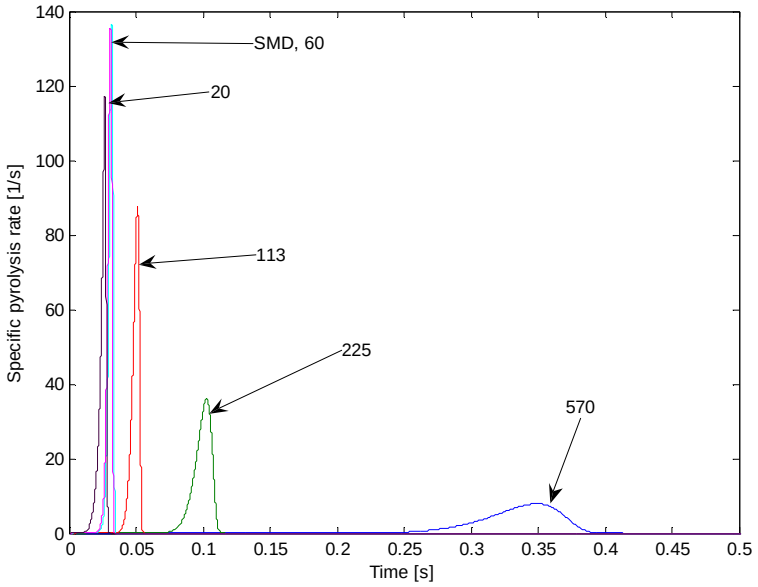

Fig. V.25. Volatile emission rate LAPC, pure air, ER = 1.

LAPC biomass releases its volatiles at a very high rate which then oxidize in the gas phase, consequently the gas stream is heated up very rapidly. The rapid release of volatiles consumes a large amount of oxygen in a very short time; this is one of the reasons why biomass is so effective in NO reduction: the higher is VM, the lower O_2 and higher the NO_x reduction.

The shape of Fig. V.25 is clearly dependent on the finite number of size groups: the spikes correspond to the five size groups. The SMD spike has been included to show the hypothetical behavior of particles with the SMD diameter. Discretizing the size distribution has forced the volatiles to evolve at some specific times. In a model with monosized fuels, there would be only one spike. The release of FN follows similar pattern.

As expected, the small particles are the first to release their volatiles as they are heated up first. It is interesting to compare the behavior of the same fuel when fired with pure and vitiated air for the SMD.

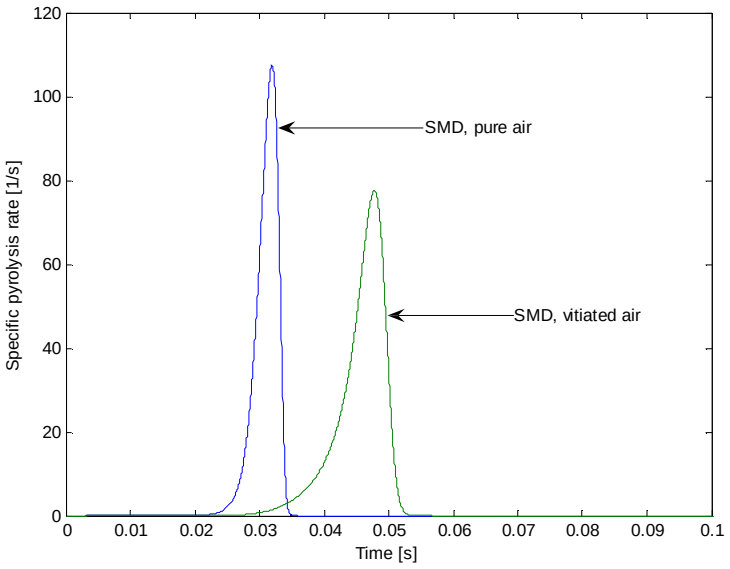

Fig. V.26. Comparison of normalized pyrolysis rate for pure and vitiated air, LAPC, ER = 1.

In Fig. V.26 the difference between the two cases is clearly seen. The pyrolysis process is delayed and the rate of release is reduced. This is due to the lower

temperatures due to the reduced oxidation rate and increased inert mass and hence slower heating rate.

It is also interesting to consider the specific mass of the various particle size groups versus time; the mass is divided by the initial particle mass. See Fig. V.27.

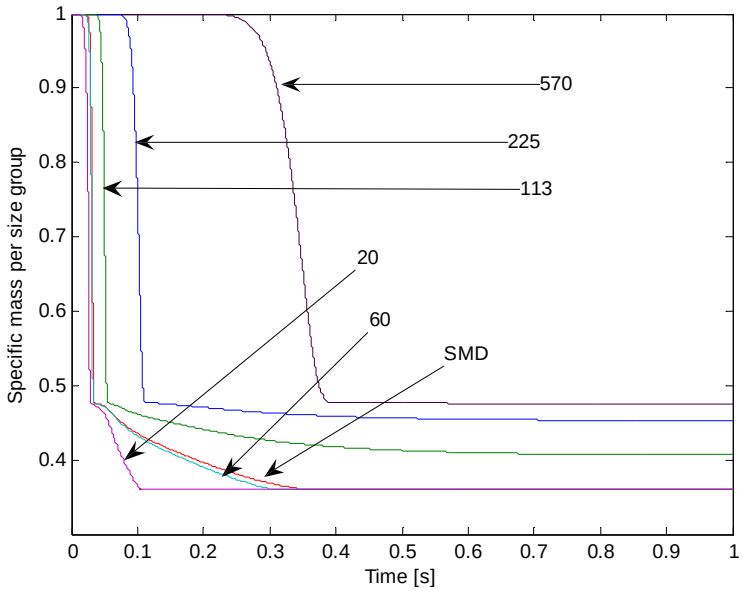

Fig. V.27. Specific mass per particle LAPC, pure air, ER = 1.

In Fig. V.27 it is possible to see that all the small particles show a first sharp decrease in their mass due to the loss of volatile matter. The largest size group presents the release of volatile matter at much later times than all the other classes.

The curves show a sharp decrease in mass loss rate due to slower heterogeneous reactions rates of fixed carbon; further this process is much slower, and occurs after the peak temperature. For the largest particles the second loss is almost negligible. It is also

possible to see the different amplitude of the two losses: the first one is much larger because the volatile content in the biomass is much larger than the fixed carbon content.

Fig. V.28 shows the fixed carbon fraction versus time, and it is clear that the fixed carbon consumption depends strongly on the particle size.

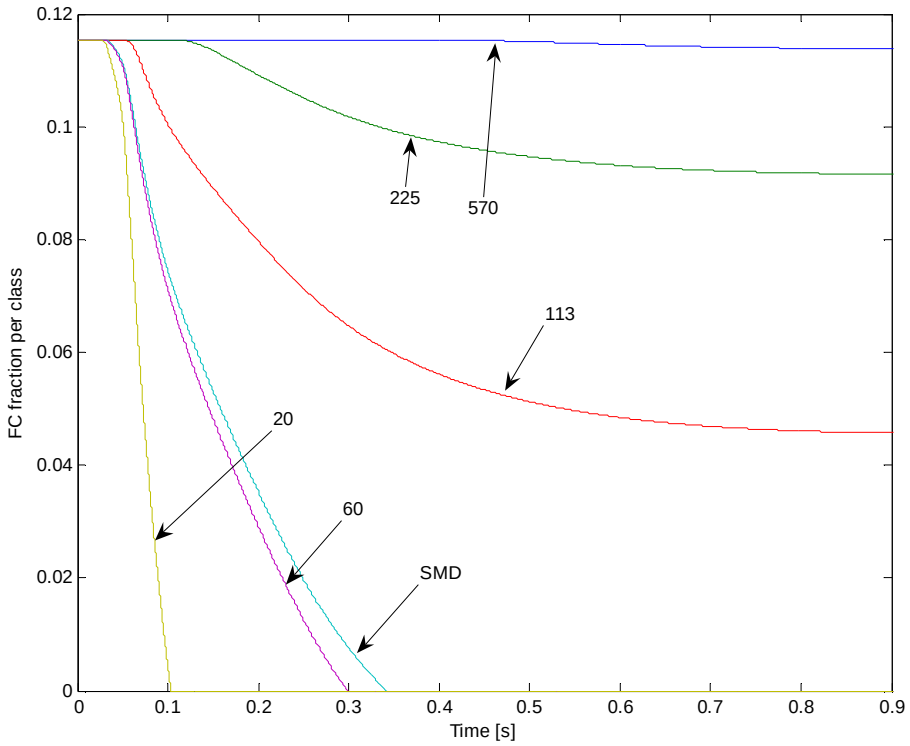

Fig. V.28. Fixed carbon fraction LAPC, pure air, ER = 1.

Only the two smallest size groups are able to burn out their fixed carbon; the SMD would be able to burn out all its fixed carbon. Particles with diameter of 113 μm and 225 μm consume only a part of their fixed carbon, while particles with diameter of 570 μm hardly consume their fixed carbon. This happens because it takes longer time for

the largest particles to be heated up; they never reach temperatures high enough for the heterogeneous reactions to become significantly fast.

Comparison with experimental data

Let us now compare the results from the simulation with the results from the experiment from Goughnour, [20].

Figs. V.29 and V.30 present a comparison of experimental data with numerical prediction for NO_x at the end of the reburn process, with the main burner providing 70% of the thermal power. In Fig. V.29 pure air is used as a carrier gas, while in Fig. V.30 vitiated air is used as a carrier gas.

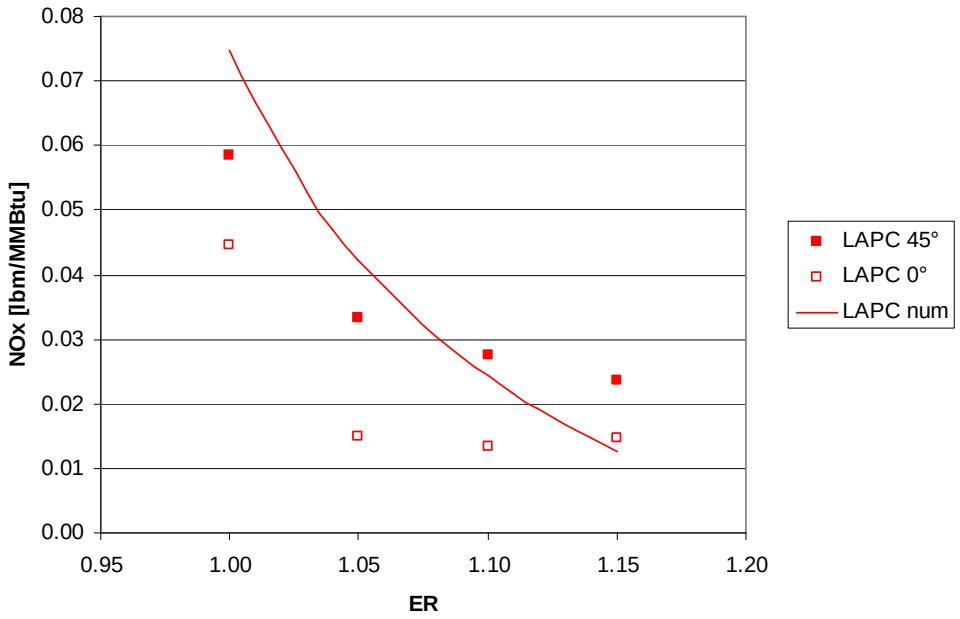

Fig. V.29. Comparison with experimental data LAPC, pure air.

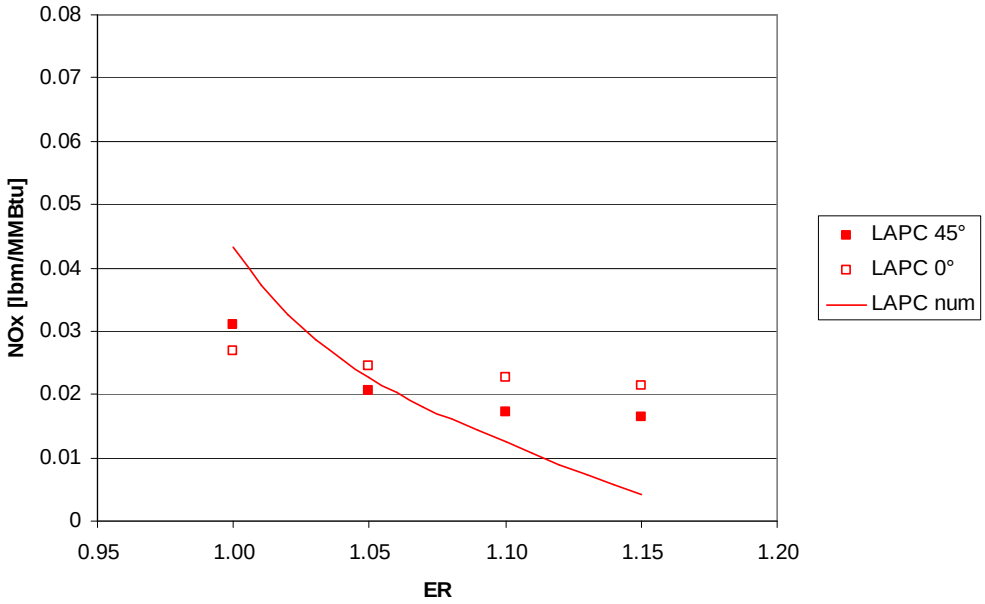

Fig. V.30. Comparison with experimental data LAPC, vitiated air.

In both cases (pure air and vitiated air) there is a good agreement between the experimental data and the numerical solution, which lends some credence to the present NO_x model. The model predicts the dependence of NO_x reduction on the ER and on the presence of vitiated air.

NO data

The NO and O_2 concentrations along the furnace are plotted when reburn gas is pure air, in order to gain a better understanding of the process (see Fig. V.31).

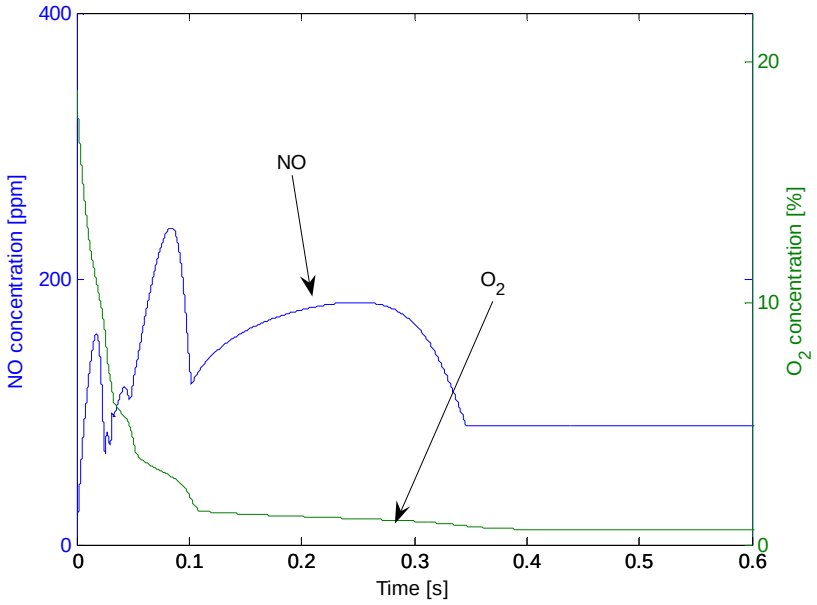

Fig. V.31. NO and oxygen concentration along the furnace, LAPC, pure air, ER = 1.

The NO concentration raises very quickly during the initial period, mainly due to the mixing of gases from the main burner which contains much NO and, partly due to the reactions of the FN that in this very first part might tend to produce NO instead of destroying it (this will be verified later). With increase in time, a sharp decrease in NO concentration occurs when some FN is released by a size group. The concentration increases again due to the contribution from the main burner gases. It is interesting to note that at the same time the oxygen concentration is rapidly decreasing and this is important in making the NO reduction even more effective; in this case, the ER is set at 1, so at the end of the process there should be no oxygen left. Actually there is a small fraction of oxygen left as it was shown that not all the fixed carbon is consumed.

The effect of ER on the NO concentration along the furnace is shown in Fig. V.32 for pure and vitiated air.

The NO concentration for the case of vitiated air is lower than the case of regular air simply because there is the dilution effect due to a larger amount of carrier gas; Figs. V.29 and V.30 have shown that the use of vitiated air does not lead to any significant improvement on the NO reduction. The shape of all the curves is somehow similar, characterized by the NO reduction when the FN is being released by a size group. The main difference between the stoichiometric and rich mixture cases is that the NO reductions due to the FN coming from the large particles (therefore reductions to take place at later times) are larger in the case of rich mixture because in the case of rich mixture there is less oxygen and so it goes down to very small concentration faster.

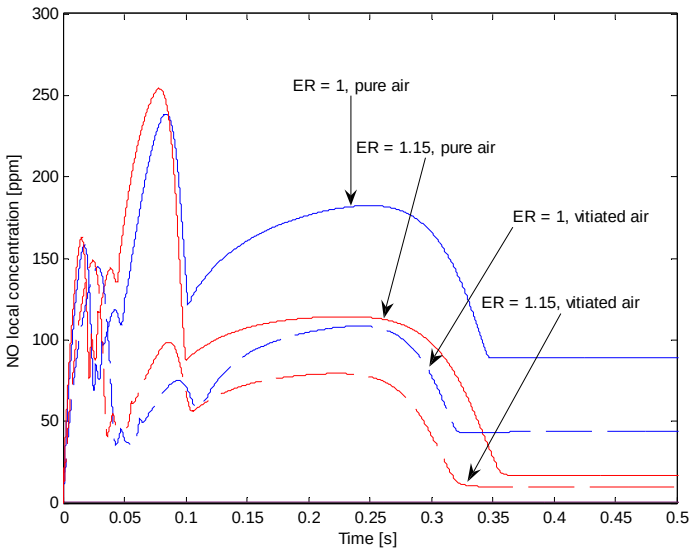

Fig. V.32. Comparison of NO concentration along the furnace, pure and vitiated air, LAPC.

It is useful to study the rate of the reactions for different reactions outlined in chapter IV that affect the NO_x chemistry in order to gain a better understanding of the NO_x reduction process.

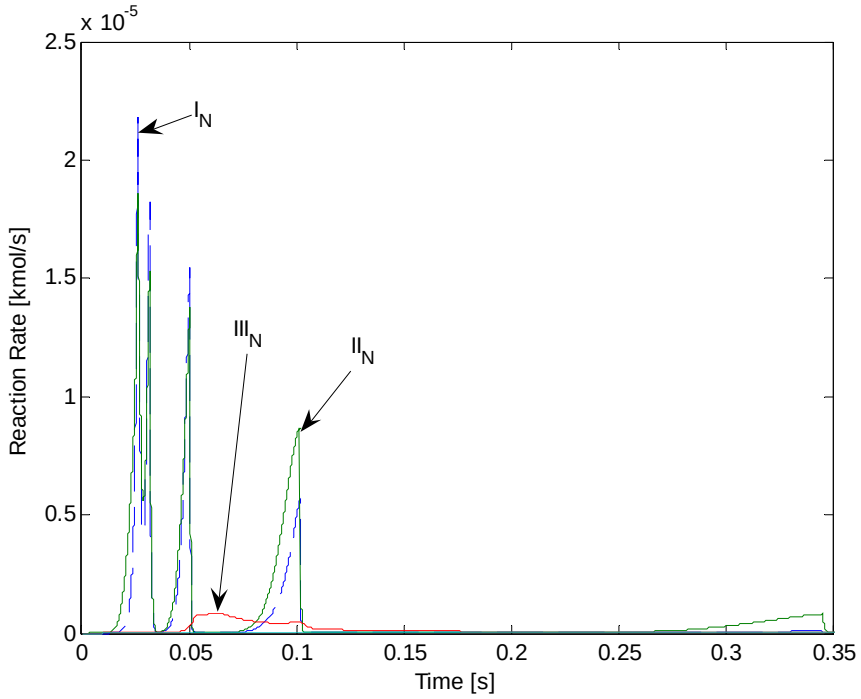

Fig. V.33. Reaction rate involving NO, LAPC, pure air, ER = 1.

Fig. V.33 shows the relative importance of the reactions: at the temperatures and conditions used in these experiments, the ammonia reactions are much more important than the reactions regarding HCN. The ammonia content in biomass is roughly the double of the HCN content, but ammonia reaction rates are much higher than double that of HCN. Thus reduction of the NO is driven by the presence of ammonia in the FN volatiles.

This plot explains the shape of the curve of the NO concentration in Fig. V.31. Initially there is still much oxygen in the gas phase, therefore when the FN is released it tends to react through oxidation reaction I_N producing more NO. It is seen from Fig. V.33 there exist three spikes reaction I_N which are faster than reaction II_N. After one tenth of a second the concentration of oxygen has decreased to a low value; so NO reduction reaction II_N becomes faster than I_N and so NO is being reduced. Also around 0.35s, when the largest size group releases FN, reaction II_N is dominant and at this point the oxygen concentration has become so low that oxidation reaction I_N is negligible. Among the reactions regarding HCN, the IV_N is absolutely negligible under these conditions. Reaction III_N, by which HCN reacts with oxygen to create NO, is present but its importance is not comparable with the ammonia reactions and as the oxygen is depleted the reactions becomes even slower.

High ash fuel

In the experiments conducted by Goughnour [20], for High Ash Partially Composted (HAPC) biomass the results for NO_x reduction do not appear to be good due to the high ash content, thus this fuel have been excluded from the modeling.

More than half of HAPC biomass is composed by ash, so in this case the ash content is so high that all the combustible may not be exposed to the reagents, besides with such a high ash content the hypothesis of the even distribution of ash in the particles is no longer valid: it is clear that it is very difficult to model successfully such a fuel.

In this case, the ash seems to be concentrated in the smallest size groups because most of the ash in this case is soil and soil can be ground into very small particles easier than regular biomass.

The importance of the HAPC fuel is very limited, as during the experiments Goughnour was able to complete only one run with HAPC biomass, as the ash content was so high to clog the furnace after only one run. Also the accuracy of the experimental results is very questionable. Due to these problems Goughnour did not have a complete test for HAPC biomass as for other fuels. The use of HAPC biomass in a pulverized fuel furnace is not advisable.

Wyoming coal

Wyoming coal is a subbituminous coal, a higher rank than lignite, and in fact it has a higher content of fixed carbon. This coal is expected to have slightly different behavior compared to lignite. It has a nitrogen content slightly lower than lignite and it is released mainly as HCN, and only in a small part as ammonia.

Temperature effect

Fig. V.34 shows the temperature profile along the furnace.

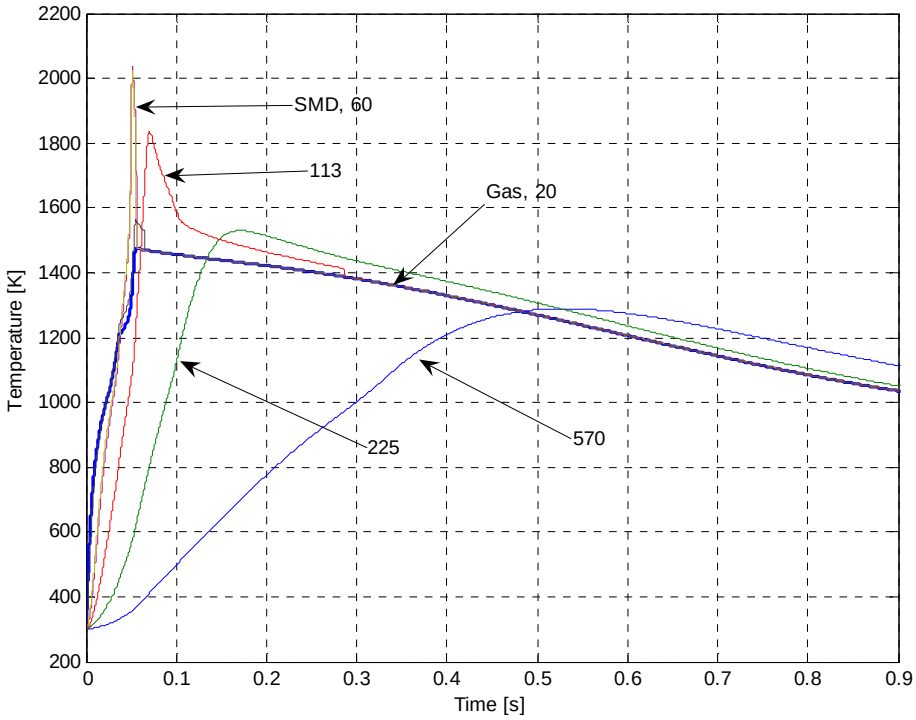

Fig. V.34. Wyoming coal temperature profile, pure air, ER = 1.

Its behavior is similar to that of Texas lignite, except that Wyoming coal has a more favorable size distribution than Texas lignite (most of the fuel is in the lower size classes) and ash content is much lower than for Texas lignite. Here the temperature of the particles can be well above that of the gas phase.

In the current case there is not much inert matter in the particle to absorb thermal energy and so the temperature of the particle raises rapidly as smaller size provides larger surface area per unit volume, making the heterogeneous reactions to proceed faster. The temperature of the particles then decreases due to the heat transfer to the gas phase that, once the fixed carbon is consumed, cools down the particles very quickly.

For the larger particle sizes, the peak temperature is lower since the oxygen has already been consumed, further surface area to volume is lower.

Particle evolution

Fig. V.35 shows the volatile emission rate for Wyoming coal.

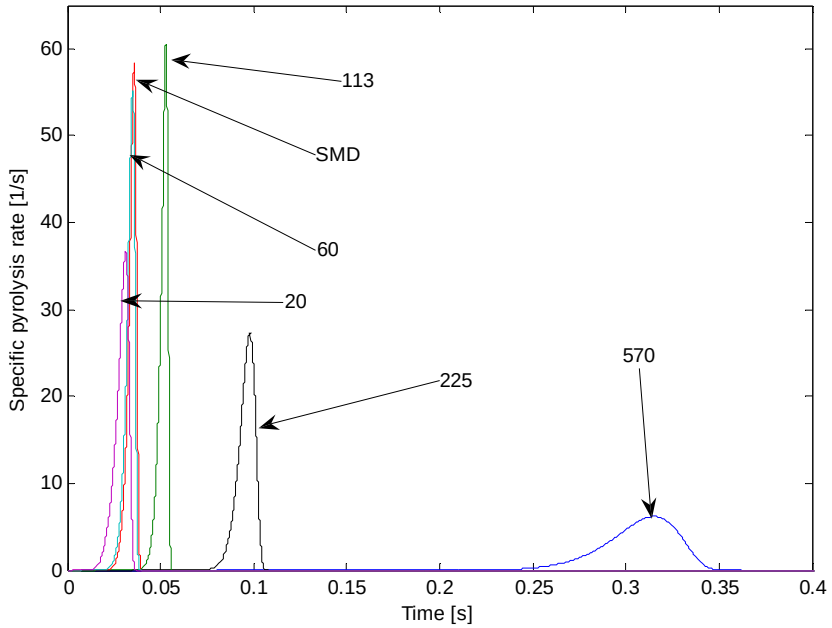

Fig. V.35. Volatile emission rate, Wyoming coal, pure air, ER = 1.

The specific pyrolysis rates are faster than those for Texas lignite because the particle temperature is higher. Also in this case it is easy to observe the emission from the various classes.

Fig. V.36 presents the mass loss for Wyoming Coal, divided by the initial mass of the particle.

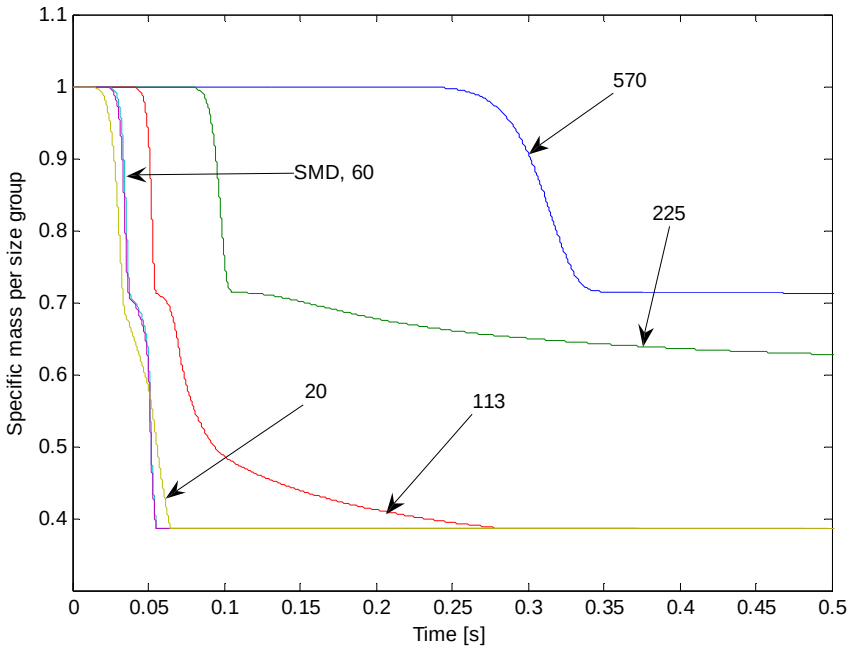

Fig. V.36. Total mass content per class, Wyoming coal, pure air, ER = 1.

Also in this case it is possible to observe the first sharp loss of mass that corresponds to the volatile loss, and afterwards a second mass loss corresponding to FC. In the two smallest particle size groups the second loss is almost as rapid as the pyrolysis as in these cases the particles reach such high temperatures that the heterogeneous reactions become very fast.

For the size group with a diameter of 113 μm, the second mass loss is still very significant, but is smoother. The class with diameter 225 μm consumes only a small fraction of its FC, and the class with 570 μm of diameter hardly consumes any FC. Also in this case the FC loss can be larger than the volatiles loss.

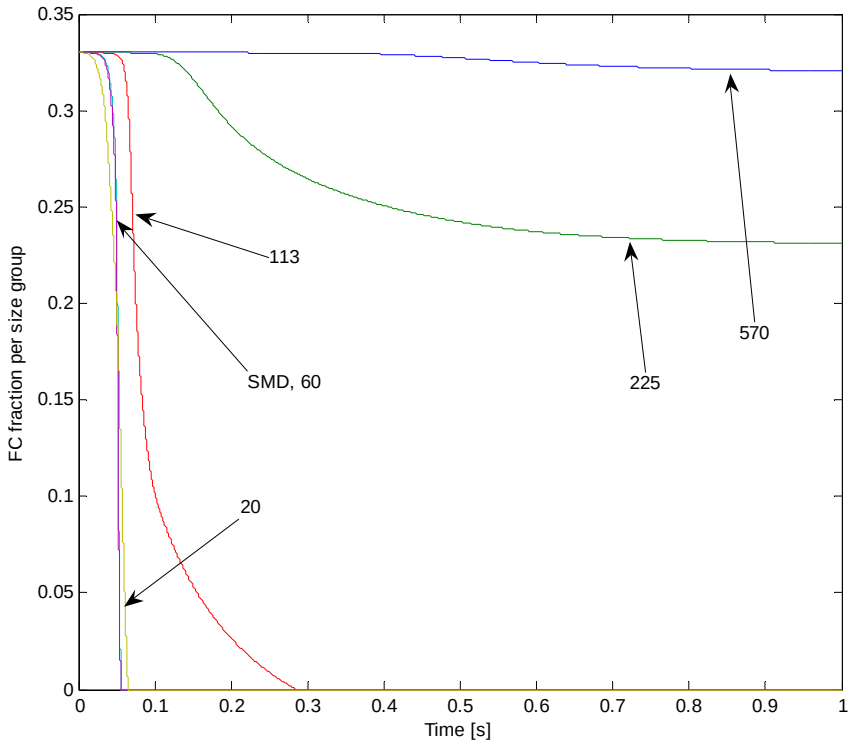

Fig. V.37. Fixed carbon fraction per group, Wyoming coal, pure air, ER = 1.

Fig. V.37 shows the FC fraction in the particles and it confirms what was revealed in the total mass plot: the three smallest size groups (and the SMD) are the only ones that are able to consume all their FC and the larger groups consume FC in part.

This plot could be misleading because it is true that also here the largest particle groups will not be able to consume all their fixed carbon, but still the amount of mass present in the largest groups is much lower than for Texas lignite, therefore the effect of this loss on the overall results is less important.

Comparison with experimental data

Figs. V.38 and V.39 show the comparison of the results from the model with the experimental results. The experimental data show poorer NO_x reduction with injection at 45° compared to 0°. However the model does not account for the effect of injection angle.

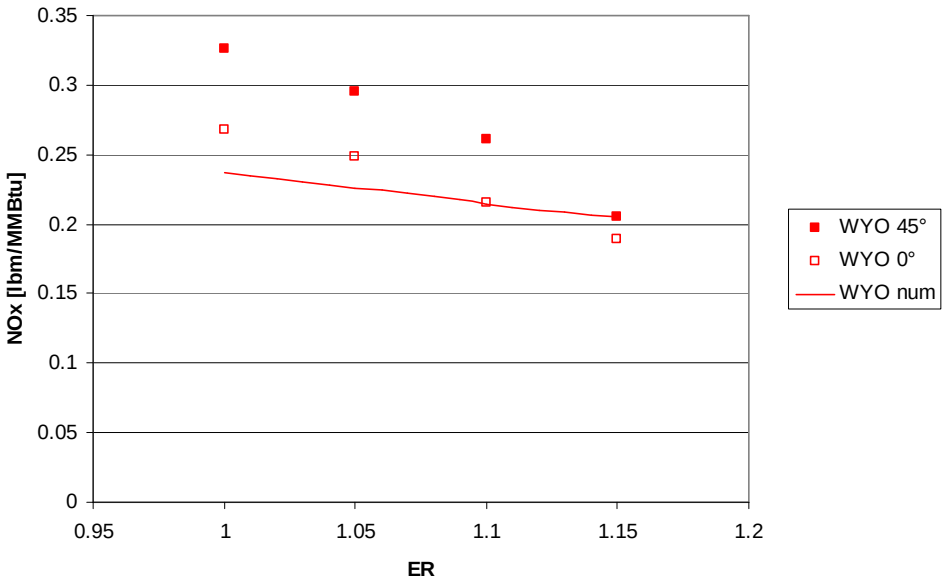

Fig. V.38. Comparison with experimental data, Wyoming coal, pure air.

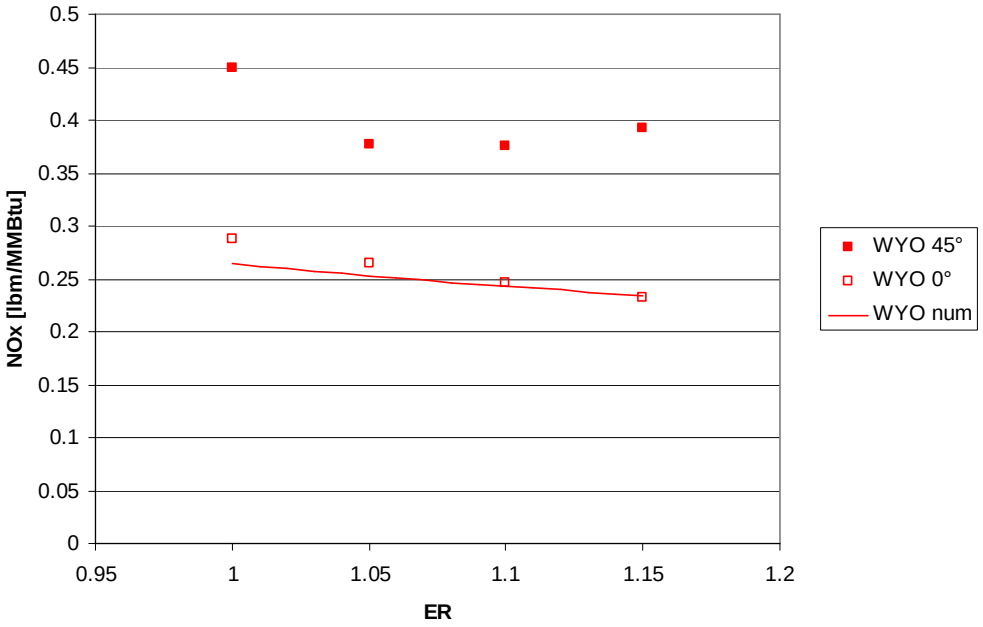

Fig. V.39. Comparison with experimental data, Wyoming coal, vitiated air.

The overall agreement is still good, especially with 0° data. In the case of pure air, the model slightly over estimates the NO emission, but as the mixture becomes richer the predicted concentration is closer to the experimental data, as shown before, as there could be more fluctuations in the experimental data near the stoichiometric condition.

In the case of vitiated air, the numerical solution matches the 0° data.

NO data

Consider now the NO and oxygen concentration along the furnace (Fig. V.40).

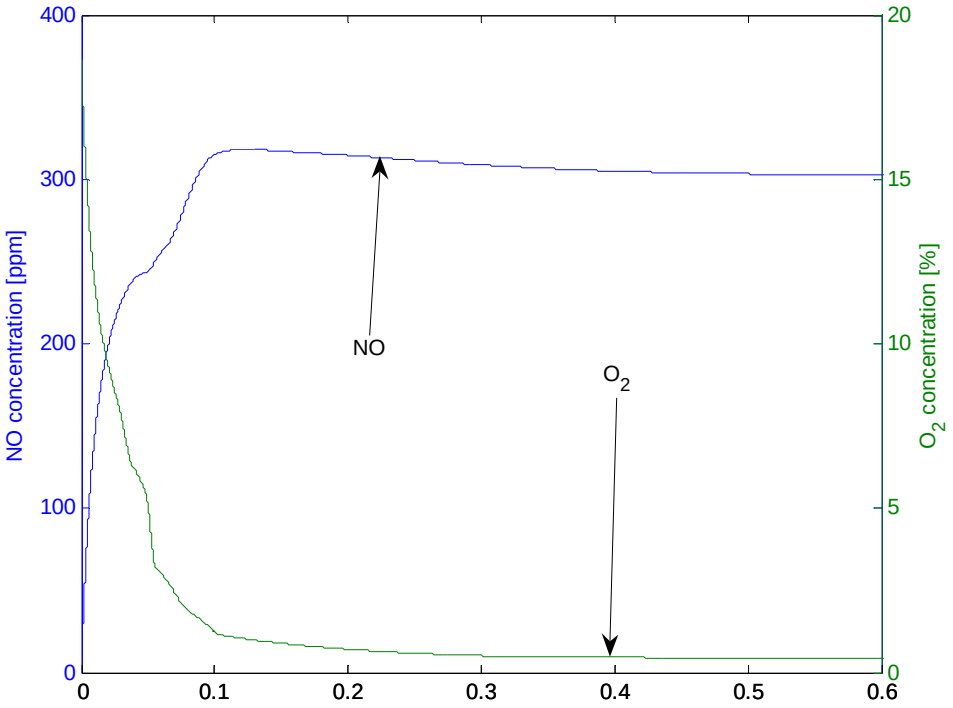

Fig. V.40. NO and oxygen concentration along the furnace, Wyoming coal, pure air, ER = 1.

This figure is similar to the one for Texas lignite. Also in this case the NO concentration raises very rapidly because of the mixing with the gas flow from the main burner and because of the reaction of the FN. The concentration of oxygen is slightly lower than the case of Texas lignite because the size distribution of Wyoming is more concentrated towards smaller size groups than for Texas lignite; therefore more coal can be burnt during the residence time and so more oxygen consumed.

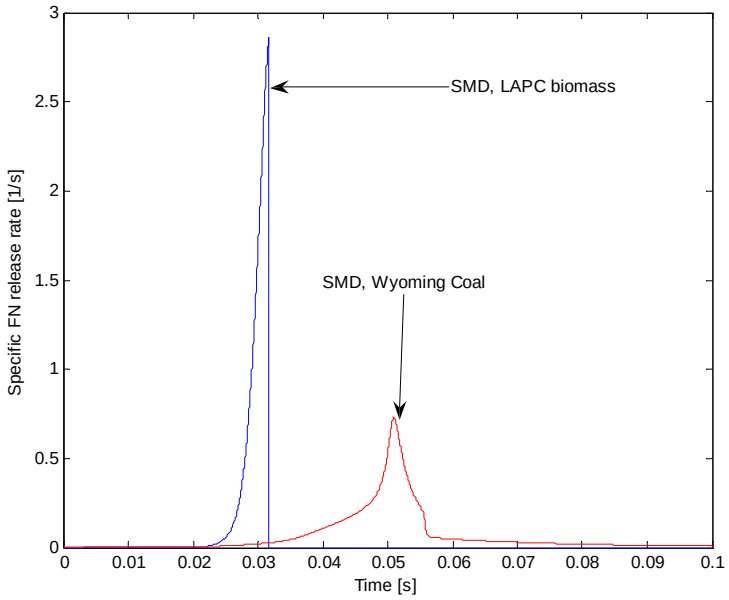

Fig. V.41. Specific FN emission rate comparison for Wyoming coal and LAPC biomass, pure air, ER = 1.

Fig. V.41 shows a comparison between the specific FN rate for LAPC biomass and Wyoming Coal. It is clear that the release rate from biomass results much faster and takes place earlier than for Wyoming Coal. The emission rate for Wyoming Coal is faster than for Texas lignite because the particles reach higher temperatures.

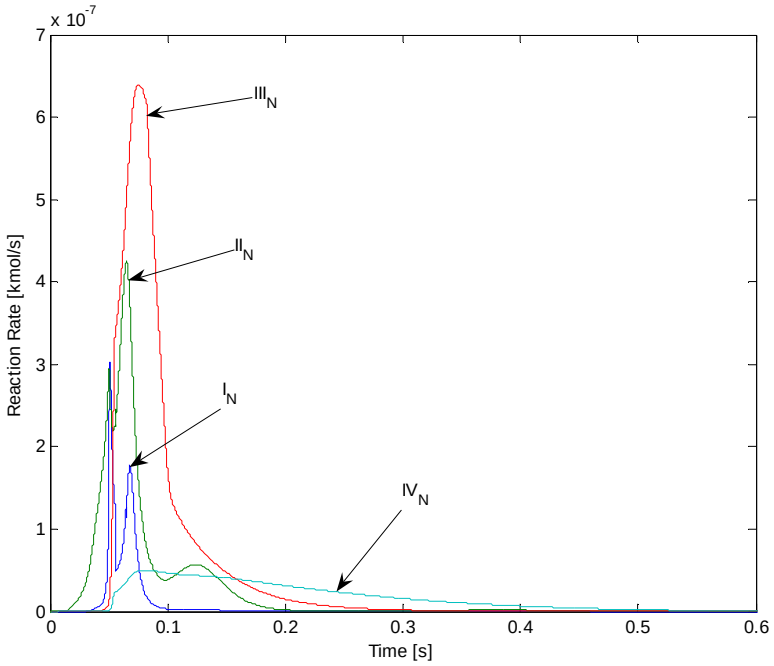

Fig. V.42. Reaction rates involving NO, Wyoming coal, ER = 1, pure air.

Fig. V.42 shows the reaction rates involving NO for Wyoming coal: the reactions are slightly faster than in the case of lignite since temperatures are slightly higher. The HCN oxidation reaction (III_N) is the dominant one, but the others cannot be neglected. As the oxygen concentration becomes low, then NO reduction reaction (IV_N) can become more important than III_N. This is what causes the small NO reduction in Fig. V.40; unfortunately the reaction contribution arrives too late when NO has already been produced and the temperature is decreasing freezing all the reactions.

Fuel blends

Let us consider the cases of fuel blends. Different blends of LAPC biomass and Texas lignite coal have been tested to determine their reburn performance. As mentioned

earlier, the composition percentages refer to mass and not to energy; this means that a 50 % TXL – 50 % LAPC blend is formulated with half biomass and half coal on mass basis. The blend, when fired to the burner must provide the same overall thermal power as that of the pure biomass or coal. The two fuels will have their own size distribution function. In all the plots, the solid lines will be for biomass while the dashed lines will be for coal.

Small amount of LAPC biomass was mixed with coal also in order to ascertain catalytic effects, if any, which may be present with LAPC biomass. However catalytic effects, if any, can be determined only by the experiments since the model does not account for these effects except through modification of kinetics constants.

The study of the behavior of blends is especially important as this might be the preferred choice in the first large scale experiments, since only a small amount of biomass would be mixed with coal therefore reducing the risks of corrosion or fouling behavior that are not completely controlled for biomass.

The main burner operation conditions are the same as for the case of single fuel, the only difference is that now there will be two different fuels injected together at the reburner. The two fuels are premixed before being put in the same hopper to be sent to the reburn injection, so it is reasonable to assume them to be well mixed.

90% Texas lignite – 10% LAPC Biomass Blend

Temperature effect

Fig. V.43 shows the particle temperature profile with the thick line representing the gas temperature. Fig. V.44 shows the same results on an enlarged scale.

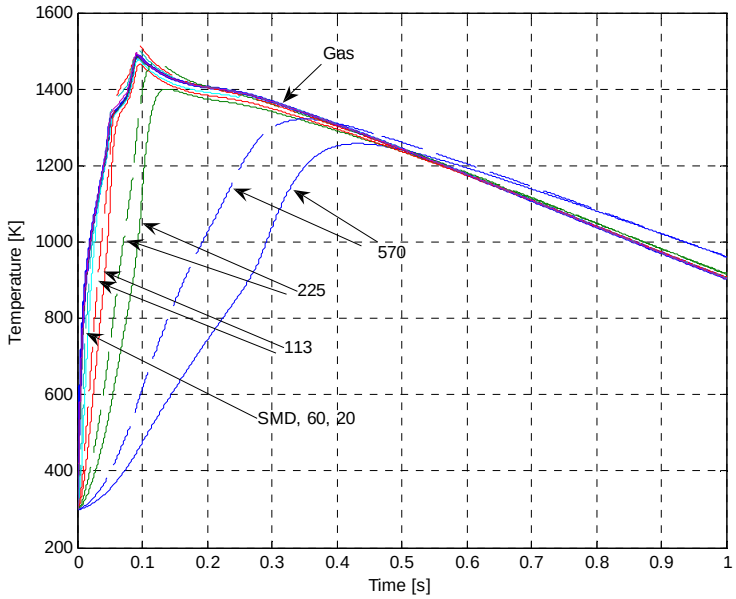

Fig. V.43. Temperature profile 90:10 Blend, pure air, ER = 1.

The particles of the two fuels behave differently in the combustion, as it could have been expected, considering the differences between the fuels.

Texas lignite is the closest fuel to biomass, so these differences may not be large but still distinct. In the initial period, the particles of coal are heated up slightly faster than those of biomass (for the same size) because of the following reasons: i) pyrolysis is an endothermic process; therefore it tries to cool down the particles; biomass has a much higher content of volatiles than coal, so during the devolatilization the absorption of heat from the pyrolysis will be larger for biomass than for coal. ii) biomass has a very low FC, and this is the only source of heat within the particle; therefore the generation of heat due to heterogeneous reactions is less important for biomass than for coal. iii) Texas lignite used in these experiments has a moisture content higher than LAPC biomass:

moisture is not bound with any strong bonds to the particle structure and so it evaporates almost instantaneously as the fuel is injected in the combustion chamber; for this reason coal particles lose a larger amount of mass due to the moisture, therefore their density decreases and so they may be heated up rapidly.

The overall difference can be noted easily on the large particles since in the smallest particles the heat up is so fast that these effects are not so evident.

Once the pyrolysis of biomass is complete, these particles have lost a large fraction of their mass, therefore the char particle will be less dense compared to coal char and so can be heated up much faster; it is seen that the slope changes after pyrolysis is completed, however they do not reach the same temperature as those of coal.

In the case of coal, the particles reach high temperature since a larger amount of FC reacts with the oxygen at the particle surface. The heat generated at the particle surface tends to drive up the particle temperature higher than the gas phase. Once the fixed carbon is consumed, the temperature of these particles decreases rapidly.

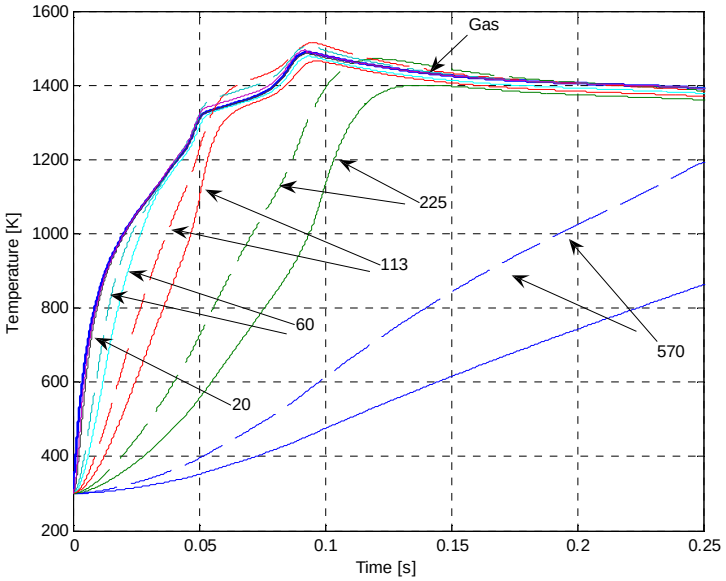

Fig. V.44. Temperature profile, 90:10 Blend, (Fig. V.43 enlarged).

The overall behavior of the gas phase is similar to what happens in the case of pure lignite as 10% content of biomass is not such a large fraction on heat basis to significantly change the results of pure coal. Still there are two important differences: the heat up time is slightly shorter and the maximum temperature is slightly higher. This is due to the biomass volatiles serving as ignition source for the coal, as they are released rapidly and at lower temperature [55], therefore providing some extra energy in the initial period of the reburn.

Let us now see the effects of the vitiated air on this fuel.

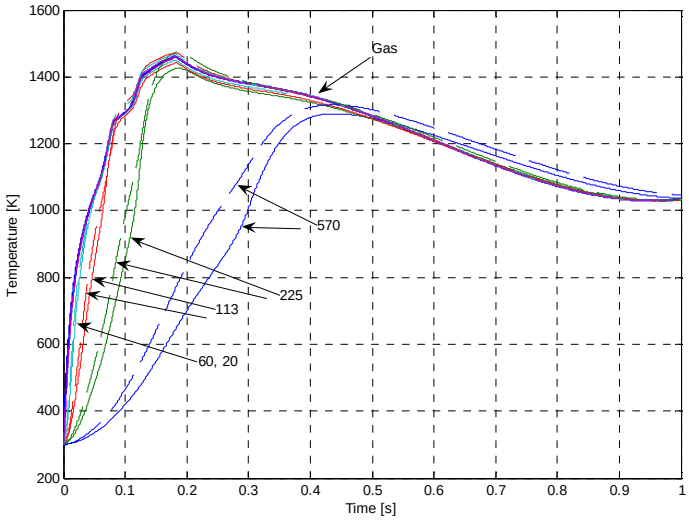

Fig. V.45. 90:10 Blend temperature profile, vitiated air, pure air, ER = 1.

Fig. V.45 shows the temperature profile for the 90:10 Blend, using vitiated air; the effect is the same observed in all the other cases: now all the temperatures are lower and the heat up time is slightly longer, due to the effect of a larger amount of inert gas.

Particle evolution

It can also be interesting to note the difference in the mass loss of the two fuels (see Fig. V.46): for clarity only the size groups of diameter 20 μm, 113 μm and 570 μm are shown. The figure confirms what was observed for the two fuels separately: the initial mass loss, corresponding to the devolatilization, is much more significant for biomass than for coal, while the second mass loss, corresponding to the fixed carbon consumption, is larger for Texas lignite. It is also seen that for both fuels, the second mass loss is much slower than the first one and the largest size groups hardly consume any fixed carbon in both cases.

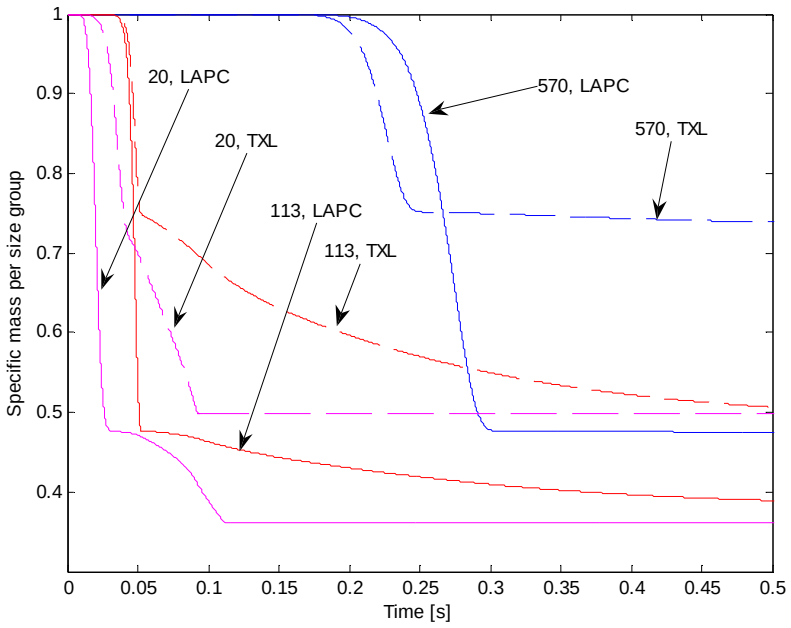

Fig. V.46. Normalized mass loss for 90:10 Blend, pure air, ER = 1.

Comparison with experimental data

The simulation data on the NO_x concentration is compared with the experimental results in Figs. V.47 and V.48.

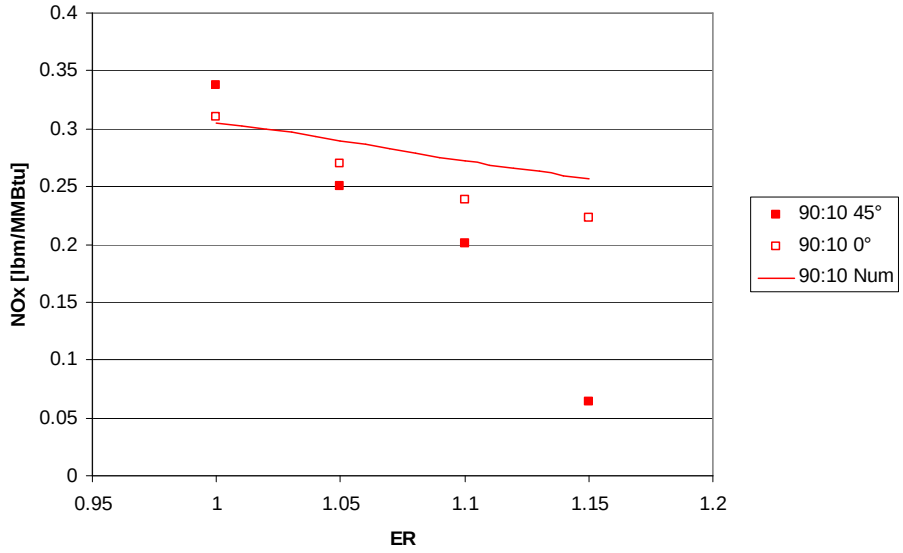

Fig. V.47. Comparison with experimental data, 90:10 Blend, pure air.

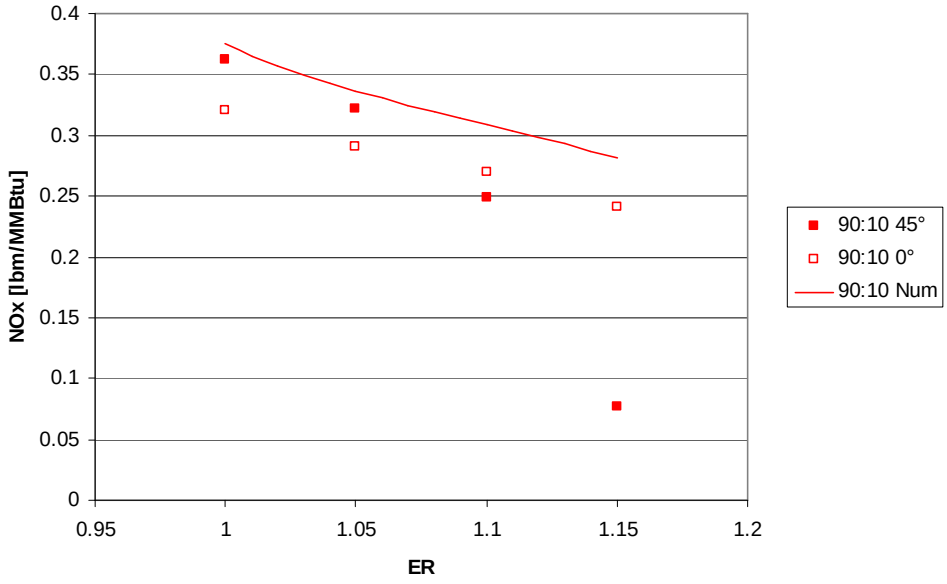

Fig. V.48. Comparison with experimental data, 90:10 Blend, vitiated air.

Recall that the reduction of NO is better for TXL with 45° injection and pure air as carrier gas, while the 0° injection is better for vitiated air (Figs. V.14 and V.15). The experimental data for the blend seems to be better at 45°.

The numerical prediction matches fairly well with the experimental data, and results are closer to data corresponding to the 0°. Also in this case the use of vitiated air does not lead to any significant improvement of the NO reduction.

NO data

Fig. V.49 shows the NO and oxygen concentration along the furnace, compared to the case of Texas lignite.

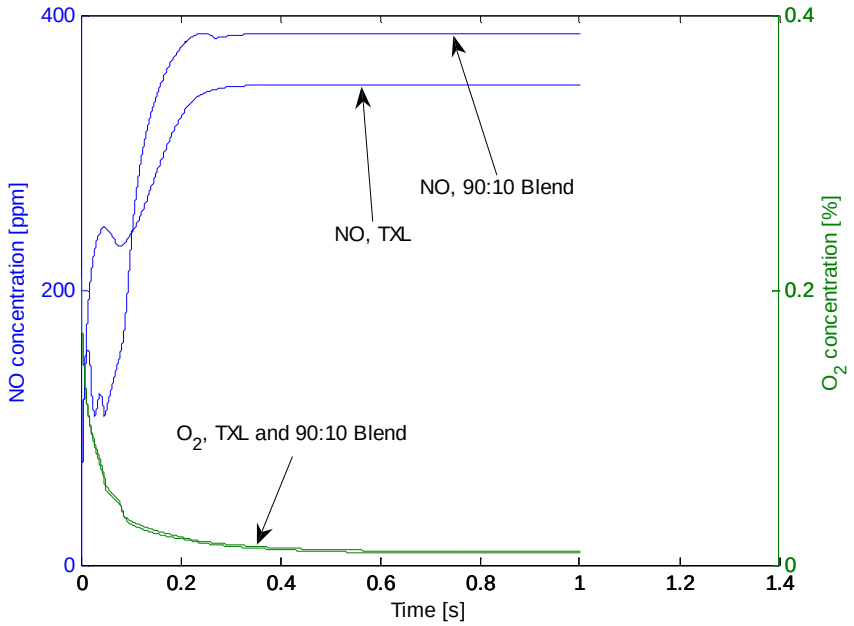

Fig. V.49. NO and oxygen concentration along the furnace, 90:10 Blend vs TXL, pure air, ER = 1.

The NO concentration reaches very high levels when gas is mixed with main burner gas as soon as the coal releases its FN as HCN; the ammonia released from biomass initially tends to reduce the NO; the line is kind of flat for a short time. However afterwards, as the lignite releases the HCN and more oxygen is available from the mixing with the main burner gases, the NO concentration increases very fast; later, when oxygen concentration becomes low it is possible to see that the NO concentration reduces a little, but it is too late to reduce it: most of the FN has already been consumed and the temperature is decreasing. The overall behavior is not far from the one of pure lignite. Small differences are noticed only in the initial part of the curve of the NO concentration, as in the case of TXL there is hardly any reduction. The oxygen concentration along the furnace is almost the same.

It is interesting to note that the final NO concentration is higher than the case of pure lignite since higher temperatures which promote more oxidation reactions with NH_3 released from biomass. This is confirmed from the experimental data.

In order to explain the process, consider the reaction rates, as shown in Fig. V.50.

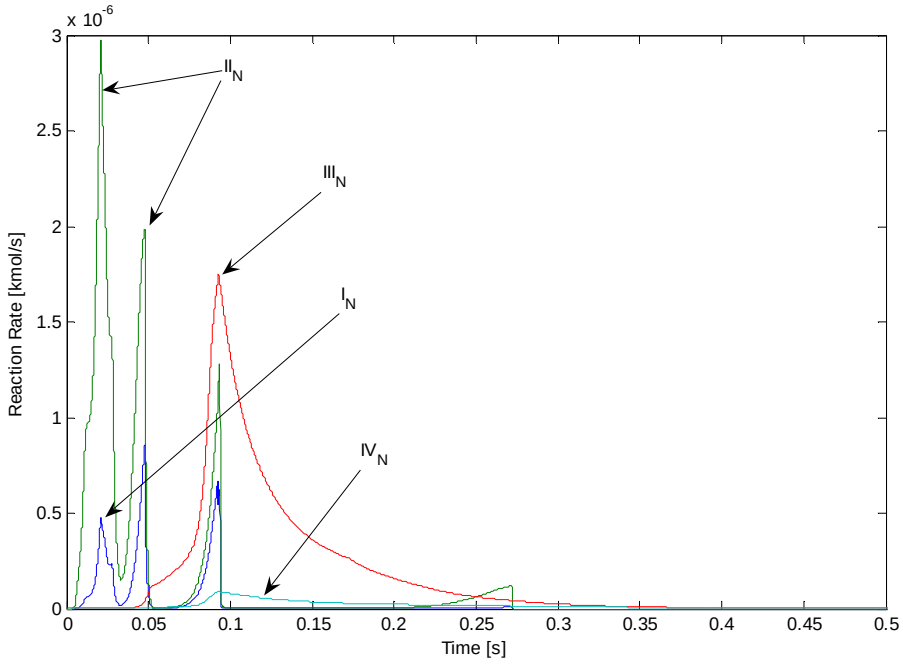

Fig. V.50. Reaction rates involving NO, 90:10 Blend, pure air, ER = 1.

Fig. V.50 offers an important insight in this case: it is possible to see that initially reaction II_N (reduction of NO with ammonia) is dominant, during which biomass is releasing its FN. Despite the small quantity of ammonia present its reactions are clearly noticeable. Later, as lignite starts releasing its FN, reaction III_N (oxidation) becomes the dominant reaction which causes the NO increase seen in Fig. V.49. A small part of the lignite FN is emitted as ammonia, and this explains the spikes of the ammonia reactions corresponding with the spike of reaction III_N; still this amount is far from being enough to lead to a NO reduction. Finally it is interesting to note that the reactions are faster than those of pure lignite as the temperatures are now slightly higher.

70% TXL – 30% LAPC Blend

Temperature effect

Let us now consider the 70:30 Blend, which has a larger fraction of biomass. Fig. V.51 shows the temperature profile.

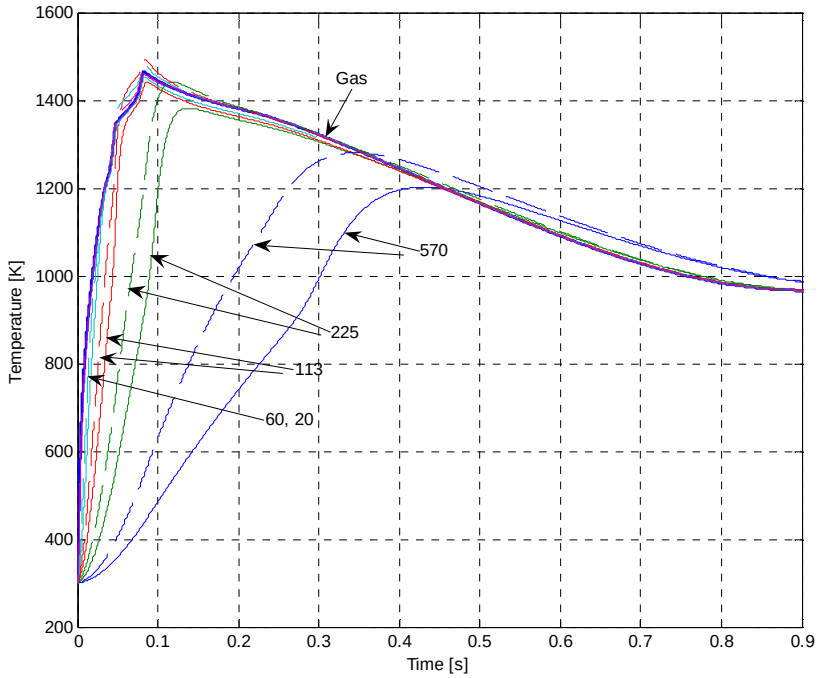

Fig. V.51. Temperature profiles 70:30 Blend, pure air, ER = 1.

As expected the heating up rate is faster than in the case of the 90:10 blend and also faster than the pure lignite case. Temperatures however are slightly lower than those of the previous case; evidently the larger fraction of biomass significantly affects the combustion of FC also lowering the maximum temperature reached by the particles. It is seen that the biomass particles never reach a temperature above the gas. The overall

temperature profile is not much different from the 90:10 blend and all the observations made are still valid.

The volatile loss and particle mass loss curves are similar to those shown for the 90:10 blend; the values will be slightly different, but the same conclusions would be drawn: biomass releases its volatiles much faster than coal, and the large particles do not have the time to consume their FC.

Comparison with the experimental results

Fig. V.52 provides a comparison of the predictions with the experimental data for pure air while Fig. V.53 presents the results for vitiated air.

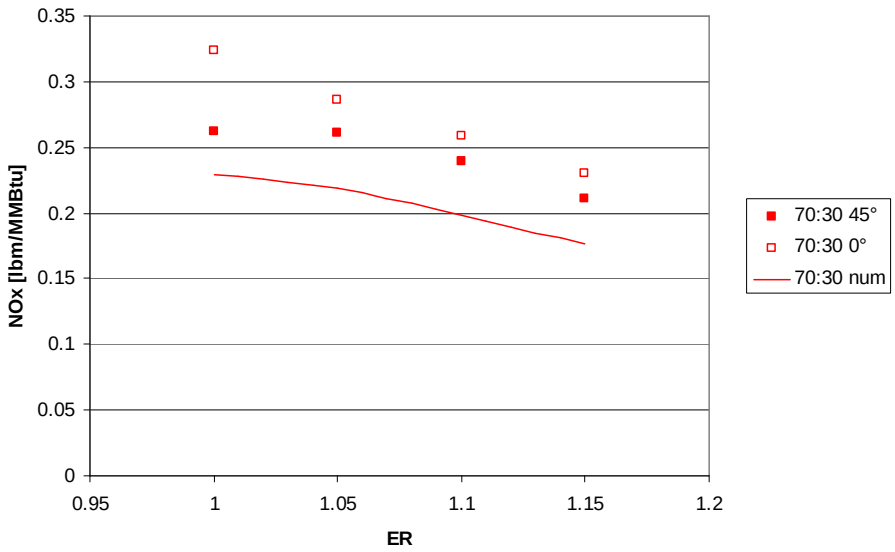

Fig. V.52. Comparison with experimental data, 70:30 Blend, pure air.

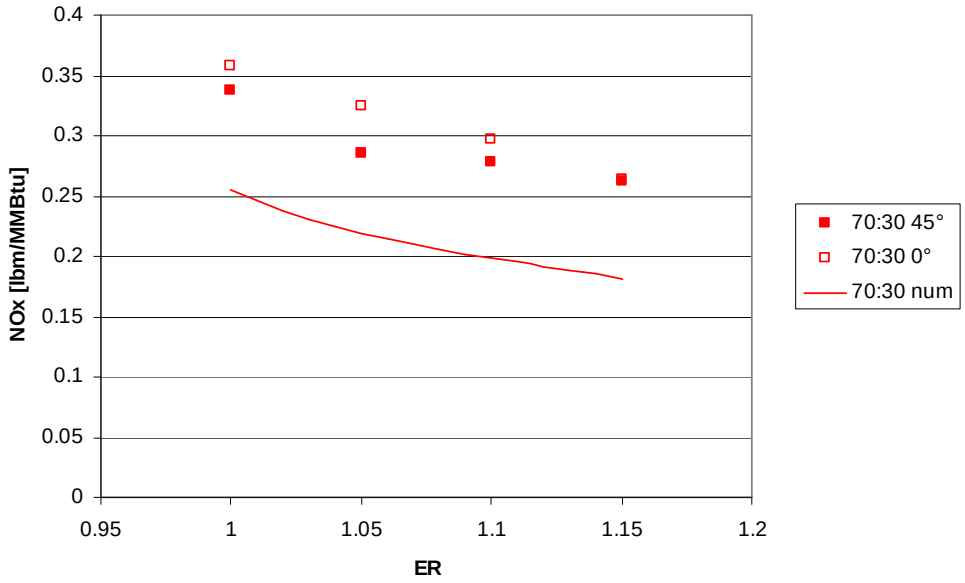

Fig. V.53. Comparison with experimental data, 70:30 Blend, vitiated air.

For the 70:30 blend, 45° is better for NO_x reduction compared to 0°, as in the case of lignite (Fig. V.14) for both pure and vitiated air.

For the case of pure air, the agreement of predictions with experimental data is not very good; in fact it is one of the worst cases studied: the prediction is off the experimental results by around 25%.

Particle evolution

Fig. V.54 shows the reaction rates for the 70:30 Blend. It is interesting to compare these rates with the ones for the 90:10 Blend (Fig. V.50).

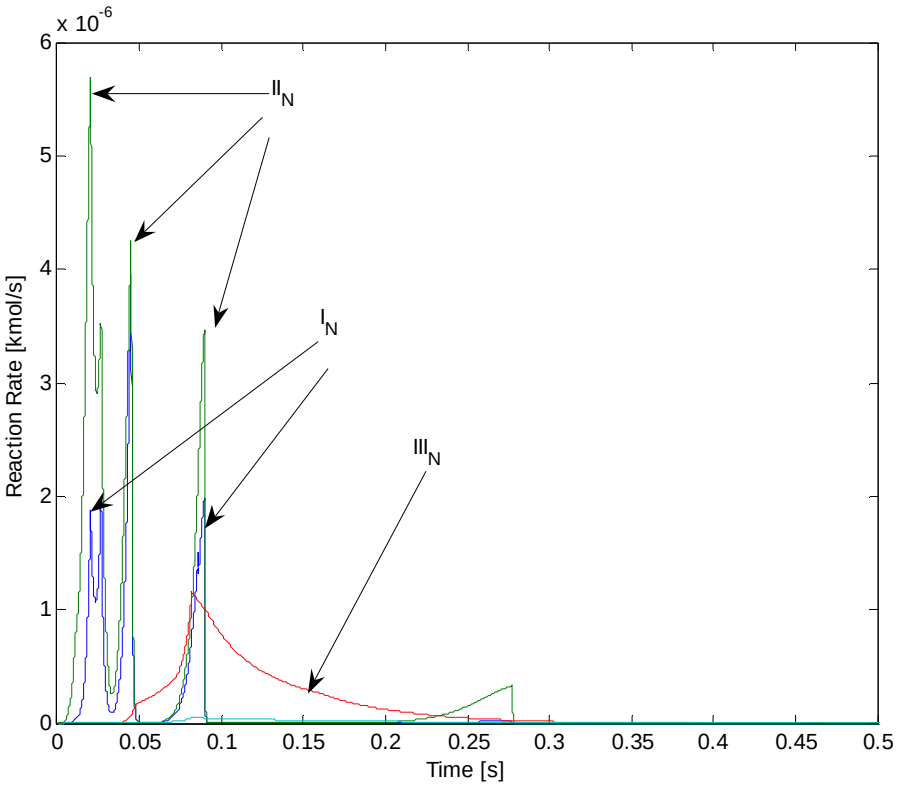

Fig. V.54. Reaction rates involving NO, 70:30 Blend, pure air, ER = 1.

Comparing this figure with the one for the 90:10 blend it is evident how the larger fraction of biomass strongly affects all the reactions: now there is much more ammonia available and less HCN, therefore the ammonia reactions (I_N and II_N) become dominant. The reaction III_N is still important but its rate has decreased.

50% TXL – 50% LAPC Blend

Temperature effect

For the 50:50 blend the contributions from coal and biomass are significant; so the expected behavior should be somewhere in between the two pure fuels.

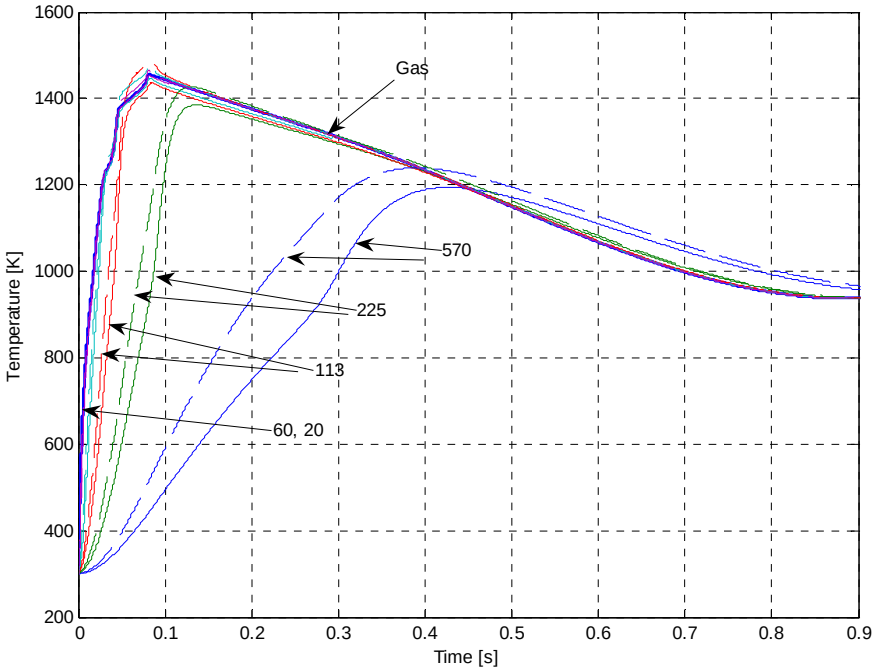

Fig. V.55. Temperature profile, 50:50 Blend, pure air, ER = 1.

As seen in Fig. V.55, the heating rates of particles in this case is faster than those of 70:30 Blend case; heating rate is closer to the case of pure biomass, as expected. As before the biomass particles have a temperature lower than those of coal particles with the same size. Also in this case, the coal particles reach temperatures higher than the gas phase.

Comparison with experimental data

Figs. V.56 and V.57 show a comparison of the numerical results with the experimental data:

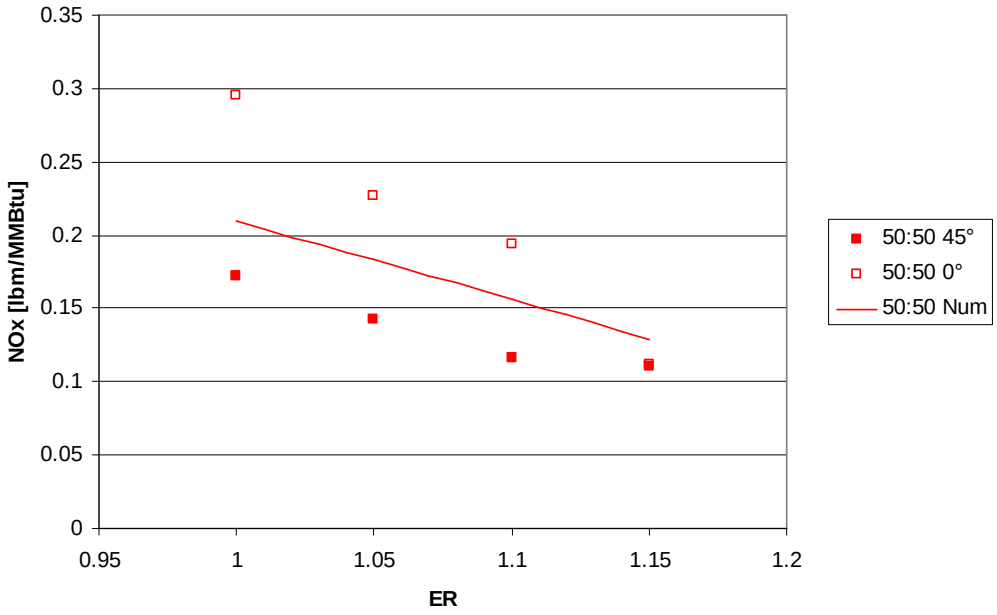

Fig. V.56. Comparison with experimental data, 50:50 Blend, pure air.

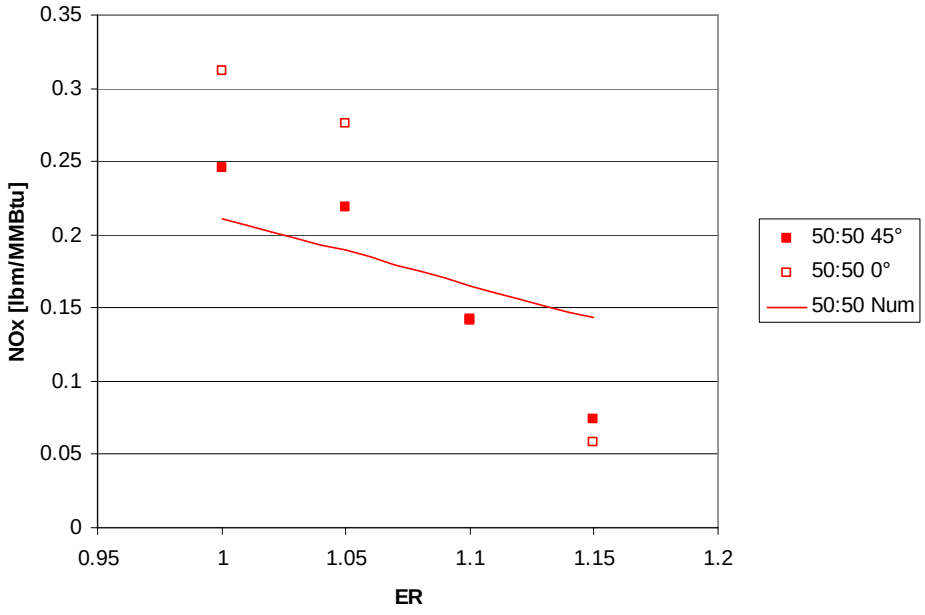

Fig. V.57. Comparison with experimental data, 50:50 Blend, vitiated air.

It is seen that the prediction lies between the two series of data and the difference between the two sets of experimental data is reduced as the RZ mixture becomes richer. Also at rich condition, the prediction is very close to the experimental points.

In the case of vitiated air, the result from the model agrees fairly well with the experimental results underestimating the dependence of the NO emission on the ER.

Summary of NO results

After having analyzed the NO emission for the pure fuels with pure air or vitiated air as carrier gas, it is useful to present the results for all fuels on the same figure in order to differentiate their effectiveness in reducing the emission of NO. As results for Texas lignite and Wyoming coal are similar, only Texas lignite is shown, and among the blends only the 50:50 is drawn.

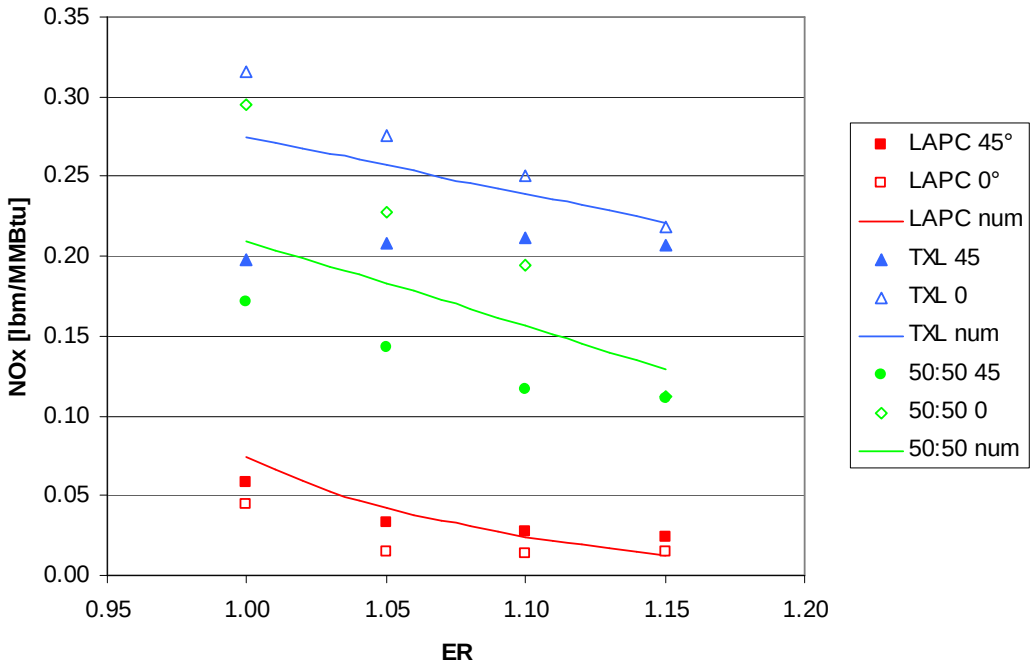

Fig. V.58. Comparison of the NO_x emission for different fuels.

From Fig. V.58 the different effectiveness of these fuels is absolutely evident: LAPC biomass is much more effective on NO reduction than what Texas lignite. The 50:50 Blend leads to results somewhere in between the two fuels, but actually closer to coal than to biomass.

Mercury results

Mercury evolution during the pyrolysis and the heterogeneous combustion is not very well understood due to its complexities. A simple model is adopted here. There is an interesting potential for gaining a large mercury oxidation fraction for the combustion of a blend of coal and biomass, as coal has a higher content of mercury but little chlorine

(when compared to biomass), while biomass has much less mercury but more chlorine than coal. This is particularly true for the coals under consideration in these experiments. Texas lignite and Wyoming coals are more widely used on Texas utilities. These are low rank coals that have a small amount of mercury, along with a small content of chlorine; in literature it is reported that higher rank coals, though having a larger content of mercury, have a larger oxidized fraction, and this is due to the larger content of chlorine [5].

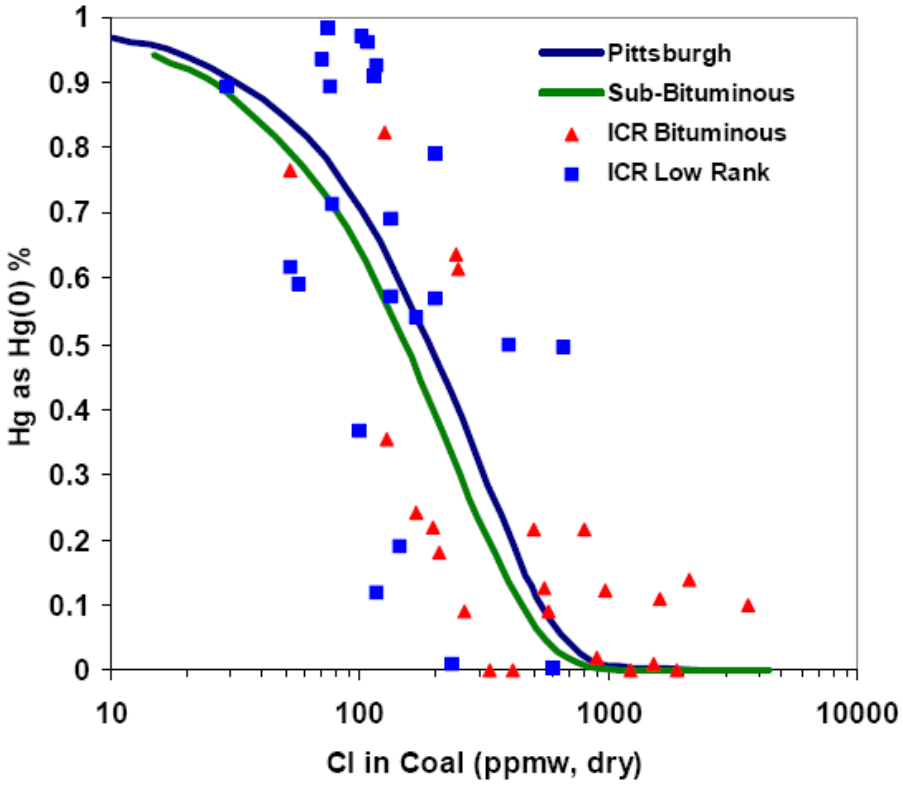

Fig. V.59. Hg and Cl content in various coals [56].

Fig. V.59 shows how the mercury and chlorine content for many coals of different ranks.

The presence of more biomass (which has a much larger chlorine content than coal) would be useful since the presence of chlorine favors the oxidation of elemental mercury (which is less soluble in water) to $HgCl_2$, which is highly soluble in water. The oxidized form of mercury is the easiest one to take out of the exhaust, particularly using wet scrubbers. The objective of this part of the model is to estimate the percentage of oxidized mercury for the different fuels.

Note that the present model does not consider Hg present in the particulate form. See Table 6 for the quantitative data on the Hg and Cl contents.

Texas lignite

Also for mercury Texas lignite is considered to be the base case fuel. Texas lignite has a mercury content three times larger than biomass and a chlorine content almost hundred times lower, therefore it is interesting to see the differences of the performance between these fuels in the oxidation of mercury. It is reasonable to expect that the mercury oxidation will be much lower than for biomass.

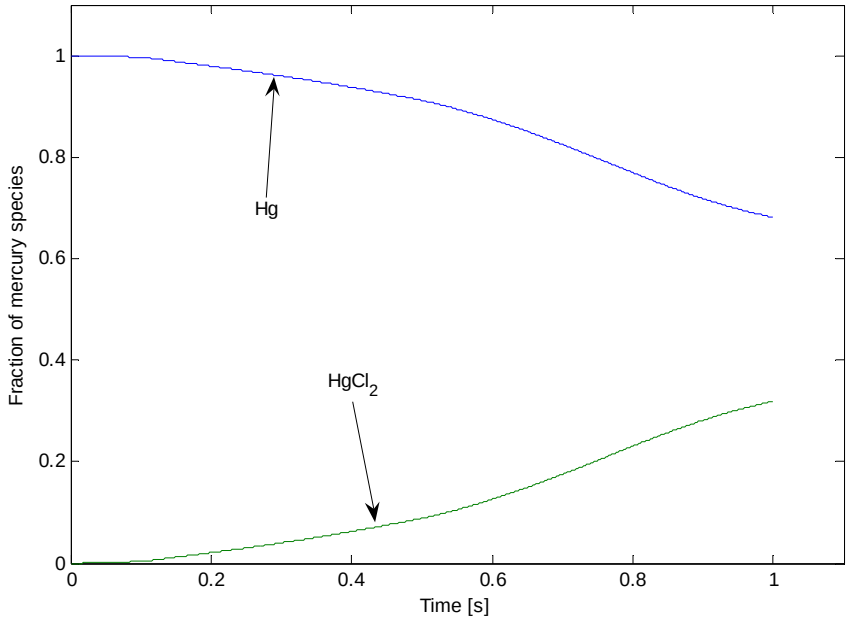

Fig. V.60. Mercury speciation in the gas phase, Texas lignite, pure air, ER = 1.

Fig. V.60 shows the mercury speciation in the gas phase for Texas lignite. It is easy to see that the elemental mercury curve is higher compared to oxidized mercury.

In this case the oxidation is smaller than 35% of the mercury present in the coal. It is important to note that this result is consistent with what has been found in literature: for most of the coal fired power plants, the amount of oxidized mercury is not larger than 40%.

Fig. V.61 shows the reaction rates for the case of Texas lignite.

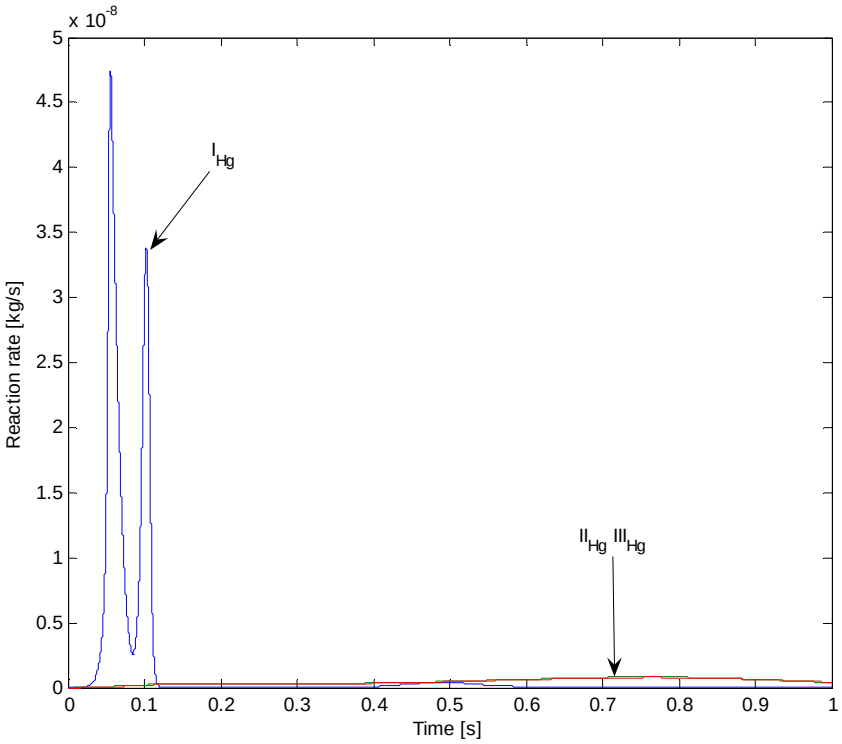

Fig. V.61. Reaction rates involving Hg, Texas lignite, pure air, ER = 1.

From the diagram it is possible to see that the reaction I_{Hg} (Cl production from HCl) is much faster than the other two: the first reaction is the one that produces the elemental chlorine from HCl, and it is reasonable to expect this reaction to be very fast, since the highest temperatures are encountered in the initial period, further the dissociation of water will be highest producing more OH.

Fig. 62 presents an enlarged version of Fig. 61.

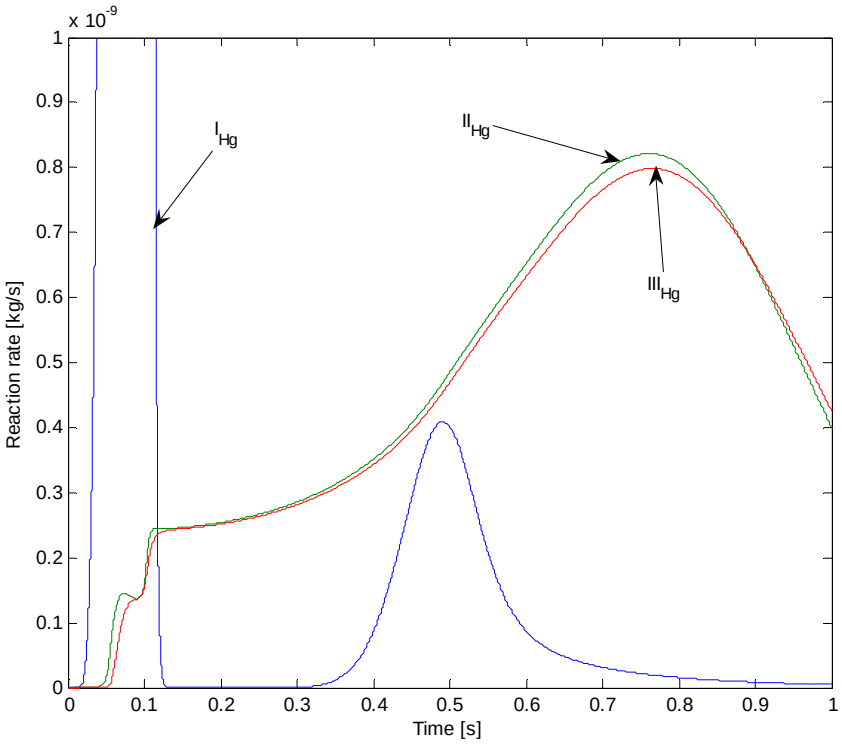

Fig. V.62. Mercury reaction rate, Texas lignite, (Fig. 61 enlarged).

The rates of reactions II_{Hg} and III_{Hg} are almost equal and they have a very smooth curve along the furnace as the mercury and chlorine is being emitted from the coal particles. They are relatively insensitive to the temperature variation along the furnace because they have very low activation energies.

Different ER would affect marginally the oxidation of mercury in this model; their only effect is to change slightly the concentration but this effect is very small. Simulations carried out with different ER confirm that the mercury reduction hardly changes, therefore results are almost independent of ER.

The use of vitiated air should not change much the results as the reactions do not depend on the oxygen concentration, except through slight temperature dependence and OH concentration. The dilution effect and the reduction of temperature should slow down all the reactions but this effect is not expected to be very important.

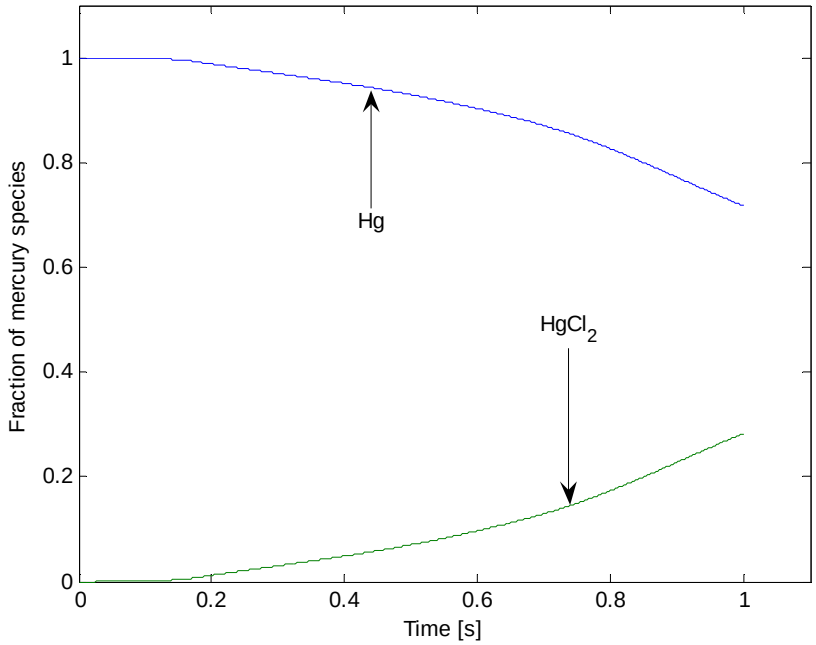

Fig. V.63. Mercury speciation in the gas phase, Texas lignite, vitiated air, ER = 1.

Fig. V.63 shows the result for the case of vitiated air: in this case the effect of dilution is slightly more significant than for biomass (see figure on page 143): the oxidation percentage is smaller than in the case of pure air, but still the difference is not significant. Also the reduction starts later as the heating rate is slower. The difference between the case of pure air and vitiated air is larger than for biomass because the

chlorine content is so small that evidently a reduction of the temperature is enough to reduce the OH concentration, therefore slowing all the reactions.

LAPC biomass

Consider the speciation of mercury in the case of reburning with LAPC biomass.

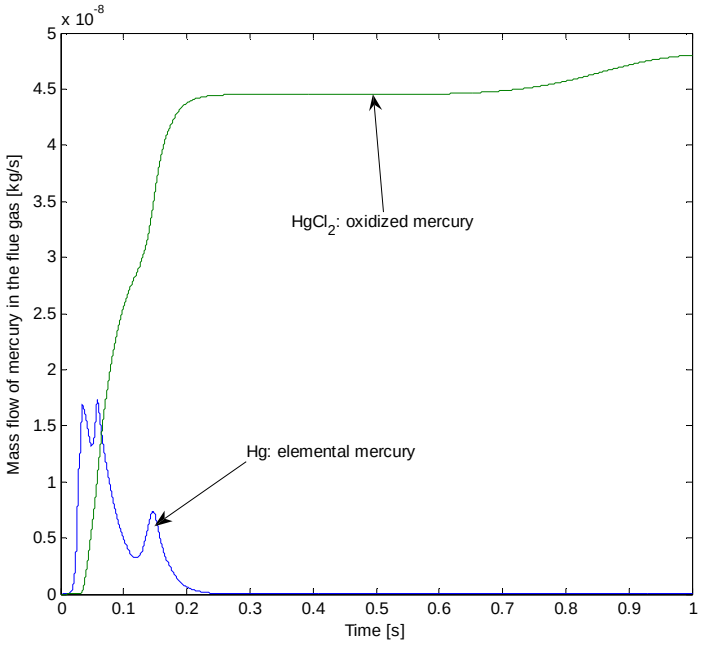

Fig. V.64. Mercury fractions, LAPC biomass, pure air, ER = 1.

Fig. V.64 shows the mass of mercury species present in the gas phase along the furnace. From this diagram it is clear that in this case most of the mercury is in oxidized form and all the amounts are extremely low. In the previous figure the amount of mercury species in the gas phase is increasing as mercury is being released from the

particles. Fig. V.65 shows how mercury is actually split into the different forms along the furnace.

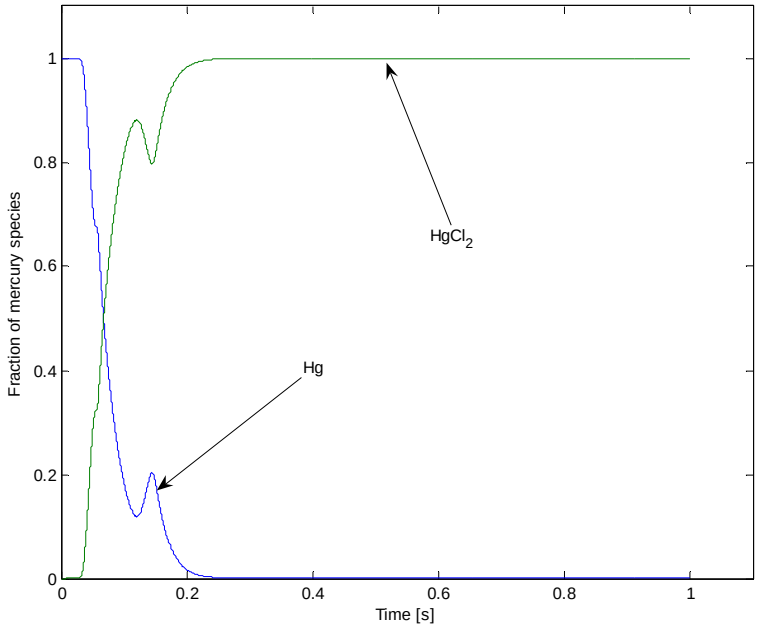

Fig. V.65. Mercury speciation in the gas phase, LAPC biomass, pure air, ER = 1.

Fig. V.65 reveals a significant reduction with biomass as a reburn fuel: all the mercury tends to be oxidized. Fig. V.66 shows the reaction rates involving Hg.

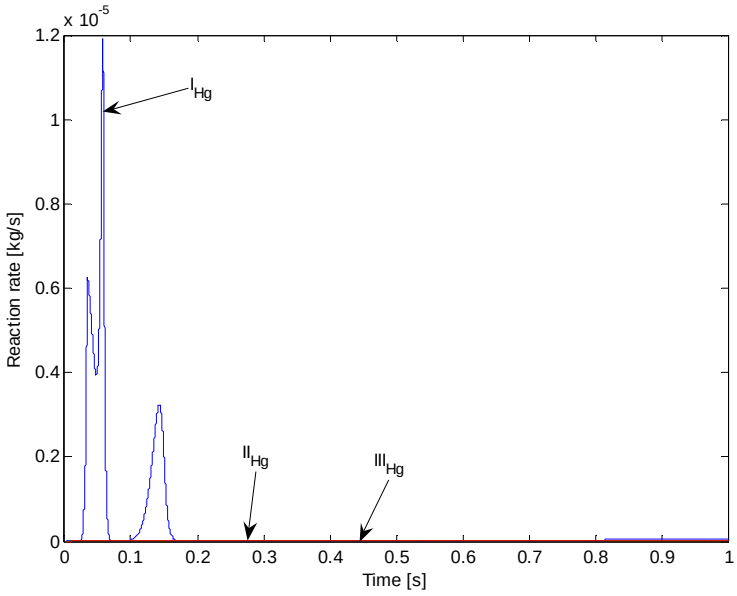

Fig. V.66. Reaction rates involving Hg, LAPC biomass, pure air, ER = 1.

Reaction I_{Hg} is much faster (around three orders of magnitude) than for Texas lignite due to the much larger content of chlorine, the peak is in the area of maximum temperature, as it is here that the OH concentration will be highest.

The previous plot is shown on a logarithmic scale in Fig. V.67.

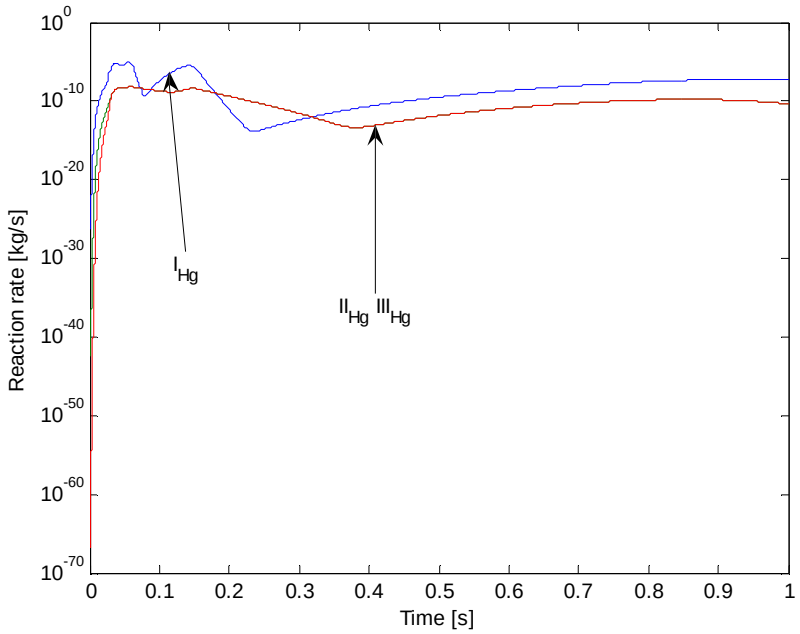

Fig. V.67. Reaction rates involving Hg, LAPC biomass, logarithmic scale, ER = 1.

The rates of reactions II_{Hg} and III_{Hg} should be almost equal. The spikes coincide with the release of mercury and chlorine along with the volatiles. The reactions of Hg are fastest in the first part since there is a larger amount of mercury and chlorine available; while they are insensitive to temperature due to low activation energy, they are indirectly affected by the temperature due to sensitivity of OH to temperature; the OH decreases as T decreases. It is interesting to note the presence of some reactions in the tail end of the curve, which corresponds to the release of mercury and chlorine from the largest particle size.

Let now consider the case of vitiated air (see Fig. V.68): in these reactions there is no dependence from oxygen, so the only effect would be the different concentration of the elements. Further the results have weak dependence on different temperature profiles

because the difference in the temperature is not dramatic and the activation energies of these reactions are very small.

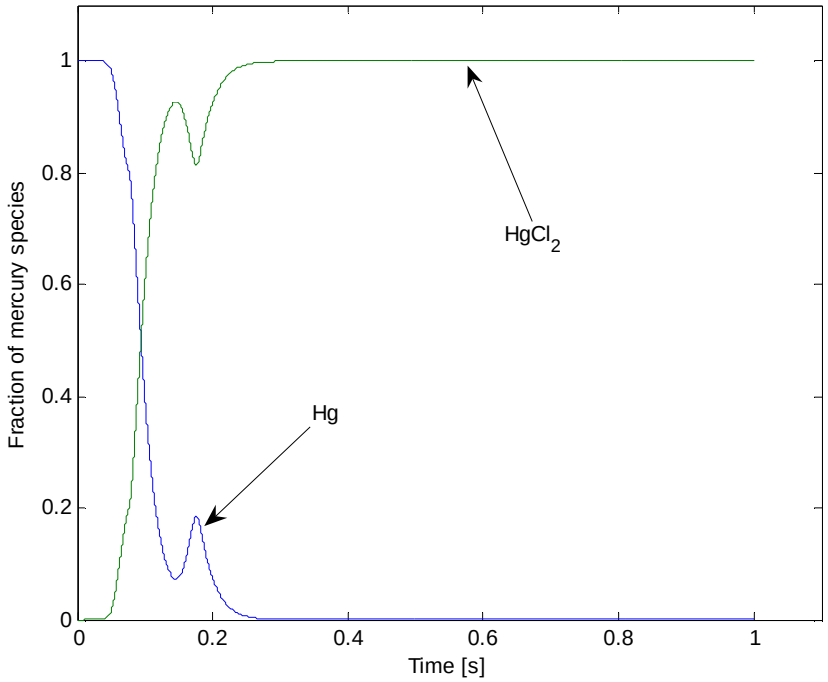

Fig. V.68. Fraction of mercury species in the gas phase, LAPC biomass, vitiated air, ER = 1.

As expected, the mercury fractions differ marginally from the case of pure air.

Wyoming coal

Wyoming coal has a mercury content slightly smaller than Texas lignite and a chlorine content larger; therefore it is expected to perform slightly better than Texas lignite, but its Hg oxidation level is not expected to reach the levels of biomass. Results are shown in Fig. V.69.

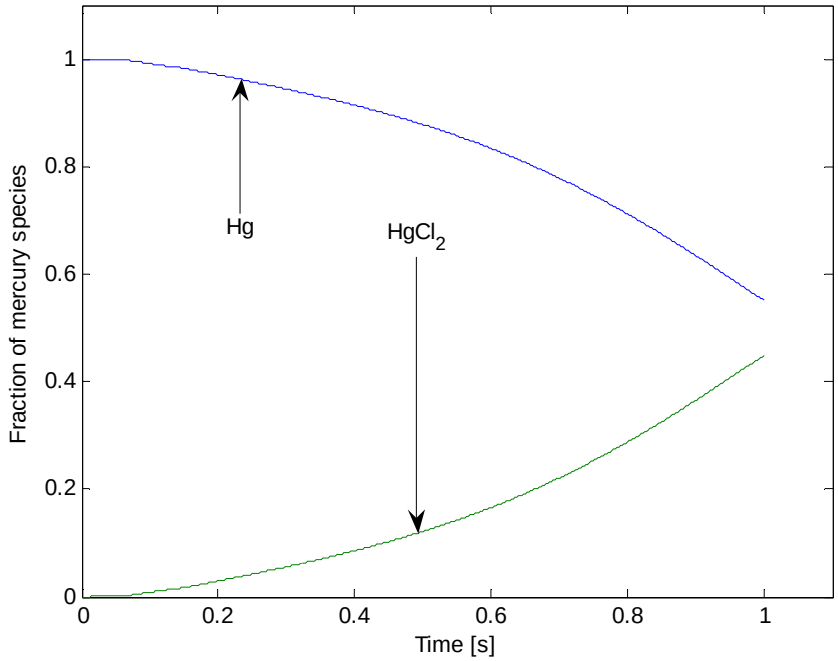

Fig. V.69. Mercury speciation in the gas phase, Wyoming coal, pure air, ER = 1.

The shape of this figure resembles the one for Texas lignite; initially the Hg is released in elemental form and afterwards it is slowly oxidized. The reduction is slightly more effective, due to the larger amount of chlorine.

90% TXL – 10% LAPC Blend

Biomass has a chlorine content more than hundred times larger than coal.

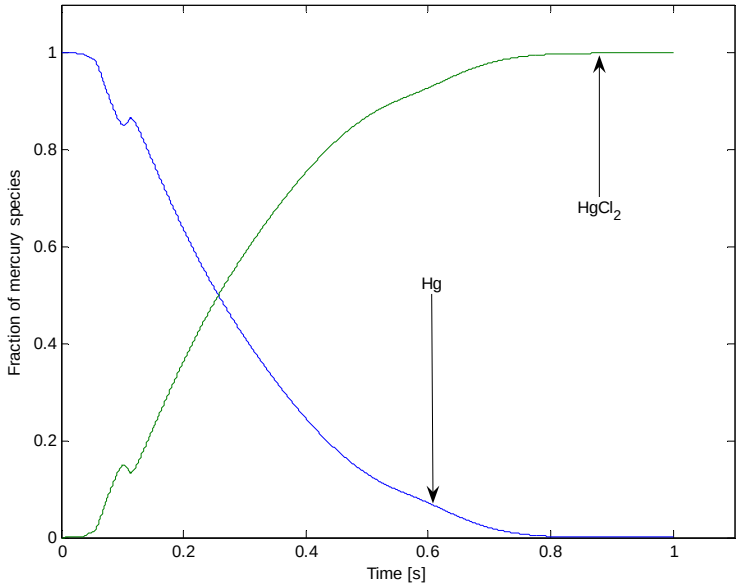

Fig. V.70. Mercury speciation in the gas phase, 90:10 Blend, pure air, ER = 1.

Fig. V.70 shows the results for the blend 90:10. Despite the presence of 90% coal in the blend, the oxidized fraction of mercury is almost comparable to that of pure biomass.

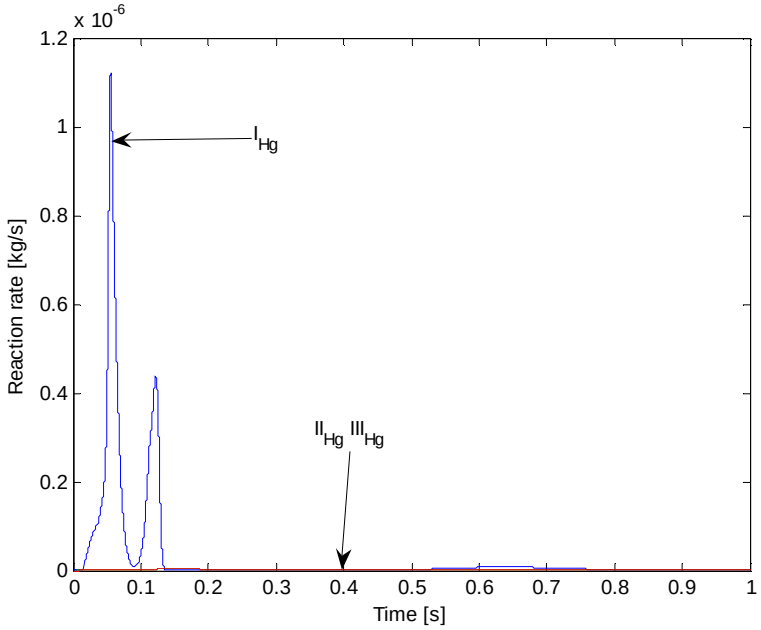

Fig. V.71. Mercury reaction rate, 90:10 Blend, pure air, ER = 1.

Fig. 71 shows the reaction rates for the 90:10 Blends. As expected, the reaction rate for reaction I_{Hg} is much faster than for coal, because now there is the contribution of chlorine from the biomass. From Fig. V.70 it is evident how the addiction of just 10% of biomass could increase significantly the oxidation reaction rate of Hg.

70% TXL – 30% LAPC Blend

For the 70:30 blend the amount of biomass is larger and the oxidation is expected to be at least as effective as before.

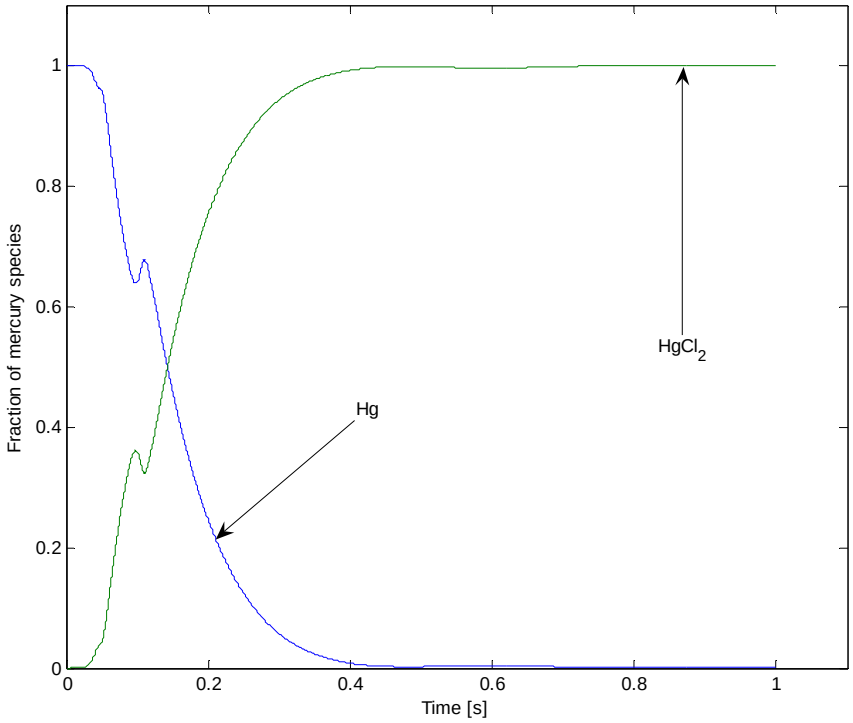

Fig. V.72. Mercury speciation in the gas phase, 70:30 Blend, pure air, ER = 1.

Fig. 72 shows the mercury speciation for the 70:30 Blend. The figure is similar to the previous ones. The only difference is that as now there is more chlorine, hence mercury oxidation is completed much earlier.

50% TXL – 50% LAPC Blend

Consider a blend made out of 50% biomass and 50% Texas lignite: in this case there will be a large amount of mercury due to the presence of coal and also a large amount of chlorine, due to the presence of biomass. As biomass contains much more

chlorine than coal Hg oxidation is expected to be comparable to the one with pure biomass.

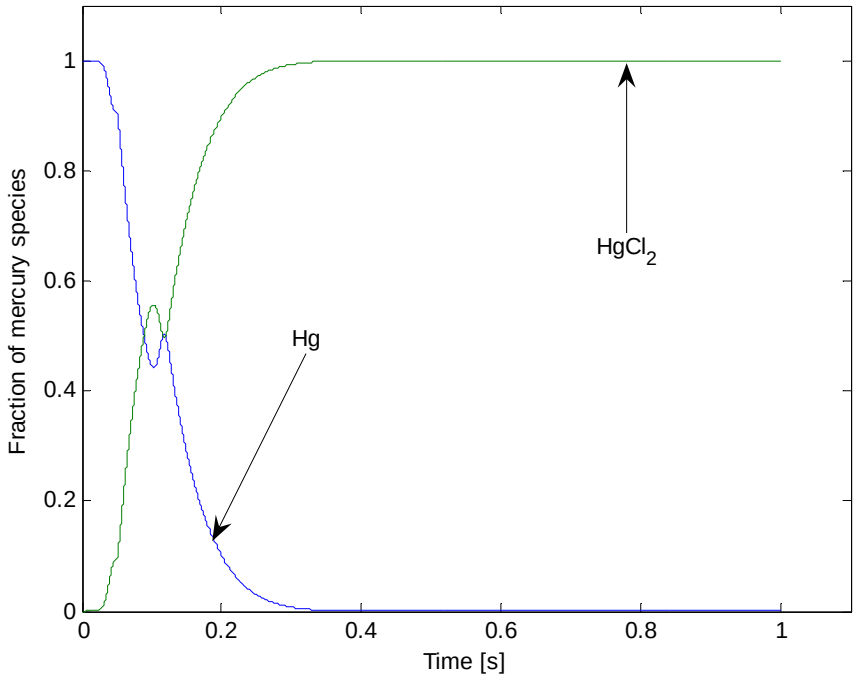

Fig. V.73. Mercury speciation in the gas phase, 50:50 Blend, pure air, ER = 1.

From Fig. V.73 it is clear that with half the fuel made out of biomass there are hardly any differences with burning pure biomass as far as Hg oxidation is concerned.

Parametric studies

The comparison of the experimental results with the prediction of the model has shown a good overall agreement, especially considering the simplicity of the model. So, it is interesting to study the effects of the many parameters on NO_x reduction. These studies can be conducted in two ways: i) by analyzing the effect of variation of the input parameters on the results in order to determine the effect of inaccuracies on the input on the results; and ii) to optimize the process by running a great variety of conditions which cannot be actually tested due to cost and duration of experiments. Using the model, parametric tests can be performed in a very reasonable time.

Mixing time

Many authors [11, 15, 17] have indicated the mixing time (τ_{mix}) to be a critical factor in the NO_x reduction. In this case the mixing time has been estimated experimentally by Goughnour [20] to be around 40 ms. This number cannot be considered absolutely accurate; therefore it is important to determine the sensitivity of the results to τ_{mix}.

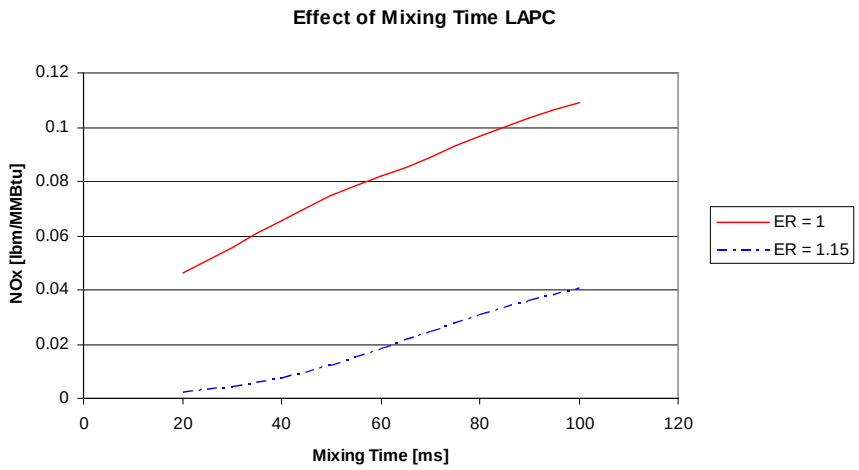

Fig. V.74. Effect of mixing time on NO_x for LAPC biomass.

Fig. V.74 shows the effect of τ_{mix} on the NO emission; as τ_{mix} is reduced, the NO level at exit decreases or % reduction is higher.

Still reasonable variation of the mixing time would not lead to dramatic variation of the NO emission, therefore the accuracy of this parameter can be considered to be not critical.

Fig. V.75 shows the same figure for Texas lignite: it is possible to see that for this coal, the mixing time τ_{mix} has hardly any effects on the NO emission, and this confirms that the accuracy of this the mixing time is not critical for TXL.

This agrees with what was found by Maly [17] that the mixing time becomes critical only for very small value, when the mixing tends toward the condition of instantaneous mixing.

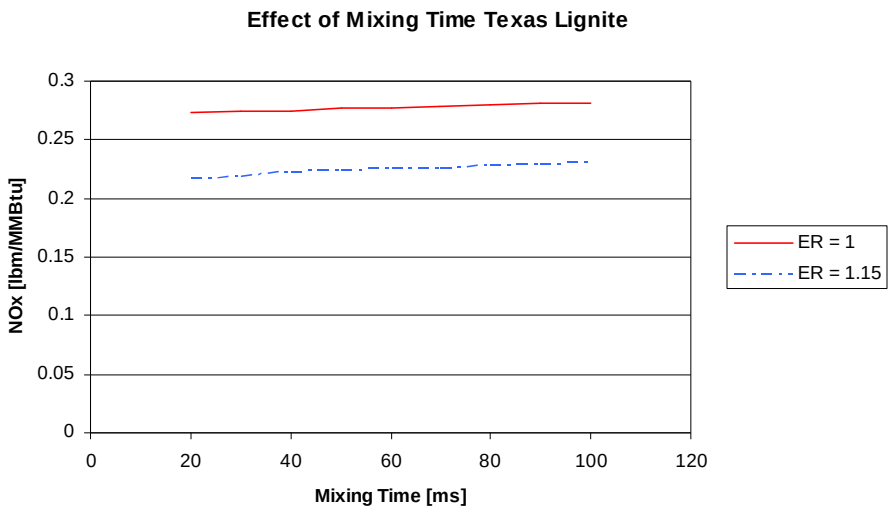

Fig. V.75. Effect of mixing time on NO_x, for Texas lignite.

Fuel nitrogen emission modeling

The release of the fuel bound nitrogen is a very important part of the reburn process; therefore it is worth studying how different models would have affected the results. The base case that was chosen was to model the FN release from biomass as proportional to the pyrolysis, since no kinetic data for FN release from biomass was available from the literature. For the purpose of this study the base case for biomass is compared with those results with kinetics scheme similar to those of coal. Note that these kinetics have been developed for coal, so their applicability to biomass is questionable [29, 49, 57].

Fig. V.76 shows the NO emissions for the various cases of release of FN.

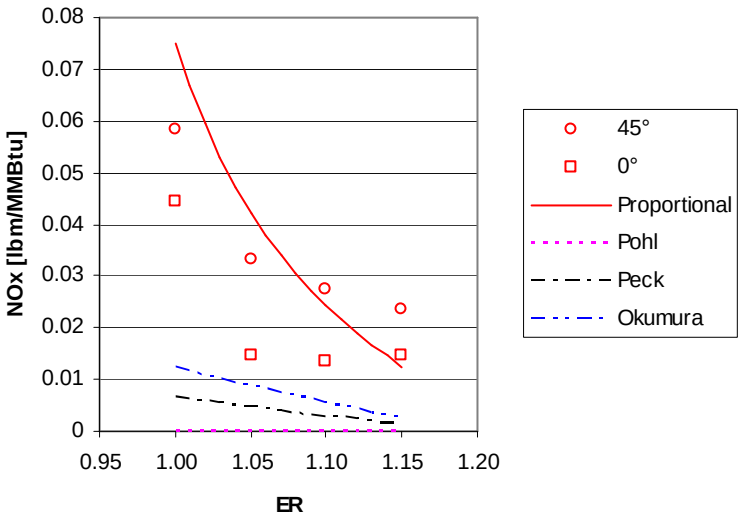

Fig. V.76. Effect of different FN models for biomass.

Fig. V.76 reveals that the assumption of having the FN to be released in proportion to the pyrolysis leads to better comparison with experimental data. The assumption of kinetics similar to coal leads to an overestimate of the NO reduction. This is expected as these kinetics have been formulated for coal, in which case nitrogen has strong bonds with the char structure; therefore the FN is released later than the pyrolysis; so when the N is released, the oxygen concentration in the gas phase is lower, leading to a more effective NO reduction.

Consider Texas lignite. For the base case, it is assumed to model the FN release using dedicated kinetics by Peck [49], which was developed for coal. It is interesting now to compare these results with the results that it would have been possible to get

using other kinetics (Pohl [29], Okumura [57]) or by assuming the FN to be emitted along with the volatiles [8]. Fig. V.77 shows the comparison.

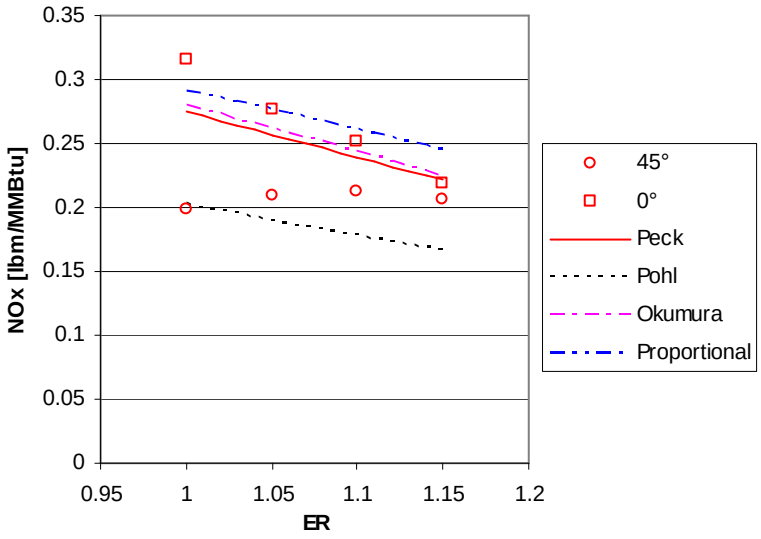

Fig. V.77. Effect of different FN emission model, Texas lignite.

It is seen that the kinetics by Peck leads to better comparison with the experimental data. Still in this case also the other models would have performed reasonably well. Modeling FN to be released along with the volatiles would have led to an underestimation of the NO reduction because in this case FN would have been released very early when there is still much oxygen in the gas phase.

With this brief analysis, it is shown that the base case choice seems to be the one that best match the experimental results.

NO reaction kinetics

The kinetics parameters for the reactions involving NO are probably the most vital parameters in the whole model, in order to get a good prediction of the NO reduction. Several kinetics data are available from literature, but sometimes their applicability to cases different from the ones in which they were formulated or for different fuels is questionable. Previously it has been said that one of the most used reduced kinetics formulation for this kind of model is the one by De Soete [37]; still this kinetics has not led to good results in the current case, probably because those kinetics were based on data points at temperatures above 2000 K, while in the current experiments the temperature is never above 1600 K. Therefore the kinetics for ammonia were substituted with the ones by Brink [38], that have been formulated specifically for biomass, and the kinetics for HCN were substituted with the ones by He [39], which are slight corrections on the De Soete's ones, to adapt them for lower temperatures. Fig. V.78 compares the NO_x predictions for different NO kinetics from literature adopted for LAPC biomass.

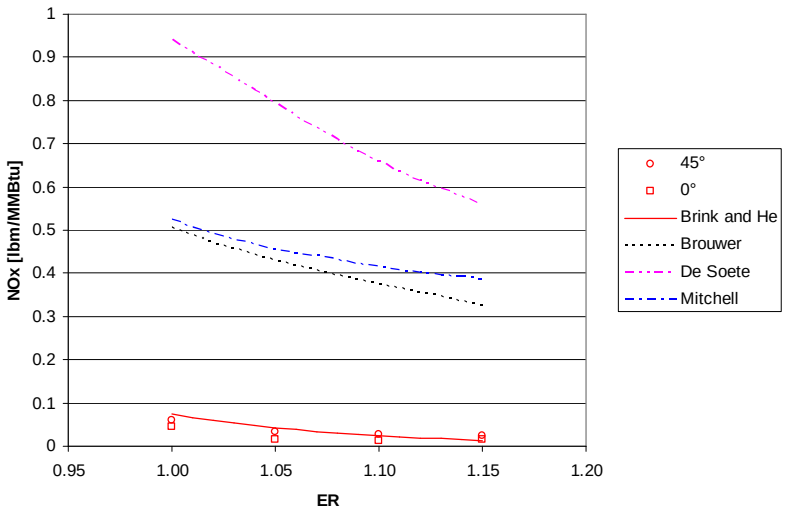

Fig. V.78. Effect of different NO kinetics on the results, LAPC biomass.

From Fig. V.78 it is evident that the choice of the proper NO kinetics is vital in matching with the experimental results. The base case proves to be the one that best matches with the experimental point. De Soete's kinetics leads to the worst results. All the kinetic data predict correct dependency on the ER, but all, except the base case kinetics, fail to lead to results comparable with those from experiments.

Fig. V.79 shows the same plot for Texas lignite; the base case kinetics are the same as used for the LAPC biomass.

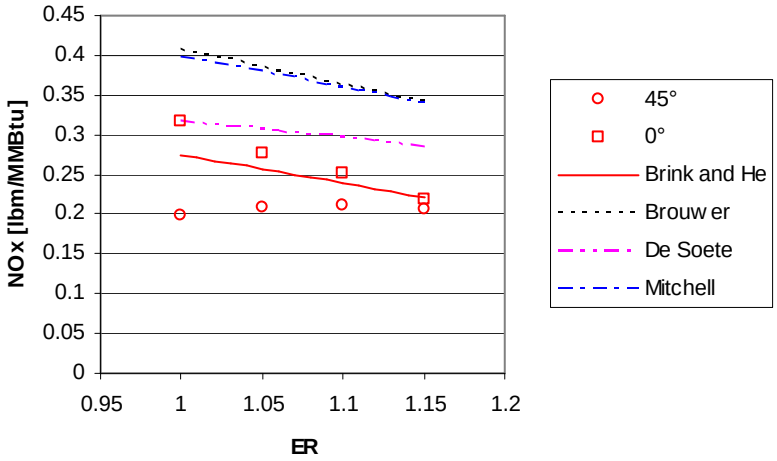

Fig. V.79. Effect of different NO kinetics on the results, Texas lignite.

The case for Texas lignite is very different from the one for biomass; in this case, the base kinetics are still the ones that best match with the experimental results, but now the other kinetics are not so far away from the experimental points.

This is interesting, and it means that the most uncertainties are about the reaction rate for ammonia, as the amount of ammonia and HCN released in the gas stream is what is really different between the two cases: coal and biomass.

The choices of the NO reaction rates are vital in modeling the reburn process, especially when there is a significant amount of ammonia in the gas stream.

Ammonia content

Another parameter that plays an important role in determining the NO reduction is the N based compounds in the volatiles. Coal normally releases significant amount of its FN as HCN and a small fraction as ammonia [8]. The amount of ammonia released

depends on the rank of the coal: the higher the rank, the smaller the fraction of ammonia. On the other hand, a large fraction of the FN from biomass is released as ammonia and a smaller fraction as HCN. The fractions of the products of FN pyrolysis have been assumed from coal and biomass literature for all the fuels. There is general agreement in literature on the values of these fraction, still small variations are possible. For the LAPC the composition of the FN gases have not been measured yet. Therefore it is necessary to consider the effect of the FN composition on the NO reduction.

Fig. V.80 shows the variation of the NO emission for LAPC according to different fraction of ammonia in the FN.

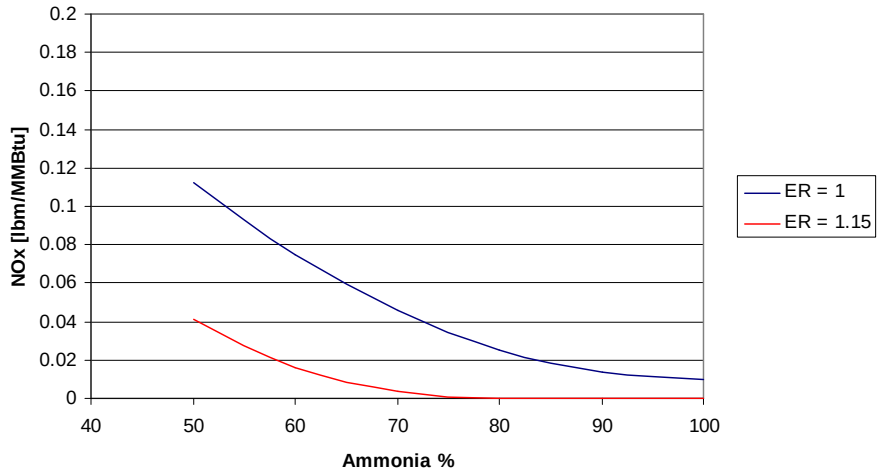

Fig. V.80. Effect of ammonia fraction, LAPC biomass.

From Fig. V.80 it is clear that the ammonia fraction plays an important role in determining the level of NO emission, therefore it is important to know the composition of FN with a good accuracy.

Fig. V.81 shows a similar plot for Texas lignite.

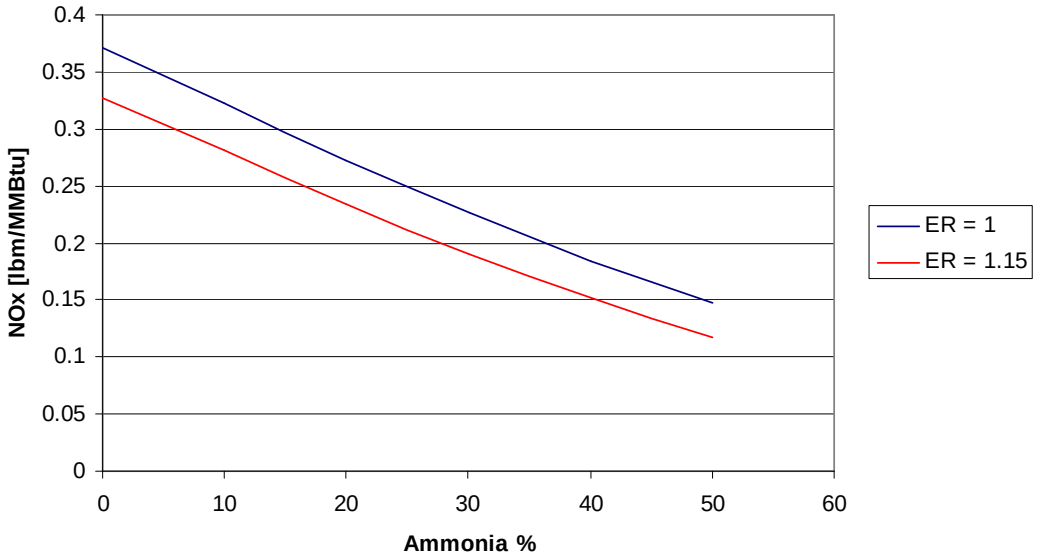

Fig. V.81.Effect of ammonia fraction, Texas lignite, pure air, ER = 1.

Also for coal it is evident that the composition of the FN is important in determining the NO emission.

Particle size distribution

Finally it is interesting to evaluate the effect of the particle size distribution on the NO emission: the base case is the one with the real size distribution that divides the particles in five groups. Since there exist differences between the use of real distribution and the SMD, the NO_x levels vary depending upon whether monosized suspension or real size distribution are used. For the monosized, the SMD is varied in order to study its effects on NO_x levels.

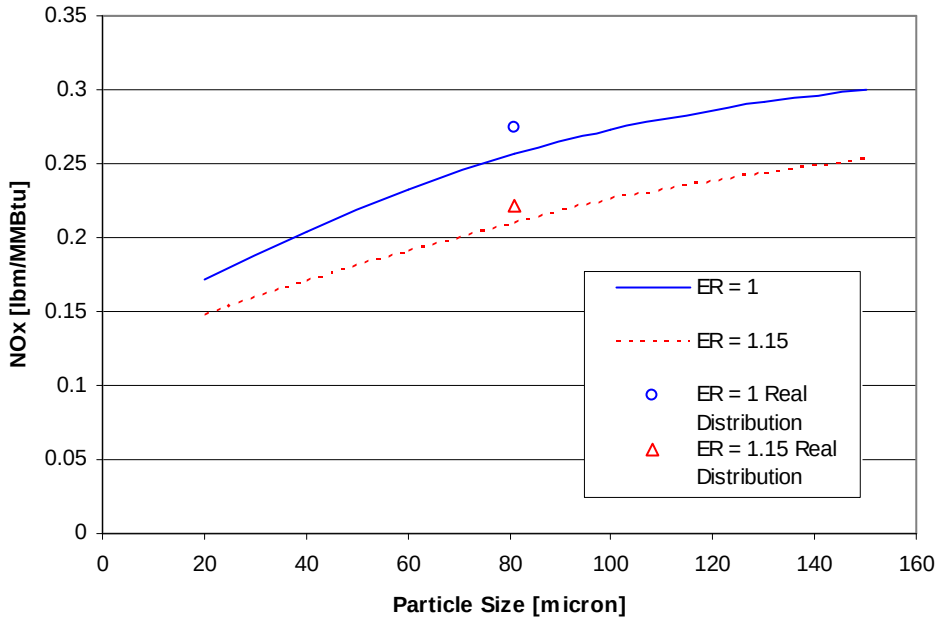

Fig. V.82.Effect of SMD or real distribution on NO emission, Texas lignite.

In Fig. V.82 two open symbols represent the NO_x obtained from the real distribution and they are placed along the X – axis in correspondence of the SMD value of that distribution. The solid lines represent the NO emission according to the SMD size of that distribution (monosized suspension).

Using just the SMD leads to slight underestimation of the NO emission; the discrepancy is visible but still not large, so if there is a strong need to reduce computational time, it is possible to describe all the fuel with monosized particle suspension. If a longer computational time is permissible, it is advisable to consider the real distribution.

It is also interesting to note that the smaller the SMD the better the NO reduction. This agrees with what has been reported in literature [11, 16] when coal was used as reburn fuel or in staged combustion. For better NO reduction, it is important to grind the fuel into small particle size, which heats up and liberate volatiles fast consuming the local oxygen; further the larger surface – volume ration results in increase of the heterogeneous reactions.

Reburn thermal energy

The fraction of thermal energy contributed by the reburner normally lies between 10% and 30% of the total thermal rating of the furnace. In the small scale experiments performed by Goughnour [20], the reburner thermal energy (RTE) fraction was fixed at 30% of the total. No experiments were performed to consider the effect of variation of RTE on the NO reduction. The effects of RTE on NO_x emission are shown in Fig. V.83.

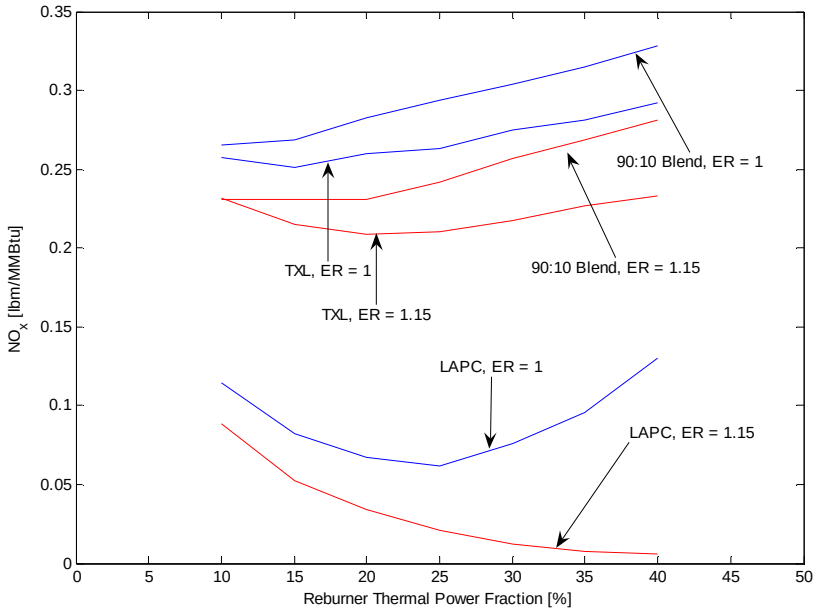

Fig. V.83. Effect of reburner thermal power fraction.

The results for 30% RTE fraction used in the experiments appear to be the best condition for biomass. For Texas lignite, the best RTE fraction is predicted to be between 15 and 20% depending on ER used. Also for the 90:10 Blend, the optimum RTE fraction is away from the 30% used in experiments. The best performance is predicted to be around 15%.

Reburner inlet temperature

In all the studies, the inlet temperatures for both the carrier gas and the reburn fuel were set at 300K, which is very close to the average temperature found in the experiments by Goughnour [20]. It is interesting to see how sensitive is the NO

reduction on such a parameter (inlet temperature of carrier gas and reburn fuel) and hence whether an optimum exists.

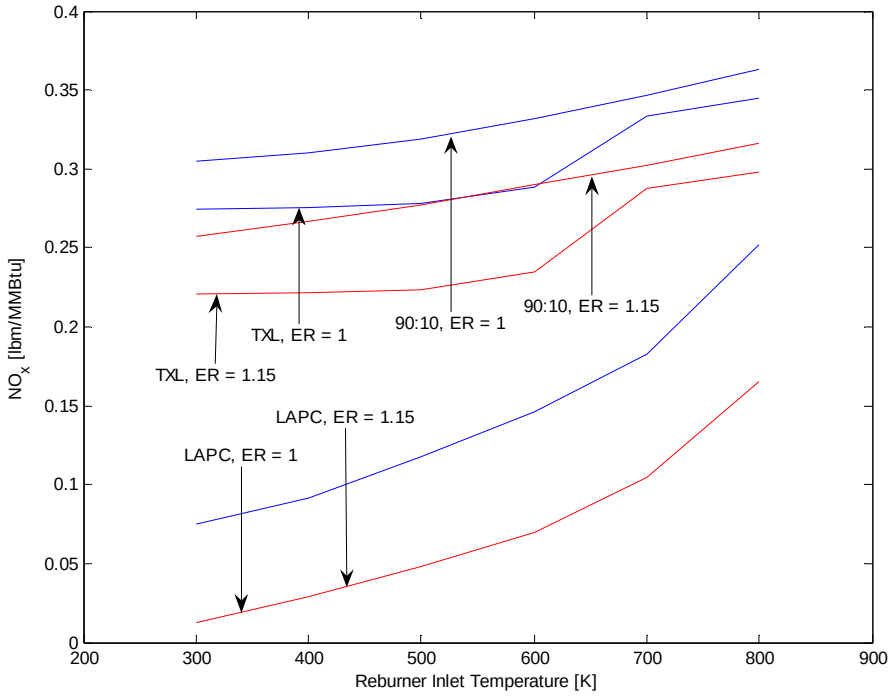

Fig. V.84. Effect of the reburner inlet temperature on the NO_x emissions.

Fig. V.84 shows that the inlet temperature affects the NO reduction and in particular the higher the temperature, the larger the NO emission. Variations due to the normal variation of the temperature of atmospheric air would not affect much the results, especially for Texas lignite and the 90:10 Blend. The situation is completely different if the inlet air and fuel were pre heated a few hundreds degree above 300 K: in this case the results are much poorer, especially for LAPC biomass. Texas lignite and the 90:10 Blend are much less sensitive on the temperature. In this case it is not possible to optimize the variable in the sense that the only direction it is possible to draw is to try to keep the reburner inlet air as cold as possible.

CHAPTER VI

CONCLUSIONS

The model supports the impressive NO_x reduction using pure LAPC biomass as reburn fuel. All the other fuels have led to poorer results and this conclusion can be drawn both from the experiments and from the model.

The model has shown a strong possibility of achieving a large mercury oxidation fraction when burning LAPC biomass or one of its blends with coal.

The other conclusions are summarized below:

1. LAPC biomass is very effective in the reburn process due to the higher amount of volatiles and the large fraction of ammonia in the fuel nitrogen.
2. The accuracy of the model is strongly dependent on the selection of kinetics applicable to the present condition.
3. The model has confirmed that higher equivalence ratios (richer mixture) reduce NO_x levels to a greater extent than lower equivalence ratios (leaner mixture).
4. The model has also confirmed that the use of finer ground fuel can lead to better NO_x reduction.
5. Blends present NO_x reduction levels somewhere between the performance of pure coal and LAPC biomass, but in general closer to coal than to biomass.
6. Some parameters such as the reburn thermal fraction might be optimized to improve the performance of the system.
7. The use of vitiated air, in this case, does not lead to significant improvements.

8. Decrease of oxygen percentage in the carrier gas from 21% down to 12.5% results in decrease of NOx from 0.02 lbm/MMBtu to 0.01 lbm/MMBtu for LAPC biomass, at ER = 1.1.
9. Increase of ER from 1 to 1.1 results in reduction of NOx from 0.07 lbm/MMBtu to 0.02 lbm/MMBtu for LAPC biomass and from 0.27 lbm/MMBtu to 0.24 lbm/MMBtu for Texas lignite, with pure air.
10. When SMD is decreased from 80μm to 40μm at ER = 1, for Texas lignite, NOx decreased from 0.27 lbm/MMBtu to 0.2 lbm/MMBtu.
11. The size distribution suspension yields lesser NO_x reduction when compared to the reburn stream with uniform size having d_p = SMD of suspension.

CHAPTER VII

FUTURE WORK

The following work would be a desirable extension of the results that have been presented here:

- The nitrogenous species such as NH_3 and HCN coming from the fuel FN should be measured in order to know the exact composition of FN products
- Modeling of the effect of the injection angle on the reburn process
- Possible 3D modeling of the reburn process using commercial software like Fluent
- Inclusion of the over fire zone in the model (if an over fire zone will be added to the furnace)
- Data on mercury oxidation should be measured in the furnace in order to validate the results from the model

REFERENCES

[1] US DOE Energy Information Administration, Electricity Statistics. (Accessed Nov 2006)
http://www.eia.doe.gov/fuelelectric.html

[2] US EPA Office of Air & Radiation. Six Principal Pollutants. (Accessed Nov. 2006)
http://www.epa.gov/airtrends/

[3] US EPA Office of Air & Radiation. NOx. (Accessed Nov 2006)
http://www.epa.gov/air/urbanair/nox/index.html

[4] DOE: Reburning Technologies for the Control of Nitric Oxides Emissions from Coal-Fired Boilers, Topical Report Number 14, May 1999

[5] J. H. Pavlish, A. S. Everett, M. D. Mann, E. S. Olson,K. C. Galbreath, D. L. Laudal et al., Fuel Processing Technology 82 (2003) 89-165.

[6] US EPA Mercury. Controlling Power Plant Emissions: Overview (Accessed Nov 2006)
http://www.epa.gov/mercury/control_emissions/index.htm

[7] L. D. Smoot and P. J. Smith, Coal Combustion and Gasification, Plenum Press, New York, 1985

[8] S. Karamba, T. Takarada, Y. Yamamoto and K. Kato, Energy & Fuels 7 (1993) 1013-1020

[9] J. Zhou, S. M. Masutani, D. M. Ishimura, S. Q. Turn and C. Kinoshita, Ind. Eng. Chem. Res. 39 (2000) 626-634

[10] K. Annamalai and I. Puri, Combustion Science and Engineering, Boca Raton, FL: CRC Press, 2006

[11] L. D. Smoot, S. C. Hill and H. Xu, Prog. Energy Combust. Sci. 24 (1998) 385-408

[12] M. A. Wojtowicz, F. P. Miknis, R. W. Grimes, W. W. Smith and M. A. Serio, Journal of Hazardous Materials 9 (2000) 74-81

[13] D. Han, M. G. Mungal, V. M. Zamansky and T. J. Tyson, Combustion and Flame 119 (1999) 483-493

[14] V. M. Zamansky, P. M. Maly, M. S. Sheldon, D. Moyeda, W. C. Gardiner and V. V. Lissianski, Second generation Advanced Reburning for High Efficiency NOx Control, DOE, Quarterly Report No. 6 for period January 1 – March 31 1997

[15] V. V. Lissianski, V. M. Zamansky and P. M. Maly, Combustion and Flame 125 (2001) 1118-1127

[16] A. Kicherer, H. Spliethoff, H. Maier and K. R. Hein, Fuel 73 (1994) 1443-1446.

[17] P. M. Maly, V. M. Zamansky, L. Ho and R. Payne, Fuel 78 (1999) 327-334.

[18] E. Hampartsoumian, O. O. Folayan, W. Nimmo and B. M. Gibbs, Fuel 82 (2003) 373-384.

[19] W. Y. Chen and L. Ma, AlChE Journal 42 (1996) 1968-1976.

[20] P. G. Goughnour, NOx Reduction with the Use of Feedlot Biomass as a Reburn Fuel, M.S. thesis, Texas A&M University, 2006.

[21] M. D. Jensen, R. C. Timpe, J. D. Laumb, Advanced Heterogeneous Reburn Fuels from Coal and Hog Manure, Final Report, U.S. Dept. of Energy, Sept. 2003.

[22] Q. Wang, W. Shen, and Z. Ma, Environ. Sci. Technol., 34 (2000) 2711-2713.

[23] T. J. Feeley, J. Murphy, J. Hoffmann and S. A. Renninger, A Review of DOE/NETL's Mercury Control Technology R&D Program for Coal-Fired Power Plants, April 2003. http://www.netl.doe.gov/technologies/coalpower/ewr/pubs/DOENETL_HgR&D_WhitePaper_Final.pdf

[24] V. M. Zamansky, M. S. Sheldon and P. M. Maly, in Proc. of the 27th Symposium (International) on Combustion, Boulder, CO, The Combustion Institute (1998), pp. 3001-3008.

[25] Y. B. Yang, E. Hampartsoumian and B. M. Gibbs, in Proc. of the 27th Symposium (International) on Combustion, Boulder, CO, The Combustion Institute (1998), pp. 3009-3017.

[26] S. Arumugam, Nitrogen Oxides Emission Control Through Reburning with Biomass in Coal-Fired Power Plants, M.S. Thesis, Texas A&M University, 2004.

[27] E. M. Suuberg, W. A. Peters and J. B. Howard, Ind. Eng. Chem. Process Des. Dev. 17 (1978) 37-46.

[28] A. A. Zabaniouto, G. Kalogiannis, E. Kappas and A. J. Karabelas, Biomass and Bioenergy 18 (2000) 411-420.

[29] J. H. Pohl and A. F. Sarofim, in Proc. of the 16th Symposium (International) on Combustion, The Combustion Institute, Pittsburgh, 1976, pp. 491-501.

[30] K. M. Nichols, P. O. Hedman and D. L. Smoot, Fuel 66 (1987) 1257-1263

[31] M. U. Alzueta, R. Bibalo and A. Millera, Energy and Fuels 12 (1998) 329-338.

[32] V. V. Lissianski, V. M. Zamansky, P. M. Maly, and M. S. Sheldon, Combustion and Flame 125 (2001) 1310-1319.

[33] M. Sami, Numerical Modeling of Coal – Feedlot Biomass Blend Combustion and NO_x emission in Swirl Burner, Ph.D. dissertation, Texas A&M University, 2000.

[34] A. L. Brown, D. C. Dayton, M. R. Nimlos and J. W. Daily, Energy & Fuels 15 (2001) 1276-1285.

[35] M. Østberg, P. Glarborg, A. Jensen, J. Johnson, L. S. Pedersen and K. Dam-Johansen, in Proc. of the 27th Symposium (International) on Combustion, The Combustion Institute, Pittsburgh, 1998, pp. 3027-3035.

[36] D. Stickler, R. Gannon, L. Toung and K. Annamalai K., Pulverized Fuel Combustion, in Proc. of International Symposium on Combustion Diagnostics, American Flame Research Committee, Akron, OH, 1983, pp. 1-21.

[37] G. G. De Soete, in the Proc. of the 15th Symposium (International) on Combustion, The Combustion Institute, Pittsburgh, 1975, pp. 1093-1102.

[38] A. Brink, P. Kilpinen and M. Hupa, Energy & Fuels 15 (2000) 1094-1099.

[39] R. He, T. Suda, M. Takafuji, T. Hirata and J. Sato, Fuel, 83 (2004) 1133-1141.

[40] J. B. Howard, G. C. Williams and D. H. Fine, in the Proc. of the 14th Symposium (International) on Combustion, The Combustion Institute, Pittsburgh, 1973, pp. 975-986.

[41] W. P. Jones and R. P. Lindstedt, Comb. Flame 73 (1988) 233-249.

[42] D. R. Van der Vaart, Ind. Eng. Chem. Res. 31 (1992) 999-1007.

[43] K. Annamalai and W. Ryan, Prog. Energy Combust. Sci. 19 (1993) 383-446.

[44] L. D. Smoot, M. L. Hobbs and P. T. Radulovic, AIChE Journal 38 (1992) 681-702.

[45] H. Yoon, J. Wei and M. M. Denn, AIChE Journal, 24 (1978) 885-903.

[46] J. G. Schoeters, The Fundamentals of Wood Gasification, in: Proc. of the Symposium on Forest Products Research International – Achievements and the Future, Pretoria, South Africa, Apr. 1984, pp. 22-26.

[47] J. W. Mitchel and J. M. Tarbell AIChE Journal 28 (1982) 302-311.

[48] X. Y. Du, Ignition and Combustion of a Dense Stream of Coal Particles, Ph.D. dissertation, Texas A&M University, 1995.

[49] R. E. Peck, K. C. Midkiff and R. A. Altenkirch, Fuel Nitrogen Transformations in one – dimensional Coal Dust Flames, Western States Section of the Combustion Inst., 1982.

[50] G. L. Borman and K. W. Ragland, Combustion Engineering, McGraw – Hill, Boston, MA, 1998.

[51] D. Shao, E. J. Hutchinson, H. Cao, W. P. Pan and C. L. Chou, Energy & Fuels 8 (1994) 399-401.

[52] M. Xu, Y. Qiao, C. Zheng, L. Li and J. Liu, Combustion and Flames, 132 (2003) 208-218.

[53] M. B. Puchakayala, Mercury Emission Behavior During Isolated Coal Particle Combustion, Ph.D. dissertation, Texas A&M University, 2006.

[54] K. Annamalai, J. Sweeten, S. Mukhtar, B. Thien, G. Wei, S. Priyadarsan, S. Arumugam and K. Heflin, Co – Firing Coal: Feedlot and Litter Biomass (CFB and CLB) Fuels in Pulverized Fuel and Fixed Bed Burners, Final Report to U.S. Department of Energy, August 2003.

[55] M. R. Brandon, Pyrolysis and Ignition Behavior of Coal, Cattle Biomass and Coal / Cattle Biomass Blends, M.S. thesis, Texas A&M University, 2006.

[56] C. Senior, D. Lignell, B. Shiley, Z. Chen and A. Sarofim, Kinetics Model for Predicting the Behavior Mercury in Coal Fired Power Plants, ACERC Annual Conference, Salt Lake City, UT, Feb. 2003.

[57] Y. Okumura, Y. Sugiyama and K. Okazaki, Fuel 81 (2002) 2317-2324.

APPENDIX A

The volumetric flow rate of the main burner air and fuel is known from Goughnour [20] for each fuel tested. Also the volumetric flow rate of the reburn air, and the nitrogen injected to simulate the vitiated air case is known.

Let consider the combustion in the main burner: as the fuel is methane the number of moles does not change with the combustion. In the reburner the emission of volatiles tends to increase the amount of volatiles in the gas phase and also the heterogeneous reactions tend to increase the number of moles in the gas phase.

Nevertheless, once the mixing between the main burner flow and the reburner flow is completed it is possible to consider the amount of moles in the gas phase as almost constant because the gas phase is dominated by the products of the main burner, as quantity, and because there are some important reactions in the gas phase that tends to reduce the number of moles (hydrogen and CO oxidation).

The sensors of the temperature are placed downstream the area where the mixing takes place and so it is possible to consider the number of moles passing at each of these sensors as constant.

Therefore, the volumetric rate flow through the burner, normalized at room temperature is known and it is simply the summation of all the volumetric flow rates (computed at room temperature):

$$\dot{V}_{RB@roomT} = \dot{V}_{air,MB} + \dot{V}_{fuel,MB} + \dot{V}_{air,RB} + \left(\dot{V}_{N_2,RB,vitiated}\right) \tag{A.1}$$

Let us suppose the mixture to follow the ideal gas law; in this case it is possible to compute the volumetric flow rate at a temperature T as:

$$\dot{V}_{RB@T} = \dot{V}_{RB@roomT} \cdot \frac{T}{T_{room}} \tag{A.2}$$

The section of the furnace is constant and the distance between two sensors is also known. To compute the time to go from one sensor to another it is necessary to know the speed of the gas flow between the two sensors.

The speed can be computed from the volumetric flow rate as:

$$u = \frac{\dot{V}_{RB@T}}{A} \tag{A.3}$$

The volumetric flow rate is a function of the temperature, and so will not be constant along the furnace. The temperature profiles from Goughnour [20] are almost linear along the furnace so in each segment between two sensors the velocity will be computed from the volumetric flow rate at the average temperature between the two extremes.

Now the average velocity u of each segment of the furnace is known, so it is possible to compute the time needed by the gas to travel from one sensor to the next simply as:

$$\Delta t = \frac{Dis\tan ce}{u} \tag{A.4}$$

Now the temperature profile can be expressed not only as a function of space but also as a function of time. The model is being integrated over time, so the temperature profile will be used as a function of time.

This function will be an interpolated function based on the point where the temperature is known from the experiments.

Summing all the time intervals between two sensors it is also possible to estimate the residence time in the furnace. This is a very important parameter in order to know how much to extend the integration on time, as results got on longer periods could not be compared with any experimental results.

APPENDIX B

The kinetic of the FN is expressed as kg of solid nitrogen being consumed per second, while in the model it is needed to know how many kg of FN products are released over time. These products will be NH_3, HCN and N_2, the composition of this flux is assumed from literature [8, 33].

Therefore the release of nitrogen will be a flow made out of:

$$\dot{N} \rightarrow \begin{cases} Frac_{NH_3} \cdot NH_3 \\ Frac_{HCN} \cdot HCN \\ Frac_{N_2} \cdot N_2 \end{cases} \rightarrow \begin{cases} Mole\_Frac_{NH_3} \cdot NH_3 \\ Mole\_Frac_{HCN} \cdot HCN \\ Mole\_Frac_{N_2} \cdot N_2 \end{cases} \tag{B.1}$$

From the mass fractions it is possible to switch easily to mole fractions of the products, as their molecular weight is known. For simplicity, let us call the mole fractions *a*, *b* and *c*.

So assuming these to be the products of the FN pyrolysis it is possible to set up a balance for the nitrogen atoms needed to provide these products:

$$(a+b+c)\cdot N(s) \rightarrow a \cdot NH_3 + b \cdot HCN + c \cdot N_2 \tag{B.2}$$

Normalizing:

$$N(s) \rightarrow \frac{a}{(a+b+c)} \cdot NH_3 + \frac{b}{(a+b+c)} \cdot HCN + \frac{c}{(a+b+c)} \cdot N_2 \tag{B.3}$$

At this point it is known how many moles of products will be generated for each mole of nitrogen consumed.

Let switch back to the mass balance:

$$N(s)\cdot M_N \rightarrow \frac{a}{(a+b+c)}\cdot M_{NH_3}\cdot NH_3 + \frac{b}{(a+b+c)}\cdot M_{HCN}\cdot HCN + \frac{c}{(a+b+c)}\cdot M_{N_2}\cdot N_2 \quad \text{(B.4)}$$

This says how many kg of products are generated from 14 kg of nitrogen:

$$14\,kg_N \rightarrow \frac{a}{(a+b+c)}\cdot M_{NH_3}\cdot kg_{NH_3} + \frac{b}{(a+b+c)}\cdot M_{HCN}\cdot kg_{HCN} + \frac{c}{(a+b+c)}\cdot M_{N_2}\cdot kg_{N_2} \quad \text{(B.5)}$$

So:

$$14\,kg_N \rightarrow \left[\frac{a}{(a+b+c)}\cdot M_{NH_3} + \frac{b}{(a+b+c)}\cdot M_{HCN} + \frac{c}{(a+b+c)}\cdot M_{N_2}\right] kg_{FBN\ pyrolysis} \quad \text{(B.6)}$$

At this point it is possible to compute the constant k_N that says how many kg of FBN products will be released for each kg of nitrogen consumed.

This constant depends only on the composition of the FBN products.

For biomass $k_N = 1.32$

For Texas lignite $k_N = 1.9$

For Wyoming coal $k_N = 1.92$

APPENDIX C

Considering the following decomposition reaction it is possible to compute the amount of OH present in the gas phase.

$$H_2O \rightarrow OH + \frac{1}{2} \cdot H_2 \tag{C.1}$$

Note that this reaction takes place in the gas phase, but the products of dissociation can be considered as trace amounts, so the total amount of moles in the gas phase n_{tot} can be considered constant. Let call n_{H2O} the number of moles of water in the gas phase.

$$n_{H2O} \cdot H_2O \rightarrow a \cdot H_2O + b \cdot OH + c \cdot H_2 \tag{C.2}$$

To find the unknowns a, b and c there are two equations from the atom balances and the equation from the equilibrium constant.

The equilibrium constant is defined as:

$$K_{eq}(T) = \frac{X_{OH} \cdot X_{H2}^{1/2}}{X_{H_2O}} \tag{C.3}$$

as the pressure is the atmospheric pressure.

So:

$$K_{eq}(T) = \frac{\frac{b}{n_{TOT}} \cdot \left(\frac{c}{n_{TOT}}\right)^{1/2}}{\frac{a}{n_{TOT}}} = \frac{b \cdot c^{1/2}}{a \cdot n_{TOT}^{1/2}} \tag{C.4}$$

The values of the equilibrium constant have been assumed from Annamalai [10].

The system to solve will be:

$$\begin{cases} 2 \cdot n_{H2O} = 2 \cdot a + b + 2 \cdot c \\ n_{H2O} = a + b \\ K_{eq}(T) \dfrac{b \cdot c^{1/2}}{a \cdot n_{TOT}^{1/2}} \end{cases} \tag{C.5}$$

Solving the system at each temporal step it is possible to estimate how much OH is present in the gas phase.

VITA

Giacomo Colmegna completed his bachelor's degree in mechanical engineering in July 2004 from Politecnico di Milano, Milan, Italy. He then started his Master of Science in Mechanical Engineering at Texas A&M University in August 2005. Giacomo may be contacted by mail at via del Monivasco, 1 22074 Lomazzo CO, Italy.